NASA TECHNICAL NOTE

NASA TN D-5901

NASA TN D-5901

c. 1

LANGLEY HOTSHOT TUNNEL OPERATIONS WITH HELIUM AT MACH NUMBERS IN EXCESS OF 30

by Charles G. Miller III

Langley Research Center
Hampton, Va. 23365

NATIONAL AERONAUTICS AND SPACE ADMINISTRATION • WASHINGTON, D. C. • JULY 1970

1. Report No.	2. Government Accession No.	3. Recipient's Catalog No.
NASA TN D-5901		

4. Title and Subtitle	5. Report Date
LANGLEY HOTSHOT TUNNEL OPERATIONS WITH HELIUM AT MACH NUMBERS IN EXCESS OF 30	July 1970
	6. Performing Organization Code
7. Author(s)	8. Performing Organization Report No.
Charles G. Miller III	L-6876
	10. Work Unit No.
9. Performing Organization Name and Address	129-01-22-06
NASA Langley Research Center Hampton, Va. 23365	11. Contract or Grant No.
	13. Type of Report and Period Covered
12. Sponsoring Agency Name and Address	Technical Note
National Aeronautics and Space Administration Washington, D.C. 20546	14. Sponsoring Agency Code

15. Supplementary Notes

The material presented herein is based on a thesis submitted in partial fulfillment of the requirements for the degree of Master of Science in Engineering Mechanics, George Washington University, Washington, D.C., Apr. 1970.

16. Abstract

The results of an exploratory study to generate extremely high Mach number helium flow in the Langley hotshot tunnel are presented for variations in reservoir pressure from 3000 to 28 000 lb/in^2 (20.7 to 193.0 MN/m^2), in reservoir temperature from 1500° to 11 000° R (833° to 6111° K), and in geometric-area ratio from 3×10^3 to 8×10^4. These variations resulted in a range of Mach numbers from 30 to 70.

The effect of wide ranges of reservoir conditions and geometric-area ratios on decay of reservoir conditions, total tunnel run time, flow quality, various nozzle test-section flow parameters, nozzle boundary-layer characteristics, and nozzle axial gradients is discussed.

Correlations of the nozzle boundary-layer thickness and displacement thickness are presented, and an existing empirical method for predicting nozzle boundary-layer displacement thickness in nitrogen was modified and extended to the Mach 30 to 60 region in helium. Semiempirical relations are presented for predicting free-stream and postnormal-shock conditions when only reservoir conditions and nozzle geometry are known.

17. Key Words (Suggested by Author(s))	18. Distribution Statement
High Mach number helium flow Hotshot tunnel Boundary-layer displacement thickness	Unclassified – Unlimited

19. Security Classif. (of this report)	20. Security Classif. (of this page)	21. No. of Pages	22. Price*
Unclassified	Unclassified	79	$3.00

*For sale by the Clearinghouse for Federal Scientific and Technical Information
Springfield, Virginia 22151

LANGLEY HOTSHOT TUNNEL OPERATIONS WITH HELIUM AT MACH NUMBERS IN EXCESS OF 30*

By Charles G. Miller III
Langley Research Center

SUMMARY

An exploratory study to generate extremely high Mach number helium flow in the Langley hotshot tunnel has been performed. Variations in reservoir pressure from 3000 to 28 000 lb/in^2 (20.7 to 193.0 MN/m^2), in reservoir temperature from 1500° to 11 000° R (833° to 6111° K), and in geometric-area ratio from 3×10^3 to 8×10^4 resulted in a range of Mach numbers from 30 to 70. The tunnel starting transient time was similar to that obtained with nitrogen as the test gas; however, the total run time in helium was approximately one-third that in nitrogen. A marked effect of variation of reservoir pressure and temperature on Mach number was observed for a given nozzle geometric-area ratio, with the Mach number increasing with increasing reservoir pressure and decreasing reservoir temperature. The conical nozzle produced an axial variation in Mach number of 0.5 percent per inch (0.2 percent per cm). The nozzle boundary-layer thickness (as determined from pitot-pressure profiles) and displacement thickness were correlated, with the use of Reynolds number evaluated at a reference temperature, to within ±20 percent, and an existing empirical method for predicting nozzle boundary-layer displacement thickness in nitrogen was modified and extended to the Mach 30 to 60 region in helium. Semiempirical relations for predicting free-stream and postnormal-shock conditions, when only reservoir conditions and nozzle geometry are known, are presented. This study indicates that hotshot tunnels provide a convenient, relatively inexpensive means of generating helium flow conditions covering a substantial portion of the earth entry corridor for return from planetary exploration (in terms of simulation parameters – that is, Mach number and free-stream Reynolds number) without requiring modification of existing hardware.

INTRODUCTION

As proposed space missions extended in scope to cislunar and translunar objectives, the need for experimental information from ground facilities concerning flow

*The material presented herein is based on a thesis submitted in partial fulfillment of the requirements for the degree of Master of Science in Engineering Mechanics, George Washington University, Washington, D.C., Apr. 1970.

characteristics about proposed entry configurations at Mach numbers in excess of 20 became apparent. One method of obtaining very high Mach numbers in a wind tunnel is to employ a test gas such as helium which requires less expansion than air or nitrogen to reach a given Mach number. Helium has been employed as the flow medium in conventional wind tunnels since the early 1950's and has thereby provided a means for performing fundamental fluid mechanic studies at hypersonic Mach numbers to approximately 26. One of the primary reasons for using helium is that it liquefies at a very low temperature; hence, Mach numbers up to approximately 26 can be generated in a wind tunnel without preheating the helium prior to expansion.

To extend the Mach number upwards into the range realized in cislunar and translunar missions, conventional facilities would require a means of preheating the helium to prevent flow condensation. Since the Langley hotshot tunnel had ample energy available for heating the test gas and was designed in such a way that the ratio of geometric nozzle-to-throat cross-sectional area could be varied rapidly, it was believed that this facility could possibly be utilized to generate Mach numbers greater than 30 with helium as the test gas. The Langley hotshot tunnel would then provide a convenient, relatively inexpensive means of simulating a substantial portion of the earth entry corridor (in terms of the simulation parameters – that is, Mach number and free-stream Reynolds number) for return from cislunar and translunar missions. Therefore, the present study was initiated to determine the feasibility of using helium as the test gas in this tunnel.

In this study, the effect of wide ranges of reservoir pressure and temperature, of nozzle-throat diameter and geometry, and of nozzle axial station on decay of reservoir conditions, total tunnel run time, flow quality, various nozzle test-section flow parameters, and nozzle boundary-layer characteristics was examined. Results presented include correlations of the nozzle boundary-layer thickness and displacement thickness, derivation of semiempirical relations for predicting free-stream and postnormal-shock conditions, and a pressure distribution measured on a spherically blunted cone at Mach 60.

SYMBOLS

The physical quantities in this paper are usually given both in U.S. Customary Units and in the International System of Units (SI) (ref. 1). Conversion factors relating these two systems of units are presented in the appendix for use in converting when only one system is given.

a	speed of sound
A	area
A_2	

A/A^*	ratio of nozzle cross-sectional area to throat cross-sectional area
C	capacitance
C_2, C_3, C_4	real-helium correction factors
c_p	specific heat at constant pressure
d	diameter
E	total electrical energy in capacitors, $\frac{1}{2}NCv^2$
h	enthalpy
L	vehicle length
l	length of cylindrical nozzle-throat section
M	Mach number
$\dot{m}$	mass-flow rate
N	number of capacitors
N_{Kn}	Knudsen number
N_{Pr}	Prandtl number
N_{Re}	Reynolds number
p	pressure
q	dynamic pressure
R	universal gas constant
r	radius
r_c	recovery factor

s	distance along model surface, measured from model stagnation point at zero angle of attack
T	temperature
t	elapsed tunnel run time
t'	total tunnel run time
U	velocity
V	reservoir volume
v	initial capacitor voltage
W	molecular weight
x	nozzle axial distance from nozzle apex
y	lateral distance from nozzle center line
γ	ratio of specific heats
δ	nozzle boundary-layer thickness
δ^*	nozzle boundary-layer displacement thickness
ϵ	energy transfer efficiency
θ	nozzle half-angle
λ	mean free path
μ	coefficient of viscosity
ρ	density
ϕ	nozzle-throat total entrance angle

Subscripts:

aw	adiabatic wall conditions
c	initial reservoir conditions
eff	effective (based on mass flow considerations)
geo	geometric
i	ideal-helium conditions
n	model nose
ref	based on reference temperature
s_b	surface length from model stagnation point to model base
t,1	reservoir stagnation conditions following arc discharge
t,2	stagnation conditions behind normal shock
w	nozzle wall
x	nozzle axial distance from nozzle apex
∞	free-stream conditions
2	static conditions immediately downstream of normal shock

Superscript:

*	conditions at nozzle throat

A bar over a symbol denotes average value across inviscid core.

FACILITY AND APPARATUS

The Langley hotshot tunnel (fig. 1) is an arc-heated, impulse-type, blowdown facility, the major components of which include a 1.9×10^3-Btu (2-MJ) capacitor bank with an

electrical charging unit, a constant-volume arc chamber incorporating coaxial electrodes (fig. 2), a 10° total-divergence-angle conical nozzle and test section, a 10° total-entrance-angle cone-cylinder diffuser having a ratio of exit to entrance area of 0.55, and a vacuum tank. A more detailed description of this facility is presented in references 2 and 3.

Lateral pitot-pressure surveys in the nozzle test section were made with the 19-probe survey rake, having a probe spacing of 1 inch (2.54 cm). (See fig. 3.) This survey rake represents a carryover from the nitrogen calibration study of reference 3. The inside diameter of the rake probes was 0.0625 inch (1.59 mm), and the length from the probe end to the leading edge of the 30° total-angle wedge section was 1.5 inches (3.81 cm). Each rake probe was provided with a contamination trap so as to minimize possible damage to the pressure transducer resulting from impact of solid contaminants in the flow. The support system consisted of a cylindrical sting, having a length of 40 inches (1.02 meters), in conjunction with a double-legged strut. The sting was adapted to the strut by a cylindrical sleeve; hence, the survey rake could be positioned at nozzle axial stations ranging from approximately 103 inches (2.62 meters) (at this station, the end probes of the survey rake would be nearly in contact with the nozzle wall) to 130 inches (3.30 meters) by simply sliding the sting within the sleeve. In the present investigation, the survey rake was maintained in a horizontal position and the center line of the center rake probe was nominally coincident with the nozzle center line. Also presented herein is the pressure distribution on a 25° half-angle spherically blunted cone having a spherical nose radius of 0.3 inch (7.62 mm) and a cone base radius of 1.5 inches (3.81 cm). (This model was employed previously in the Mach 20 nitrogen investigation of ref. 4.) Ten pressure orifices having diameters of 0.038 inch (0.965 mm) were positioned at various increments along a ray.

INSTRUMENTATION

Nozzle test-section pitot pressures and surface pressures on the spherically blunted cone were measured with differential, variable-reluctance, wafer-type pressure transducers (ref. 5). In the measurement of nozzle wall pressures less than 0.1 lb/in^2 (689.5 N/m^2), differential, variable-reluctance, barrel-type pressure transducers were used. Geometric details of this barrel-type pressure transducer are shown in reference 6. All the pressure transducers were excited by 5-volt 20-kilocycle carrier amplifiers. The output signal drove galvanometers in a light-beam-type oscillograph having a variety of chart speeds. The wafer-type pressure transducers were calibrated before each tunnel test, in order to compensate for any time-varying characteristics associated with the transducers and amplifiers, by utilizing a bellows and manometer system. The barrel-type pressure transducers were calibrated under vacuum with a high-precision capacitive pressure meter used as a calibration standard. The reference side of all

test-section pressure transducers was maintained at a constant pressure of approximately 4×10^{-5} lb/in^2 (0.28 N/m^2) by an external vacuum source. Initial charge pressure in the reservoir (arc chamber) was measured with a Bourdon gage having an operating range from 0 to 5000 lb/in^2 (0 to 34.5 MN/m^2). The reservoir stagnation pressure was measured by a high-response, strain-gage transducer having a full-scale rating of 20 000 lb/in^2 (138 MN/m^2). Although this strain-gage transducer was subjected to reservoir pressures up to approximately 30 000 lb/in^2 (207 MN/m^2), no physical damage or appreciable change in calibration characteristics was observed.

OPERATING PROCEDURE

Following evacuation of the nozzle and vacuum tank to approximately 2×10^{-5} lb/in^2 (0.14 N/m^2), the reservoir (arc chamber) is initially pressurized at ambient temperature with the test gas. A quantity of stored electrical energy is then discharged across the coaxial electrodes when the arc gap is broken down by exploding a trigger wire between the electrodes. The resulting increase in pressure and temperature within the reservoir results in the rupture of the diaphragm between the reservoir and evacuated nozzle. The gas then expands through the diverging conical nozzle into the vacuum tank.

The operating procedure with helium is, with a few exceptions, the same as that with nitrogen. One exception is that less electrical energy is required for helium to produce similar reservoir pressure and temperature. The range of reservoir pressure and temperature in figure 4 represents, roughly, practical operating conditions as determined from tunnel-hardware considerations and arc-discharge characteristics. To demonstrate the use of this working chart, assume that for a tunnel test, a reservoir pressure of 12 000 lb/in^2 (82.7 MN/m^2) and a reservoir temperature of 5400° R (3000° K) are desired immediately following arc discharge (tunnel run time of zero). These conditions are denoted by the shaded circle in figure 4 and observed to correspond to an initial reservoir pressure (reservoir charge pressure) of approximately 1200 lb/in^2 (8.3 MN/m^2). By following the dashed line, it can be seen that a representative reservoir volume for the Langley hotshot tunnel is 180 in^3 (2950 cm^3). In the present study, the energy transfer efficiency (defined as the ratio of the difference in internal energy of the test gas to the electrical energy supplied to the gas, with any residual voltage neglected) was observed to vary randomly from 0.52 to 0.62. For the purpose of illustration, an energy transfer efficiency of 0.55 is assumed. By following the dashed line and noting that the total number of capacitors for this tunnel is 720, it is observed that 4050 volts are required in conjunction with the initial reservoir pressure of 1200 lb/in^2 (8.3 MN/m^2), to yield the desired reservoir conditions. For comparison, a similar working chart in reference 2 shows that to obtain the same reservoir pressure and temperature in nitrogen, an initial reservoir pressure of approximately 1100 lb/in^2 (7.6 MN/m^2) is required, but in

conjunction with 5800 volts, again with an energy transfer efficiency of 0.55 assumed. Of course, a working chart such as that of figure 4 is extremely useful when a facility is to be operated over a wide range of reservoir pressure and temperature as in the present investigation.

A second difference in procedure (with helium used instead of nitrogen) is that an added precaution was taken to minimize the amount of air contamination present in the test gas. As discussed in reference 7, and verified accidentally during the course of the present study, the presence of air in the helium test gas can have a significant effect on test-section flow parameters. The usual procedure for nitrogen operation was to purge the reservoir with nitrogen prior to charging (pressurizing). However, for helium operation, the reservoir was evacuated to approximately 3×10^{-4} lb/in^2 (2.07 N/m^2) prior to charging. An air-in-helium analyzer was used to monitor the purity of the helium supply, and for the present test the air contamination by mass was less than 0.2 percent.

Although the tunnel starting transient time with helium was not significantly different from that with nitrogen, the total run time for helium was shorter, being approximately one-third that for nitrogen. A comparison is shown in figure 5 where representative oscillograph pressure traces obtained with the survey rake are presented for helium and nitrogen at similar values of reservoir pressure and temperature immediately following arc discharge and for a nozzle-throat diameter of 0.15 inch (3.81 mm). The survey rake was located at an axial station of 122 inches (3.10 meters). (See fig. 1 for relative nozzle-axial-station locations.) Rake probe number 1 is closest to the nozzle wall and probe number 10 is nominally coincident with the nozzle center line. The run times in helium were of sufficient length to obtain useful data with existing tunnel instrumentation, but did necessitate such minor adjustments as advancing the dump-valve actuation, increasing the oscillograph record speed, and advancing the schlieren spark when schlieren photographs were attempted.

In the course of the present helium study, a series of "misfires" occurred during attempts to obtain charge voltages in excess of approximately 5500 volts. Similar misfires had occurred in the past with nitrogen; however, they were random, usually being caused by breakdowns in the laminated plastic insulators (fig. 2), and did not appear to be an explicit function of charge voltage. When a high-voltage, low-current source was placed across the electrodes for a given reservoir charge pressure with nitrogen, no arcing was observed for voltages to approximately 7000 volts. However, when this test was repeated with helium for the same charge pressure, arcing occurred in the neighborhood of 5000 to 5500 volts. Thus, for helium operation, a ceiling on the charge voltage was necessary, this ceiling being approximately 5500 volts. (Only one helium test involving a charge voltage in excess of approximately 5500 volts was obtained successfully in the present study; three attempts to repeat this test were characterized by premature arc discharges, all of which occurred in the neighborhood of 5500 volts.)

DATA REDUCTION AND ACCURACY

The reservoir, nozzle-throat, free-stream, and postnormal-shock conditions were calculated by using the real-helium data reduction method of reference 8. This method was derived primarily to meet the needs of hotshot wind tunnels where, as in the present study, the only direct measurements made to define the flow conditions are of reservoir pressure and test-section stagnation pressure behind a normal shock. A third known flow quantity in the present study (required by the system of equations) is the reservoir density. At a tunnel run time of zero (immediately following arc discharge), the reservoir density is equal to the reservoir charge density as calculated from the measured reservoir charge pressure and ambient temperature. Time variation of the reservoir density is obtained by using a mass-flow iteration procedure, for which the assumption of uniform density throughout the reservoir during a tunnel test is made. The flow is assumed to be isentropic, one dimensional, and in thermodynamic equilibrium.

Uncertainties involved in the pressure measurements and the reading of oscillograph traces of this study are believed to be less than the following:

$p_{t,1}$, percent	±10
$p_{t,2}$, percent	±10
p_w, percent	±30

For the most unfavorable conditions, these uncertainties result in the following maximum inaccuracies in calculated free-stream parameters:

p_∞, percent	±21
ρ_∞, percent	±18.5
T_∞, percent	±6
M_∞, percent	±6.5
$N_{Re,\infty}$, percent	±13
$(A/A^*)_{eff}$, percent	±18

A recent survey (ref. 9) revealed that use of Keesom's empirical expression for viscosity (ref. 10) at free-stream static temperatures below about 14° R (7.8° K) can result in appreciable errors in free-stream Reynolds number. Since the data reduction method of reference 8 employs Keesom's expression and since most of the present data were obtained for free-stream static temperatures below 14° R (7.8° K), a correction was applied to the present values of free-stream Reynolds number by using the viscosity relations of reference 9.

A quantity of interest in the present study, which was not discussed in reference 8, is the nozzle boundary-layer displacement thickness. This quantity, with one-dimensional flow assumed, is given by the relation

$$\delta^* = r_{geo} - r_{eff} \tag{1}$$

where

$$r_{eff} = r_{eff}^* \left(\frac{A}{A^*}\right)_{eff}^{1/2}$$

and $(A/A^*)_{eff}$ is determined from the continuity equation. With the assumption that the displacement thickness at the nozzle throat is zero $\left(r_{geo}^* = r_{eff}^*\right)$, equation (1) becomes

$$\delta^* = r_{geo} - r_{geo}^* \left(\frac{A}{A^*}\right)_{eff}^{1/2} \tag{2}$$

which can be expressed, for a conical nozzle, in the nondimensional form

$$\frac{\delta^*}{x} = \tan \theta - \frac{d^*}{2x}\left(\frac{A}{A^*}\right)_{eff}^{1/2} \tag{3}$$

Since the measured pitot pressure serves as a basic input to the method of reference 8, a value of $(A/A^*)_{eff}$ was determined for each survey-rake pitot-pressure measurement within the inviscid core; the average of these inviscid-core values of $(A/A^*)_{eff}$ was employed in equation (3). The maximum inaccuracy in calculated nozzle boundary-layer displacement thickness is believed to be less than ±15 percent.

RESULTS AND DISCUSSION

In determining the feasibility of generating extremely high Mach number flow by using helium as the test gas in the Langley hotshot tunnel, the first concern was, of course, whether the flow would establish. If so, would the total run time be sufficient to obtain usable data with existing instrumentation and would the flow be quasi-steady? Also, would flow characteristics such as uniformity, repeatability, and inviscid-core size be of sufficient quality to permit aerodynamic testing? The present study represents an attempt to answer these questions and to examine the effects of large variations in reservoir pressure and temperature, of nozzle-throat diameter and geometry, and of nozzle axial station on various flow characteristics.

Decay of Reservoir Conditions

In the operation of a hotshot wind tunnel, a decay of reservoir conditions (and hence a decay of free-stream thermodynamic quantities and velocity) occurs during the total run time (defined herein as the time increment between the diaphragm rupture immediately following arc discharge and the termination of useful flow) because of heat loss to the cold (ambient-temperature) reservoir wall and because of mass flow from the reservoir.

Since the useful flow establishes sometime after diaphragm rupture, reservoir and free-stream conditions corresponding to this flow may differ appreciably from those immediately following arc discharge. To determine the extent of heat loss to the reservoir wall, the nozzle throat was blocked, as in reference 2, and flow from the reservoir following arc discharge was thereby prevented. The tests were repeated with a 0.15-inch (3.81-mm) nozzle-throat diameter so that the loss due to mass flow from the reservoir could be estimated.

Figure 6 shows the relative decay of reservoir pressure (see fig. 6(a)) and reservoir temperature (see fig. 6(b)) with elapsed run time for several values of reservoir pressure at zero run time. The blocked-throat tests (no flow) correspond to a constant density and thereby permit the reservoir temperature to be determined, at various elapsed run times, from the measured reservoir pressure. The reservoir temperature at zero run time was nearly the same for the three reservoir-pressure levels of figure 6, being approximately 5000° R (2778° K). (The blocked-throat test for the lowest reservoir-pressure level is not shown in fig. 6 because of a probable leak past the solid nozzle insert.) From figure 6(a), the relative decay of reservoir pressure is observed to be essentially independent of reservoir-pressure level, with the approximate decay due to heat loss to the wall being around 15 percent and with the mass-flow loss contributing an additional 20 percent or so for the 30-msec test time. Since the blocked-throat test corresponds to a constant reservoir density, the relative decay of reservoir temperature (fig. 6(b)) due to heat loss to the wall very nearly equals that of reservoir pressure and thus is approximately 15 percent. From figure 6(b), the mass-flow loss is observed to contribute an additional 5 percent or so to the relative decay of reservoir temperature for the 30-msec test time.

The relative decay of reservoir pressure and reservoir temperature with elapsed run time for several values of reservoir temperature at zero run time is shown in figure 7. The reservoir pressure at zero run time was approximately 11 500 lb/in^2 (79.3 MN/m^2) for the four reservoir-temperature levels. From figure 7(a), the relative decay of reservoir pressure is observed to increase with increasing reservoir-temperature level. The contribution of wall heat loss to this decay increases from approximately 5 percent to 20 percent with increasing reservoir-temperature level, whereas the contribution corresponding to mass-flow loss remains nearly constant at 20 percent or so for the 30-msec test time. The trends of figure 7(a) apply to the relative decay of reservoir temperature in figure 7(b), where the magnitude of wall heat loss is very nearly the same (approximately 5 percent to 20 percent) and the mass-flow loss is somewhat less.

The relative decay of reservoir pressure, temperature, and density is shown in figure 8 for four nozzle-throat diameters. To minimize the effect of reservoir temperature on the relative decay of reservoir conditions, the results of figure 8 were selected

in such a way that the reservoir temperature at zero test time was nearly the same for all nozzle-throat diameters, being approximately 3000° R (1667° K). (See fig. 8(b).) The reservoir pressure at zero test time increased with increasing nozzle-throat diameter (see fig. 8(a)); however, on the basis of the results of figure 6, it is assumed that no significant effect of reservoir pressure exists. With the assumption that the wall heat-loss contribution for all nozzle-throat diameters is similar (the validity of this assumption is questionable, especially for the nozzle-throat diameter of 0.375 inch (9.53 mm)), the results of figure 8 show that the mass-flow contribution to the decay of reservoir conditions increases markedly with increasing nozzle-throat diameter as expected, since mass-flow rate is proportional to the square of the nozzle-throat diameter. The large relative reservoir-pressure decay, ranging from 20 percent during the 35-msec test for the 0.10-inch-diameter (2.54-mm) throat to 65 percent during the 20-msec test for the 0.375-inch-diameter (9.53-mm) throat, illustrates the importance of time correlation between the reservoir and nozzle test-section pressure measurements. The large decay of reservoir density illustrates the importance of proper choice of time increment in the data reduction method of reference 8.

Tunnel Test Time

Characteristic of impulse-type facilities are extremely short usable run times, usually not exceeding 0.15 second for hotshot tunnels employing nitrogen as the test gas. Several factors are known to affect the run time of hotshot facilities, one of the more important being diffuser configuration. For example, in reference 3 the total run time of the Langley hotshot tunnel with nitrogen was increased from approximately 0.04 to 0.12 second with the installation of a 10° total-angle cone-cylinder diffuser having a ratio of entrance area to exit area of 0.55 and a ratio of cylinder length to entrance diameter of 2. (This diffuser was also used throughout the present investigation.) Other factors possibly affecting the total run time that were varied in the present investigation are reservoir pressure, reservoir temperature, and nozzle-throat diameter.

In figure 9, variation in total run time for a wide range of reservoir pressure is shown for nozzle-throat diameters of 0.15 inch (3.81 mm) (see fig. 9(a)) and 0.10 inch (2.54 mm) (see fig. 9(b)). The values of total run time were obtained from the pressure record of the center pitot-pressure probe of the survey rake; the center line of this probe was nominally coincident with the nozzle center line. The survey rake was positioned at a nozzle axial station of 122 inches (3.10 meters). The total run time was defined as the time increment between the initial deflection of the center-rake-probe oscillograph record and the termination of usable flow (see fig. 5) and thereby included the 5- to 8-msec starting transient time. The bars in figure 9 illustrate the reservoir-pressure decay during the total run time. Although a corresponding decay of reservoir temperature also exists for both nozzle-throat diameters, this decay was essentially the same for all levels

of reservoir pressure for the respective nozzle-throat diameter. From figure 9, the total run time is observed to decrease with increasing reservoir pressure, this decrease being roughly proportional to $p_{t,1}^{-1/4}$ for both nozzle-throat diameters.

Figure 10 illustrates the variation in total run time for a wide range of reservoir temperature and for nozzle-throat diameters of 0.15 inch (3.81 mm) (see fig. 10(a)) and 0.10 inch (2.54 mm) (see fig. 10(b)). The bars denote the decay of reservoir temperature during the total run time. The corresponding decay of reservoir pressure was essentially the same for all reservoir-temperature levels for a nozzle-throat diameter of 0.10 inch (2.54 mm), but increased with increasing reservoir-temperature level for a nozzle-throat diameter of 0.15 inch (3.81 mm). This larger decay of reservoir pressure for the higher reservoir-temperature levels is expected to contribute to a somewhat shorter total run time. Then, from figure 10, the effect of reservoir temperature on total run time is considered to be essentially negligible.

Total run time as a function of nozzle-throat diameter is shown in figure 11. In this figure, the bars indicate the variation in total run time, with each bar representing several tunnel runs at somewhat different reservoir conditions. From figure 11, the total run time is observed to decrease approximately 50 percent for the present increase in nozzle-throat diameter from 0.075 to 0.375 inch (1.91 to 9.53 mm), this decrease being roughly proportional to $(d^*)^{-1/2}$. From this finding, in conjunction with the previous finding that $t' \propto p_{t,1}^{-1/4}$ and the assumption that $t' \propto T_{t,1}^{1/8}$ (which is good to within ±15 percent for the present range of $T_{t,1}$), it can be shown through the use of the ideal-gas expression

$$\dot{m} = \rho^* U^* A^* = \left[\gamma\left(\frac{2}{\gamma+1}\right)^{\frac{\gamma+1}{\gamma-1}}\right]^{1/2} \left(\frac{W}{RT_{t,1}}\right)^{1/2} p_{t,1} A^* \tag{4}$$

that $t' \propto \dot{m}^{-1/4}$.

Time Variation of Flow Conditions

As observed from figures 6 to 8, a monotonic decay in reservoir conditions occurs which, in turn, causes a decay in free-stream flow quantities with elapsed run time. In figure 12, the average-stagnation-pressure ratio and corresponding average Mach number across the inviscid core are shown as functions of elapsed run time for several nozzle-throat diameters. (Determination of $\overline{p_{t,2}}/p_{t,1}$ and $\overline{M}_\infty$ is discussed in a subsequent section.) These data correspond to the reservoir conditions of figure 8. For the three smallest nozzle-throat diameters of figure 12, the average-stagnation-pressure ratio (fig. 12(a)) and average Mach number (fig. 12(b)) are essentially invariant with elapsed run time and thereby correspond to a quasi-steady flow condition. However, for the

largest nozzle-throat diameter, the average-stagnation-pressure ratio increases and corresponding Mach number decreases with increasing elapsed run time. This variation with elapsed run time is believed to be due to the large decay of reservoir conditions which is associated with this nozzle-throat diameter ($d^* = 0.375$ in. (9.53 mm)) and which influences the nozzle boundary-layer characteristics. (The effect of reservoir pressure and temperature on average-stagnation-pressure ratio is discussed subsequently.)

Effect of Reservoir Conditions on Test-Section Flow Characteristics

Lateral profiles of stagnation-pressure ratio (survey-rake pitot pressure nondimensionalized by reservoir pressure) and corresponding inviscid-core Mach number profiles for nozzle-throat diameters of 0.15 inch (3.81 mm) and 0.10 inch (2.54 mm) are shown in figure 13 for various reservoir pressures and in figure 14 for various reservoir temperatures. For both figures, the survey rake was located at a nozzle axial station of 122 inches (3.10 meters). The inviscid core was defined as the relatively flat section of the lateral pitot-pressure profile about the nozzle center line, for which the stagnation-pressure-ratio variation is, in general, within ±10 percent of the average value. This ±10 percent variation in stagnation-pressure ratio corresponds to a ±3.2 percent variation in Mach number. The boundaries of the inviscid core, as determined from the lateral pitot-pressure profiles and represented by the plotted values of Mach number, were uncertain in many instances because of the seemingly random data scatter, nature of the lateral pitot-pressure distributions, and relatively large survey-rake probe spacing of 1 inch (2.54 cm). This uncertainty is not expected to have an appreciable influence on the magnitude or trends to be discussed subsequently, with a possible exception being the nozzle boundary-layer-thickness results.

Test repeatability, always a primary concern with impulse-type facilities, is shown in figures 13 and 14 where the different symbols denote repeat tests for a given reservoir pressure or reservoir temperature, respectively. With a few exceptions, repeatability of stagnation-pressure ratio across the inviscid core was within ±10 percent for the present range of reservoir pressure and reservoir temperature for both nozzle-throat diameters.

The average-stagnation-pressure ratio and average Mach number across the inviscid core, as obtained from the profiles of figures 13 and 14, are presented as functions of reservoir pressure and reservoir temperature in figures 15 and 16, respectively. Also shown in figures 15 and 16 are the corresponding variations of free-stream Reynolds number per foot (per meter) and free-stream Knudsen number (where the effective nozzle diameter was chosen as the characteristic flow dimension). The free-stream Knudsen number is determined with the use of the viscosity expression for the rigid-elastic-sphere model of kinetic theory (ref. 11). By solving this expression for the mean-free path and utilizing the definitions of Mach number and Reynolds number, the following relation is obtained:

$$N_{Kn,\infty} = \frac{\lambda_\infty}{d_{eff}} = \sqrt{\frac{\pi\gamma_\infty}{2}} \frac{M_\infty}{(N_{Re,\infty})_{d_{eff}}} \tag{5}$$

From figure 15(a), the average-stagnation-pressure ratio for both nozzle-throat diameters is observed to decrease with increasing reservoir pressure; figure 15(b) shows a corresponding increase in average Mach number with increasing reservoir pressure. The trend of decreasing stagnation-pressure ratio with increasing reservoir pressure and constant reservoir temperature is well substantiated by the lower Mach number helium studies of references 12 and 13, the recent higher Mach number helium results of reference 14, the air results of reference 15, and the nitrogen results of reference 16. From figure 15(c), the average free-stream Reynolds number per foot (per meter) is observed to increase with increasing reservoir pressure. (This trend is predicted by the ideal-helium relation (ref. 17)

$$N_{Re,\infty} \approx \frac{(1.028 \times 10^9) p_{t,1}}{T_{t,1}^{1.147} M_\infty^{1.706}} \tag{6}$$

where $N_{Re,\infty}$ is per foot, $p_{t,1}$ is in lb/in^2, and $T_{t,1}$ is in $^\circ$R. As is shown subsequently, $M_\infty \propto p_{t,1}^{0.129}$; thus, from equation (6), the free-stream Reynolds number varies roughly as $p_{t,1}^{0.87}$. It should be noted that equation (6) was derived by using the helium viscosity expression of reference 10 and thus is in error for conditions corresponding to free-stream static temperatures less than about 14° R (7.8° K) (see ref. 9).) From figure 15(d), the average free-stream Knudsen number decreases with increasing reservoir pressure for both nozzle-throat diameters. Since the Knudsen number is much less than 1 for the present range of conditions, intermolecular collisions dominate over collisions with the boundaries (assumed to be the effective nozzle), and the flow is in the continuum region (ref. 18).

From figure 16(a), the average-stagnation-pressure ratio for both nozzle-throat diameters is observed to increase with increasing reservoir temperature; figure 16(b) shows a corresponding decrease in average Mach number with increasing reservoir temperature. No comparison of the trends exhibited in figures 16(a) and 16(b) could be made with results of the lower Mach number helium studies (refs. 12 and 13) because of the lack of temperature variation at the lower Mach numbers. Although not stated explicitly in the nitrogen study of reference 19, the Mach number decreased and hence stagnation-pressure ratio increased as reservoir temperature increased from 2000° to 8100° R (1111° to 4500° K) for a nozzle-throat diameter of 0.15 inch (3.81 mm). However, the air results of reference 15 showed no appreciable effect of reservoir temperature from 2460° to 3750° R (1367° to 2083° K); these results (ref. 15) are in agreement with the stated

nitrogen results of reference 16 for a range of reservoir temperature from 2880° to 4320° R (1600° to 2400° K). (It should be noted, however, that one figure in reference 16 shows a trend of increasing stagnation-pressure ratio with increasing reservoir temperature, this trend becoming more pronounced as reservoir pressure decreases.) The expected decrease in average free-stream Reynolds number per foot (per meter) and increase in average free-stream Knudsen number with increasing reservoir temperature are shown in figures 16(c) and 16(d), respectively, for both nozzle-throat diameters. For the given range of reservoir temperature and for both nozzle-throat diameters, continuum flow exists.

Opposite trends were observed in figures 15 and 16 for increasing reservoir pressure at constant reservoir temperature (fig. 15) and increasing reservoir temperature at constant reservoir pressure (fig. 16). Since these increases in reservoir pressure and reservoir temperature also correspond to opposite trends in reservoir density, it may prove to be more convenient to relate the trends of figures 15 and 16 to reservoir density. For this reason, the results of figures 15 and 16 are shown in figure 17 where the average-stagnation-pressure ratio and average free-stream Mach number are plotted as functions of reservoir density for two nozzle-throat diameters. The data of figures 15 and 16 are observed to be in fair agreement for the same range of reservoir density for both nozzle-throat diameters. (An exception is the lowest-reservoir-density result for the nozzle-throat diameter of 0.10 inch (2.54 mm), which corresponds to the minimum reservoir pressure result of figure 15. For this test, the flow failed to establish during the initial attempt; hence, this result is marginal concerning proper flow establishment and thus is subject to question.)

Effect of Reservoir Conditions on Nozzle Boundary-Layer Characteristics

Before discussing the effect of reservoir conditions on nozzle boundary-layer characteristics, a comment concerning the type (turbulent or laminar) of nozzle boundary layer experienced in the present study is believed in order. As shown in the oscillograph pressure traces for helium in figure 5, the flow region encompassing survey rake probes 7 to 13 is encircled by a region characterized by relatively large and somewhat erratic pitot-pressure fluctuations. Between this region of high fluctuations and the nozzle wall exists a region of low pitot pressure having little, if any, noticeable fluctuations. Thus, it appears that the nozzle boundary layer may have a relatively thick region of laminar-like characteristics adjacent to the nozzle wall, with an outer region having turbulent-like characteristics. The existence of such a nozzle boundary layer at high Mach numbers (27 to 47) in helium has been observed previously (ref. 14). In the present study the ratio of the thickness of the laminar-like region (determined from pitot-pressure fluctuation) to the nozzle boundary-layer thickness (determined from lateral pitot-pressure survey) was in the neighborhood of 0.5 to 0.65. Thus, the nozzle boundary layer appears to be as much

laminar-like as turbulent-like, and therefore a straightforward classification of its type is not possible.

Figures 18 and 19 show the nozzle boundary-layer displacement thickness and nozzle boundary-layer thickness as functions of reservoir pressure and reservoir temperature, respectively, for two nozzle-throat diameters. The nozzle boundary-layer thickness results of figures 18(b) and 19(b) were determined from the lateral stagnation-pressure-ratio profiles of figures 13 and 14, respectively. As mentioned previously, precise determination of the nozzle boundary-layer thickness was not possible. An estimate of the uncertainty involved in determining nozzle boundary-layer thickness is indicated by the barred symbols of figures 18(b) and 19(b). From figure 18(a), the nozzle boundary-layer displacement thickness is observed to decrease with increasing reservoir pressure for both nozzle-throat diameters, as expected from figure 15(b). (An increase in Mach number with increasing reservoir pressure (fig. 15(b)) corresponds to an increase in effective nozzle expansion angle, which in turn corresponds to a decrease in nozzle boundary-layer displacement thickness.) The nozzle boundary-layer thickness for the nozzle-throat diameter of 0.15 inch (3.81 mm) (fig. 18(b)) initially decreases, then increases and becomes essentially constant with increasing reservoir pressure; for the nozzle-throat diameter of 0.10 inch (2.54 mm), the nozzle boundary-layer thickness is essentially constant over the range of reservoir pressure. From figure 19(a), the nozzle boundary-layer displacement thickness is observed to increase with increasing reservoir temperature for both nozzle-throat diameters, again as expected. The nozzle boundary-layer thickness for the nozzle-throat diameter of 0.15 inch (3.81 mm) (fig. 19(b)) is essentially constant over the range of reservoir temperature with the exception of a dip occurring in the neighborhood of 3700° R (2056° K). Within the experimental accuracy, the nozzle boundary-layer thickness for the nozzle-throat diameter of 0.10 inch (2.54 mm) is essentially constant over the range of reservoir temperature. (Since a decrease in nozzle boundary-layer thickness is generally associated with a decrease in stagnation-pressure ratio (increase in Mach number) for a given geometric-area ratio, apparent discrepancies exist between the trends observed in figures 15 and 16 and those observed in figures 18 and 19, respectively. The reason for such discrepancies is not known at this time.)

The results of figures 18 and 19 are shown in figure 20 where the nozzle boundary-layer displacement thickness and nozzle boundary-layer thickness are plotted as functions of reservoir density for two nozzle-throat diameters. The data of figures 18 and 19 are observed to be in fair agreement for the same range of reservoir density for both nozzle-throat diameters.

Nozzle Axial Gradients

As mentioned previously, the Langley hotshot tunnel employs a 10° total-divergence-angle conical nozzle. As is well recognized, although the conical nozzle does not involve the design problems and higher fabrication expense of the contoured nozzle, it has the undesirable characteristics of source flow (namely, flow angularity and nozzle axial gradients) which can create a problem in data analysis (ref. 20). Detection of flow angularity was not possible with the pitot-pressure survey rake since pitot pressure is relatively insensitive to flow angularity (the maximum deviation in pitot pressure for the present nozzle was calculated to be roughly 1.5 percent). However, nozzle axial gradients were examined by positioning the survey rake at various nozzle axial stations.

Lateral stagnation-pressure-ratio profiles and corresponding inviscid-core Mach number profiles are shown in figure 21 for various nozzle axial stations and three nozzle-throat diameters. The reservoir pressure was approximately 11 500 lb/in^2 (79.3 MN/m^2) for all three nozzle-throat diameters, and the reservoir temperature ranged from 2400° to 2800° R (1333° to 1556° K). Again, different symbols for a given nozzle-throat diameter and nozzle axial station denote repeat tests. No significant variation in flow uniformity or repeatability with nozzle axial station was observed for any of the three nozzle-throat diameters.

The values of average-stagnation-pressure ratio and average Mach number across the inviscid core, corresponding to the profiles of figure 21, are shown in figure 22 as functions of nozzle axial station; also shown are values for the ratios of average free-stream static pressure and average free-stream density. The variation of average-stagnation-pressure ratio and average Mach number with nozzle axial station is observed from figures 22(a) and 22(b), respectively, to be essentially linear for all three nozzle-throat diameters. The approximate nozzle axial gradients per inch (per cm) for the three free-stream quantities of figure 22 are as follows:

d^*, inch (mm)	$\bar{M}_\infty$ gradient		$\bar{p}_\infty/p_{t,1}$ gradient		$\bar{\rho}_\infty/\rho_{t,1}$ gradient	
	per in.	per cm	per in.	per cm	per in.	per cm
0.375 (9.53) . . .	+0.15	+0.059	-1.4×10^{-8}	-5.51×10^{-9}	-2.8×10^{-6}	-1.10×10^{-6}
0.25 (6.35)	+0.16	+0.063	-4.8×10^{-9}	-1.89×10^{-9}	-1.3×10^{-6}	-5.12×10^{-7}
0.15 (3.81)	+0.20	+0.079	-1.3×10^{-9}	-5.12×10^{-10}	-6.2×10^{-7}	-2.44×10^{-7}

(A plus sign indicates an increasing value and a minus sign indicates a decreasing value with increasing nozzle axial station.) These gradients correspond approximately to an axial variation in Mach number of 0.5 percent per inch (0.2 percent per cm), a variation in free-stream static-pressure ratio of 2 percent per inch (0.8 percent per cm), and a

variation in free-stream density ratio of 1 percent per inch (0.4 percent per cm) for all three nozzle-throat diameters. The present axial Mach number gradient is approximately 1.5 to 2 times that reported in reference 21 for a Mach number of approximately 40 in helium. The results of reference 21 were obtained in the Ames Mach 50 helium tunnel; this tunnel is equipped with a contoured nozzle and thus would be expected to have a smaller axial Mach number variation in the nozzle test section.

Axial variations of nozzle boundary-layer displacement thickness and nozzle boundary-layer thickness, corresponding to the lateral profiles of figure 21, are shown in figure 23 for three nozzle-throat diameters. The nozzle boundary-layer displacement thickness δ^* (fig. 23(a)) is observed to increase linearly approximately 1.5 to 1.75 percent per inch (0.6 to 0.7 percent per cm) with increasing nozzle axial station for all three nozzle-throat diameters. According to figure 23(a), the flow is still expanding in this section of the nozzle. For the two largest nozzle-throat diameters in figure 23(b), the nozzle boundary-layer thickness δ increases linearly with increasing nozzle axial station. (This increase results from the increase in nozzle radius with increasing nozzle axial station, since, as observed in the profiles of fig. 21, the inviscid core is essentially constant over this variation in nozzle axial station.) However, for the nozzle-throat diameter of 0.15 inch (3.81 mm), the nozzle boundary-layer thickness increases abruptly between axial stations 118 inches (3.00 meters) and 122 inches (3.10 meters). The nozzle test section is equipped with two opposed circular plate-glass windows, the leading edges of which are at an axial station of 121.5 inches (3.09 meters). These windows do not conform to the nozzle contour and thus were considered as a possible source of flow disturbance. (The magnitude of pitot-pressure fluctuations was observed to increase appreciably between axial stations 118 inches (3.00 meters) and 122 inches (3.10 meters).) Contoured window blanks conforming to the nozzle were installed and several repeat tests were performed in this range of nozzle axial station for the nozzle-throat diameter of 0.15 inch (3.81 mm). However, no discrepancies in the trend of the data in figure 23(b) were observed. A possible explanation for this increase in nozzle boundary-layer thickness between axial stations 118 and 122 inches (3.00 and 3.10 meters) is that the nozzle boundary layer may have separated from the nozzle wall in this region. (In a recent study performed in the Ames Mach 50 helium tunnel at Mach numbers from 27 to 47 (ref. 14), it was speculated that nozzle boundary-layer separation occurred around an axial station of 110 inches (2.79 meters) at some test conditions.)

Effect of Nozzle-Throat Diameter and Geometry

Average-stagnation-pressure ratio and corresponding average Mach number are shown in figure 24 as functions of geometric-area ratio. The data for geometric-area ratios less than 3×10^4 correspond to nozzle-throat diameters of 0.375, 0.25, and 0.15 inch (9.53, 6.35, and 3.81 mm) and were obtained from the lateral profiles of

figure 21; for geometric-area ratios greater than 3×10^4, the data correspond to nozzle-throat diameters of 0.10 and 0.075 inch (2.54 and 1.91 mm). The reservoir pressure was approximately 11 500 lb/in^2 (79.3 MN/m^2) and the reservoir temperature ranged from 2400^o to 2800^o R (1333^o to 1556^o K).

In figure 24(a), the average-stagnation-pressure ratio is observed to decrease by nearly a factor of 9 for the present increase in geometric-area ratio (decrease in nozzle-throat diameter). The corresponding increase in Mach number from approximately 30 to 60 with increasing geometric-area ratio is shown in figure 24(b). Also shown in figure 24(b) are the nitrogen results of reference 3 for the same range of geometric-area ratio. These nitrogen results were obtained for a range of reservoir pressure from 7000 to 11 500 lb/in^2 (48.3 to 79.3 MN/m^2) and a range of reservoir temperature from 4000^o to 4700^o R (2222^o to 2611^o K). For a given geometric-area ratio and nearly the same reservoir pressure and temperature, the Mach number for helium would be roughly 2.5 times that for nitrogen.

The present nozzle boundary-layer displacement thickness and nozzle boundary-layer thickness are shown in figure 25 as functions of geometric-area ratio; also shown are the nitrogen results of reference 3. From figure 25(a), the helium nozzle boundary-layer displacement thickness is observed to increase by a factor of approximately 2.5 for the present increase in geometric-area ratio. For the same reservoir pressure and temperature, the nozzle boundary-layer displacement thickness for helium would be roughly 1.5 to 2 times that for nitrogen. The helium nozzle boundary-layer thickness is observed from figure 25(b) to increase by a factor of approximately 2 for the present increase in geometric-area ratio. Extrapolation of this result shows that fully viscous flow would occur, for the present reservoir conditions, at a geometric-area ratio of about 1.5×10^5. This extrapolation corresponds to a Mach number of approximately 70 in figure 24(b).

The trend of nozzle boundary-layer thickness for nitrogen (ref. 3) does not conform to the present trend for helium. (See fig. 25(b).) As speculated in reference 3, the trend for nitrogen may be due to the boundary layer being turbulent at the lower values of geometric-area ratio (corresponding to lower values of Mach number and higher values of free-stream Reynolds number) and laminar at the higher values of geometric-area ratio.

To determine if any advantages could be achieved by varying the nozzle-throat geometry, two additional nozzle-throat geometries were examined. Sketch (1) of figure 26 illustrates the nozzle-throat geometry used in obtaining the previously discussed helium results for a nozzle-throat diameter of 0.15 inch (3.81 mm). The two additional nozzle-throat geometries are shown in sketches (2) and (3) of figure 26. The nozzle-throat geometry in sketch (2) was obtained by drilling out a 20^o total-entrance-angle

nozzle throat with a 0.10-inch (2.54-mm) diameter to a diameter of 0.15 inch (3.81 mm) and thereby providing a constant-area length-to-diameter ratio of 2.85. Sketch (3) shows a 50° total-entrance-angle nozzle throat having a ratio of cylinder length to diameter of 1.15. This nozzle throat was originally 0.125 inch (3.18 mm) in diameter, but was drilled out to 0.15 inch (3.81 mm). These nozzle-throat geometries were tested for a range of reservoir temperature from approximately 1500° to 6000° R (833° to 3333° K) and a reservoir pressure of approximately 9400 lb/in^2 (64.8 MN/m^2). The results at a reservoir temperature of 6000° R (3333° K) are not shown for the nozzle-throat geometry of sketch (3) because of severe throat erosion experienced during testing. (The nozzle throat with this geometry was stainless steel, whereas the two other throats, the geometries of which are shown in sketches (1) and (2), were copper-filled sintered tungsten.) As observed from figure 26, no significant effect of nozzle-throat geometry on average-stagnation-pressure ratio, or corresponding average free-stream Mach number, occurred for the three test geometries.

Nozzle Wall Pressure

During several of the helium tests, nozzle wall pressures in the nozzle test section were measured. In figure 27, nozzle-wall-pressure ratios are shown as functions of average free-stream Mach number. These results correspond to a reservoir pressure of approximately 11 500 lb/in^2 (79.3 MN/m^2), reservoir-temperature range of 2400° to 2800° R (1333° to 1556° K), and nozzle-throat diameters of 0.375, 0.25, and 0.15 inch (9.53, 6.35, and 3.81 mm). The nozzle wall pressure was measured at an axial station of 121.5 inches (3.09 meters) and the pitot-pressure survey rake was positioned at a station of 122 inches (3.10 meters); hence, the calculated average free-stream static pressure used to nondimensionalize the measured nozzle wall pressure (fig. 27(b)) corresponds to essentially the same nozzle axial station as the wall pressure. No nozzle wall pressures were measured with the rake and support system removed from the tunnel; thus, the effect of the rake and strut on the wall pressures is not known.

The bars of figure 27 represent the uncertainty of the nozzle-wall-pressure measurements. From figure 27(b), the nozzle-wall-pressure ratio is observed to increase with increasing Mach number, with the wall pressure being three to four times the average free-stream static pressure at a Mach number of approximately 30 and six to 11 times the average free-stream static pressure at a Mach number of approximately 50. Nozzle wall pressures greater than the calculated average free-stream static pressure were also observed in the Mach 27 to 47 helium study of reference 14. The present results and those of reference 14 indicate that the commonly made assumption of constant static pressure through the boundary layer is subject to question at these high Mach numbers. In general, the nozzle wall pressure remained essentially constant or increased somewhat with increasing axial station from 112.5 to 124.5 inches (2.86 to 3.16 meters) for the

present tests. A rise in nozzle wall pressure with increasing nozzle axial station was observed in reference 14 and was attributed to nozzle boundary-layer separation.

Test Region

Figure 28 presents the test experience in terms of Mach number and free-stream Reynolds number in the Langley hotshot tunnel with helium. The shaded test region results from variations in reservoir pressure from 3000 to 28 000 lb/in^2 (20.7 to 193.0 MN/m^2), in $T_{t,1}$ from 1500° to 11 000° R (833° to 6111° K), and in $(A/A^*)_{geo}$ from 3×10^3 to 8×10^4 and corresponds to theoretically uncondensed flow. Also shown in figure 28 is a trajectory for earth entry at 50 000 ft/sec (15.2 km/sec) of a vehicle having a lift-drag ratio of 1.0 and an arbitrarily chosen length L of 30 feet (9.1 meters). (The value of L used to determine the present helium value of $(N_{Re,\infty})_L$ was 1 foot (0.305 meter).) The range of M_∞ for helium is approximately 30 to 70; this range in conjunction with the Mach number range for nitrogen in references 3 and 19 results in a range of M_∞ for the two gases of approximately 10 to 70. This range is believed to be the most extensive variation in M_∞ ever reported from a single facility. (However, it should be noted that aerodynamic testing of models at the highest values of M_∞ in helium and nitrogen is, in all probability, not feasible because of the existence of extremely thick boundary layers at these high Mach numbers.) It appears that helium testing in hotshot tunnels with even smaller values of $(A/A^*)_{geo}$ than those of the present study would cover a substantial portion of the earth entry corridor for return from planetary exploration in terms of the simulation parameters M_∞ and $(N_{Re,\infty})_L$. Thus, the hotshot tunnel provides a convenient, relatively inexpensive means of generating a substantial portion of the earth entry corridor without requiring modification of existing hardware.

Comparison of Existing Empirical Methods for Predicting Nozzle Boundary-Layer Displacement Thickness

Over the past decade, the empirical relations of references 22 and 23 for predicting hypersonic nozzle boundary-layer displacement thickness have received considerable usage. These relations were obtained from conical and contoured nozzle data for Mach numbers of 6 to 16 in air. A recent study showed that extrapolation of the empirical relations of references 22 and 23 to Mach numbers greater than those from which they were obtained resulted in overestimation of the nozzle boundary-layer displacement thickness (ref. 24). An empirical relation employing the same parameters used in references 22 and 23 (free-stream Mach number and free-stream Reynolds number based on nozzle axial station) was derived by Jack D. Whitfield of Arnold Engineering Development Center (and presented by Edenfield in ref. 24) from higher Mach number data so as to more accurately predict the nozzle boundary-layer displacement thickness for Mach numbers from

approximately 12 to 19. The following table presents the empirical relations from references 22 to 24 (in the present notation) for predicting turbulent nozzle boundary-layer displacement thickness and the conditions for which they were obtained:

Source	Relation	Gas	Range of M_∞	Range of $(N_{Re,\infty})_x$	Nozzle
Burke (ref. 22)	$\frac{\delta^*}{x} = 0.0463 \frac{M_\infty^{1.311}}{(N_{Re,\infty})_x^{0.276}}$	Air	8 to 16	10^5 to 10^7	Conical and contoured
Whitfield (as presented in ref. 24)	$\frac{\delta^*}{x} = 0.22 \frac{M_\infty^{0.5}}{(N_{Re,\infty})_x^{0.25}}$	Nitrogen	12 to 19	10^6 to 10^8	Conical
Lee (ref. 23)	$\frac{\delta^*}{x} = 0.0064 \frac{M_\infty^{1.25}}{(N_{Re,\infty})_x^{0.14}}$	Air	6 to 13	10^6 to 10^7	Conical and contoured

Predictions, as applied to the present range of reservoir pressure for nozzle-throat diameters of 0.15 and 0.10 inch (3.81 and 2.54 mm), are shown in figure 29. The symbols in figure 29 represent average values of the data presented in figure 18(a). The relations of Burke and Lee overpredict the present data by a factor of about 2, and Lee's relation fails to predict the trend of decreasing nozzle boundary-layer displacement thickness with increasing reservoir pressure for a nozzle-throat diameter of 0.15 inch (3.81 mm); both relations fail to predict the trend for a nozzle-throat diameter of 0.10 inch (2.54 mm). Although the empirical prediction of Whitfield underestimates the magnitude of the present data for a nozzle-throat diameter of 0.15 inch (3.81 mm) by approximately one-third, it predicts the trend with surprising accuracy. (It is interesting to note that for hypersonic flow over a flat plate, the displacement thickness in air is about three-fifths that in helium for the same value of Mach number and Reynolds number (ref. 25). This air-helium simulation factor (3/5) is surprisingly close to the relationship of Whitfield's prediction to the present data (2/3). Although this agreement is probably fortuitous, it may imply that the relation of Whitfield will provide reasonably accurate predictions of nozzle boundary-layer displacement thickness in nitrogen (or air) at Mach numbers in excess of 19 or so.) Thus, the constant of Whitfield's relation (0.22) was modified (changed to 0.37) to bring the prediction into agreement with the present data for a nozzle-throat diameter of 0.15 inch (3.81 mm). To account for the difference between the free-stream specific heat

ratio of the present study $(\gamma_\infty = 5/3)$ and that of Whitfield $(\gamma_\infty = 7/5)$, the constants were assumed to be functions of γ_∞ only. Also, a third constant, corresponding to a value for γ_∞ of 1.21, has been obtained recently by James L. Hunt at the Langley Research Center in the pilot model hypersonic CF_4 blowdown tunnel at a free-stream Mach number of 6.13 and free-stream Reynolds number, based on nozzle axial distance, of 5.75×10^5. The three constants were plotted as functions of γ_∞, and a simple, second-order polynomial curve fit was applied. The resulting expression is

$$\frac{\delta^*}{x} = \left(1.07\gamma_\infty{}^2 - 2.73\gamma_\infty + 1.945\right)\frac{M_\infty{}^{1/2}}{\left(N_{Re,\infty}\right)_x^{1/4}} \tag{7}$$

for $1.21 < \gamma_\infty < 1.67$. Discretion should be used in applying this equation at conditions other than those for which the three constants just discussed were obtained. As shown in figure 29(a), equation (7) predicts the nozzle boundary-layer displacement thickness for the present range of reservoir pressure, as expected; however, for a nozzle-throat diameter of 0.10 inch (2.54 mm) (fig. 29(b)), the prediction of equation (7) is somewhat less satisfactory at the lower values of reservoir pressure.

The nozzle boundary-layer displacement-thickness results for the present range of reservoir temperature are shown in figure 30 for nozzle-throat diameters of 0.15 inch (3.81 mm) (see fig. 30(a)) and 0.10 inch (2.54 mm) (see fig. 30(b)). The symbols in figure 30 represent average values of the data in figure 19(a). The predictions of Burke (ref. 22) and Lee (ref. 23) are again shown to yield values about twice those of the present data. Equation (7), which represents a modification of Whitfield's expression as presented in reference 24, provides a reasonable prediction of the nozzle boundary-layer displacement thickness over the present reservoir-temperature range for both nozzle-throat diameters.

Figure 31, where nozzle boundary-layer displacement thickness is plotted as a function of geometric-area ratio, is a repeat of the helium results of figure 25(a) along with the prediction of equation (7). For geometric-area ratios less than 3×10^4, equation (7) provides a reasonably good estimate of the displacement thickness; however, for geometric-area ratios greater than 3×10^4, the prediction of equation (7) becomes somewhat poorer.

Correlation of Nozzle Boundary-Layer Thickness and Displacement Thickness

In reference 22, results for hypersonic nozzle boundary-layer displacement thickness were correlated in terms of Reynolds number evaluated at a reference enthalpy for a Mach number range of approximately 8 to 16 and a range of free-stream Reynolds number, based on nozzle axial distance from nozzle apex, of 1.5×10^5 to 8×10^6 in air. In the more recent study of reference 24, a similar correlation is presented for a Mach

number range of 5 to 22 and an approximate range of free-stream Reynolds number, based on nozzle axial distance, of 1×10^5 to 1×10^8. In reference 24, which includes nitrogen and air results, the nozzle boundary-layer displacement thickness was correlated to within ±20 percent.

By following the example of references 22 and 24, a similar correlation was tried with the present results; all the nozzle boundary-layer displacement-thickness data obtained in the present helium study, as well as those obtained in the Mach 27 to 47 helium study of reference 14, are shown in figure 32(a) as functions of Reynolds number based on a reference temperature. This reference Reynolds number is defined as

$$\left(N_{Re,ref}\right)_x = \frac{\rho_{ref} U_\infty x}{\mu_{ref}} \tag{8}$$

where the density ρ_{ref} and viscosity μ_{ref} are evaluated at the reference temperature. The reference enthalpy used in reference 24 is given by Eckert's expression (ref. 26)

$$h_{ref} = 0.5\left(h_w + h_\infty\right) + 0.22\left(h_{aw} - h_\infty\right) \tag{9}$$

The adiabatic-wall enthalpy is

$$h_{aw} = h_\infty + r_c \frac{U_\infty^2}{2} \tag{10}$$

where r_c is the recovery factor. Since the pressure level corresponding to the nozzle wall and reference conditions is on the order of the free-stream pressure (which ranged from approximately 10^{-4} to 10^{-2} lb/in^2 (0.69 to 69 N/m^2) in the present study), ideal-helium behavior can be assumed at these conditions (that is, $h_{ref} = c_{p,ref} T_{ref}$, $h_w = c_{p,w} T_w$, and $h_\infty = c_{p,\infty} T_\infty$). Also, since the specific heat is essentially constant for a monatomic gas, $c_{p,ref} = c_{p,w} = c_{p,\infty} = \frac{\gamma}{\gamma - 1} \frac{R}{W}$. Thus, equation (9) becomes

$$T_{ref} = 0.5\left(T_w + T_\infty\right) + 0.22 r_c \frac{\gamma - 1}{2\gamma} \frac{W}{R} U_\infty^2 \tag{11}$$

If the nozzle boundary layer is assumed to be turbulent, the recovery factor can be approximated by

$$r_c \approx N_{Pr,ref}^{1/3} \tag{12}$$

By using the relation

$$U_\infty^2 = \gamma \frac{R}{W} T_\infty M_\infty^2 \tag{13}$$

equation (11) can be expressed as

$$T_{ref} = \frac{T_w}{2} + T_\infty\left[0.5 + 0.11N_{Pr,ref}^{1/3}(\gamma - 1)M_\infty^2\right] \tag{14}$$

Since the Prandtl number $N_{Pr,ref}$ is a function of the reference temperature, it was set equal to unity in order to approximate the present range of reference temperature. For the present tests, the reference temperature varied from roughly 550° to 1800° R (306° to 1000° K). Over this temperature range, the Prandtl number is essentially constant and equal to 0.69 (ref. 27), thereby corresponding to a recovery factor of 0.884. The nozzle wall temperature T_w is assumed ambient (532° R (296° K)), and the ratio of specific heats γ is 5/3 for helium. Hence the present reference temperature is a function only of free-stream static temperature T_∞ and free-stream Mach number.

The reference density ρ_{ref} is evaluated from the ideal-gas equation of state

$$\rho_{ref} = \frac{Wp_\infty}{RT_{ref}} \tag{15}$$

and the reference viscosity is determined from the empirical helium expression of reference 10

$$\mu = 5.023T^{0.647} \times 10^{-6} \tag{16a}$$

where μ is in poises and T is in $^\circ$K. With μ in slugs/ft-sec and T in $^\circ$R, this equation (for reference viscosity) would be

$$\mu_{ref} = 7.173T_{ref}^{0.647} \times 10^{-9} \tag{16b}$$

Equation (8) then becomes

$$\left(N_{Re,ref}\right)_x = \left(2.324 \times 10^8\right)\frac{p_\infty M_\infty T_\infty^{1/2} x}{T_{ref}^{1.647}} \tag{17}$$

where p_∞ is in lb/in^2, T_∞ and T_{ref} are in $^\circ$R, and x is in feet.

From figure 32(a), the nozzle boundary-layer displacement-thickness results of the present study and those of reference 14 are observed to correlate in terms of reference Reynolds number and are predicted to within ±20 percent by the relation

$$\frac{\delta^*}{x} = 0.3\left(N_{Re,ref}\right)_x^{-0.257} \tag{18}$$

The nozzle boundary-layer thickness data of the present study and those of reference 14 are shown in figure 32(b) in terms of the reference Reynolds number. As in figure 32(a), the present data encompass the entire range of reservoir conditions and geometric-area ratio of the present study. From figure 32(b), the nozzle boundary-layer

thickness is observed to correlate in terms of reference Reynolds number and can be predicted to within ±20 percent by the relation

$$\frac{\delta}{x} = 0.284\left(N_{Re,ref}\right)_x^{-0.197} \tag{19}$$

Thus,

$$\frac{\delta^*}{\delta} = 1.056\left(N_{Re,ref}\right)_x^{-0.06} \tag{20}$$

and for the present investigation, $0.57 \leqq \frac{\delta^*}{\delta} \leqq 0.70$.

In figure 33, the nozzle boundary-layer displacement thickness is shown plotted against a function involving the three primary variables of this study (reservoir pressure, reservoir temperature, and geometric-area ratio). Figure 33 shows that all the displacement-thickness data of this investigation can be correlated in terms of this function and predicted to within approximately 5 percent by the expression

$$\frac{\delta^*}{x} = \left(5.423 \times 10^{-3}\right) T_{t,1}^{0.170} \left(\frac{A}{A^*}\right)_{geo}^{0.248} p_{t,1}^{-0.203} \tag{21}$$

where $p_{t,1}$ is in lb/in^2 and $T_{t,1}$ is in ^oR. Unlike equations (7) and (18), equation (21) provides a means of estimating the nozzle boundary-layer displacement thickness without knowledge of free-stream flow conditions. The results of reference 14, which were obtained with a contoured nozzle and different reservoir conditions, are also shown in figure 33. Although the results of reference 14 correlate in terms of this function, they are approximately 1.2 to 1.4 times the values given by equation (21). Changing the constant in equation (21) from 5.423×10^{-3} to 6.38×10^{-3} yields an expression that predicts the displacement-thickness results of both the present study and reference 14 to within ±20 percent, which is the same uncertainty associated with usage of equation (18).

Since equation (21) is dimensional (dependent on the system of units employed), an attempt was made to formulate a nondimensional expression for nozzle boundary-layer displacement thickness independent of free-stream conditions. From equation (21), it is observed that $\frac{\delta^*}{x} \propto \rho_{t,1}^{-b}$, where the power b is between 0.170 and 0.203. At the nozzle throat, the fact that $U^* = a^*$ infers that $U^* \propto \left(T^*\right)^{1/2}$. For helium, $\mu^* \propto \left(T^*\right)^c$ where c is about 1/2. Thus, the unit nozzle-throat Reynolds number is roughly proportional to ρ^* or $\rho_{t,1}$ (because the T^* dependence on U^* and μ^* approximately cancels), and therefore the displacement thickness might be expressed as a function of nozzle-throat Reynolds number and geometric-area ratio. The present displacement-thickness results were plotted against such a function and observed to correlate and be predicted to within roughly ±5 percent by the nondimensional expression

$$\frac{\delta^*}{x} = \left(3.72 \times 10^{-2}\right)\left(\frac{A}{A^*}\right)_{geo}^{0.187}\left(N_{Re}{}^*\right)_{d^*}^{-0.126} \tag{22}$$

Semiempirical Prediction of Free-Stream and Postnormal-Shock Flow Conditions

When performing a helium test in the Langley hotshot tunnel, estimations of the nozzle test-section flow conditions, corresponding to given reservoir conditions and nozzle geometry, have been possible only if previous tests have been performed at similar conditions. (In determining nozzle test-section before-shock and postnormal-shock flow conditions, at least one nozzle flow quantity must be known in conjunction with the reservoir conditions.) Thus, simple expressions allowing prior determination of nozzle flow quantities as functions only of reservoir conditions $\left(p_{t,1}\right.$ and $\left.T_{t,1}\right)$ and nozzle geometry (d^*, x, and θ) could be quite useful.

To derive such expressions, the Mach number results of this study were plotted against a function involving reservoir pressure, reservoir temperature, and geometric-area ratio, as shown in figure 34. Also shown in figure 34 are the results of reference 14. The Mach number can be correlated in terms of such a function, and both the present Mach number data and the Mach number data of reference 14 can be predicted to within approximately 6 percent by the expression

$$M_\infty = 4.34 p_{t,1}{}^{0.129}\left(\frac{A}{A^*}\right)_{geo}^{0.209} T_{t,1}{}^{-0.109} \tag{23}$$

where $p_{t,1}$ is in lb/in^2 and $T_{t,1}$ is in $^\circ R$ and where, of course, for a conical nozzle

$$\left(\frac{A}{A^*}\right)_{geo} = \left(\frac{2x \tan \theta}{d^*}\right)^2$$

Equation (23) thus provides a means of determining a nozzle flow quantity (Mach number) in terms of reservoir conditions and nozzle geometry.

To account for real-helium effects, the expressions presented in the appendix of reference 8 are used. The real-helium correction factors (ratio of real-helium value of a particular flow parameter to its ideal-helium value) of reference 8, as required in this study, are given by

$$C_2 \equiv \frac{p_\infty/p_{t,1}}{\left(p_\infty/p_{t,1}\right)_i} = 1 + p_{t,1}\left(\frac{1.454}{T_{t,1}{}^{1.364}} - \frac{1.380 \times 10^3}{T_{t,1}{}^{2.823}}\right) \tag{24a}$$

and

$$C_3 \equiv \frac{T_\infty/T_{t,1}}{(T_\infty/T_{t,1})_i} = 1 + p_{t,1}\left(\frac{0.790}{T_{t,1}^{1.363}} - \frac{2.431 \times 10^1}{T_{t,1}^{2.129}}\right) \tag{24b}$$

where, in conformity with the system of units of reference 8, $p_{t,1}$ is in atm and $T_{t,1}$ is in ^oK. Likewise, an additional correction factor may be given by

$$C_4 \equiv \frac{A^*/A}{(A^*/A)_i} = 1 + p_{t,1}\left(\frac{1.730}{T_{t,1}^{1.378}} - \frac{5.397 \times 10^2}{T_{t,1}^{2.603}}\right) \tag{24c}$$

The correction factors C_2 and C_3 are accurate to within 0.2 percent for Mach numbers above 20. The correction factor C_4, although not presented in reference 8, was obtained at the same time and has an uncertainty of approximately 0.5 percent for reservoir temperatures above 900^o R (500^o K) and Mach numbers above 20. For ideal helium, $C_2 = C_3 = C_4 = 1$. The desired real-helium relations, in terms of reservoir pressure, reservoir temperature, and Mach number, for various free-stream quantities are then

$$p_\infty = \frac{15.5885 p_{t,1} C_2}{(M_\infty^2 + 3)^{2.5}} \quad , \text{atm} \tag{25}$$

$$T_\infty = \frac{3 T_{t,1} C_3}{M_\infty^2 + 3} \quad , {}^oK \tag{26}$$

$$a_\infty = \left[\gamma\left(\frac{R}{W} \times 10^7\right) T_\infty\right]^{1/2} \quad , \text{cm/sec} \tag{27}$$

$$U_\infty = a_\infty M_\infty \quad , \text{cm/sec} \tag{28}$$

$$q_\infty = 0.833 p_\infty M_\infty^2 \quad , \text{atm} \tag{29}$$

and

$$\left(\frac{A^*}{A}\right)_{eff} = \frac{16 M_\infty C_4}{(M_\infty^2 + 3)^2} \tag{30}$$

where R is taken to be 8.3143 joules/mole-^oK and $W = 4.003$ g/mole. With the assumption of ideal-helium behavior in the free stream, the free-stream density in g/cm^3 is given by

$$\rho_\infty = \frac{W p_\infty}{R T_\infty} \tag{31}$$

where R is taken to be 82.0597 $\frac{\text{atm-cm}^3}{\text{mole-}^\circ\text{K}}$. From reference 9, the free-stream coefficient of viscosity is given by the set of relations

$3.6^\circ \leqq T_\infty \leqq 10^\circ$ K $\qquad \mu_\infty = \left(-1.5691 + 3.4167T_\infty - 0.10317T_\infty{}^2\right) \times 10^{-6}$ (32a)

$1.2^\circ < T_\infty < 3.6^\circ$ K $\qquad \mu_\infty = \left(5.0200 - 3.2241T_\infty + 2.0308T_\infty{}^2 - 0.22351T_\infty{}^3\right) \times 10^{-6}$ (32b)

$0.2^\circ \leqq T_\infty \leqq 1.2^\circ$ K $\qquad \mu_\infty = \left(2.1630 - 26.665T_\infty + 120.54T_\infty{}^2 - 187.4T_\infty{}^3 + 126.82T_\infty{}^4 - 31.823T_\infty{}^5\right) \times 10^{-6}$ (32c)

where μ_∞ is in poises for T_∞ in $^\circ$K. (For free-stream temperatures greater than 10° K, eq. (16a) is used to obtain values of free-stream viscosity.) Then the free-stream Reynolds number per foot is given by

$$N_{Re,\infty} = \left(8.748 \times 10^3\right) \frac{M_\infty p_\infty}{T_\infty{}^{1/2} \mu_\infty} \tag{33}$$

where p_∞ is in atm, T_∞ is in $^\circ$K, and μ_∞ is in poises. Since the correction factors for p_2/p_∞, ρ_2/ρ_∞, T_2/T_∞, and $p_{t,2}/p_\infty$ are within 0.05 percent of unity for Mach numbers greater than 20 (ref. 8), the postnormal-shock conditions may be found from the ideal-helium expressions (see ref. 17)

$$p_2 = \frac{5}{4} p_\infty M_\infty{}^2 \quad \text{, atm} \tag{34}$$

$$\rho_2 = \frac{4\rho_\infty M_\infty{}^2}{M_\infty{}^2 + 3} \quad \text{, g/cm}^3 \tag{35}$$

and

$$p_{t,2} = 1.469 p_\infty M_\infty{}^2 \quad \text{, atm} \tag{36}$$

Equation (23) predicts the Mach number with an uncertainty of 6 percent. Corresponding uncertainties in free-stream quantities calculated by using equations (25) to (33) are given in the previously discussed section "Data Reduction and Accuracy."

Surface Pressure Distribution on Spherically Blunted Cone

A nozzle-throat diameter of 0.10 inch (2.54 mm) was used in a test made on a 25° half-angle spherically blunted cone, having a ratio of nose radius to base radius (which was 1.5 inch (3.81 cm)) of 0.10, at zero angle of attack. The primary purpose of this test

was to determine whether flow would establish about the model and, if so, to evaluate the present schlieren system at these conditions. From the pressure records corresponding to the various pressure orifices on the model surface, the flow appeared to establish about the model, although the density level was too low to provide significant resolution on the photographs obtained by using this schlieren system. The resulting pressure distribution, with the surface pressure p nondimensionalized by the model stagnation pressure $(p)_{S=0}$, is shown in figure 35. The present experimental results are observed to be in reasonable agreement with the inviscid prediction of reference 28, as well as the Mach 20 nitrogen results of reference 4.

CONCLUDING REMARKS

An exploratory study to generate extremely high Mach number helium flow in the Langley hotshot tunnel has been performed. Variations in reservoir pressure from 3000 to 28 000 lb/in^2 (20.7 to 193.0 MN/m^2), in reservoir temperature from 1500° to 11 000° R (833° to 6111° K), and in geometric-area ratio from 3×10^3 to 8×10^4 resulted in a range of Mach numbers from 30 to 70. The tunnel starting transient time was similar to that obtained with nitrogen as the test gas; however, the total run time in helium was approximately one-third that in nitrogen. A marked effect of variation of reservoir pressure and temperature on Mach number was observed for a given nozzle geometric-area ratio, with the Mach number increasing with increasing reservoir pressure and decreasing reservoir temperature. The conical nozzle produced an axial variation in Mach number of 0.5 percent per inch (0.2 percent per cm). The nozzle boundary-layer thickness (as determined from pitot-pressure profiles) and displacement thickness were correlated to within ±20 percent by using Reynolds number evaluated at a reference temperature, and an existing empirical method for predicting nozzle boundary-layer displacement thickness in nitrogen was modified and extended to the Mach 30 to 60 region in helium. Semiempirical relations for predicting free-stream and postnormal-shock conditions, when only reservoir conditions and nozzle geometry are known, are presented. This study indicates that hotshot tunnels provide a convenient, relatively inexpensive means of generating helium flow conditions covering a substantial portion of the earth entry corridor for return from planetary exploration (in terms of simulation parameters – that is, Mach number and free-stream Reynolds number) without requiring modification of existing hardware.

Langley Research Center,
National Aeronautics and Space Administration,
Hampton, Va., April 24, 1970.

APPENDIX

CONVERSION OF U.S. CUSTOMARY UNITS TO SI UNITS

The International System of Units (SI) was adopted by the Eleventh General Conference on Weights and Measures held in Paris in 1960 (ref. 1). Conversion factors for units used herein are given in the following table:

Physical quantity	U.S. Customary Unit	Conversion factor (*)	SI Unit (**)
Length or distance . .	in.	0.0254	meters (m)
	ft	0.3048	
Pressure	lbf/in^2	6895	newtons per sq meter (N/m^2)
	atm	101 325	
Temperature	^oR	5/9	degrees Kelvin (^oK)
Density	$slugs/ft^3$	515.379	kilograms per cubic meter (kg/m^3)
Viscosity	poises	0.100	newton-second per sq meter ($N\text{-}sec/m^2$)
	slugs/ft-sec	47.880258	
Volume	in^3	1.6387064×10^{-5}	cubic meters (m^3)
Energy	Btu	1055.87	joules (J)

*Multiply value given in U.S. Customary Unit by conversion factor to obtain equivalent value in SI unit.

**Prefixes to indicate multiple of units are as follows:

Prefix	Multiple
kilo (k)	10^3
mega (M)	10^6
centi (c)	10^{-2}
milli (m)	10^{-3}
micro (μ)	10^{-6}

REFERENCES

1. Mechtly, E. A.: The International System of Units – Physical Constants and Conversion Factors. NASA SP-7012, 1964.

2. Smith, Fred M.; Harrison, Edwin F.; and Lawing, Pierce L.: Description and Initial Calibration of the Langley Hotshot Tunnel With Some Real-Gas Charts for Nitrogen. NASA TN D-2023, 1963.

3. Miller, Charles G., III; Creel, Theodore R., Jr.; and Smith, Fred M.: Calibration Experience in the Langley Hotshot Tunnel for Mach Numbers From 12 to 26. NASA TN D-3278, 1966.

4. Harris, Julius E.: Aerodynamic Characteristics of a Spherically Blunted 25° Cone at a Mach Number of 20. NASA TN D-4098, 1967.

5. Smotherman, W. E.: A Miniature Wafer-Style Pressure Transducer. AEDC-TR-60-11, U.S. Air Force, Oct. 1960.

6. Miller, Charles G., III: An Experimental Investigation of Support Interference on a Blunt Body of Revolution at a Mach Number of Approximately 20. NASA TN D-2742, 1965.

7. Henderson, Arthur, Jr.; and Swalley, Frank E.: Effects of Air Contamination in a Helium Tunnel. NASA TN D-406, 1960.

8. Miller, Charles G., III; and Wilder, Sue E.: Real-Helium Hypersonic Flow Parameters for Pressures to 3600 Atmospheres and Temperatures to 15 000° K. NASA TN D-4869, 1968.

9. Maddalon, Dal V.; and Jackson, Willis E.: A Survey of the Transport Properties of Helium at High Mach Number Wind-Tunnel Conditions. NASA TM X-2020, 1970.

10. Keesom, W. H.: Helium. Elsevier, 1942.

11. Present, R. D.: Kinetic Theory of Gases. McGraw-Hill Book Co., Inc., 1958, p. 222.

12. Orlik-Rückemann, K. J.; and LaBerge, J. G.: NAE Helium Hypersonic Wind Tunnel. Nat. Res. Counc. Can. Quart. Bull., no. 3, 1965, pp. 1-31.

13. Wagner, Richard D., Jr.; and Watson, Ralph: Reynolds Number Effects on the Induced Pressures of Cylindrical Bodies With Different Nose Shapes and Nose Drag Coefficients in Helium at a Mach Number of 24. NASA TR R-182, 1963.

14. Kemp, Joseph H., Jr.; and Sreekanth, A. K.: Preliminary Results From an Experimental Investigation of Nozzle Wall Boundary Layers at Mach Numbers Ranging From 27 to 47. AIAA Pap. No. 69-686, June 1969.

15. Clark, Louis E.: Description and Initial Calibration of the Langley 12-Inch Hypersonic Ceramic-Heated Tunnel. NASA TN D-2703, 1965.

16. Vas, I. E.; and Koppenwallner, G.: The Princeton University High Pressure Hypersonic Nitrogen Tunnel N-3. AFOSR 64-1422, U.S. Air Force, July 1964.

17. Mueller, James N.: Equations, Tables, and Figures for Use in the Analysis of Helium Flow at Supersonic and Hypersonic Speeds. NACA TN 4063, 1957.

18. Liepmann, H. W.; and Roshko, A.: Elements of Gasdynamics. John Wiley & Sons, Inc., c.1957.

19. Miller, Charles G., III: Experimental Base Pressures on 9^{o} Spherically Blunted Cones at Mach Numbers From 10.5 to 20. NASA TN D-4800, 1968.

20. Henderson, Arthur, Jr.; Watson, Ralph D.; and Wagner, Richard D., Jr.: Fluid Dynamic Studies at $M = 41$ in Helium. AIAA J., vol. 4, no. 12, Dec. 1966, pp. 2117-2124.

21. Horstman, C. C.; and Kussoy, M. I.: Hypersonic Viscous Interaction on Slender Cones. AIAA J., vol. 6, no. 12, Dec. 1968, pp. 2364-2371.

22. Burke, Andrew F.: Turbulent Boundary Layers on Highly Cooled Surfaces at High Mach Numbers. Proceedings of Symposium on Aerothermoelasticity, ASD Tech. Rep. 61-645, U.S. Air Force, 1961, pp. 704-741.

23. Lee, John D.: Axisymmetric Nozzles for Hypersonic Flows. Rep. No. TN(ALOSU)459-1 (WADC TN 59-228), Ohio State Univ. Res. Found., June 1959.

24. Edenfield, E. E.: Contoured Nozzle Design and Evaluation for Hotshot Wind Tunnels. AIAA Pap. No. 68-369, Apr. 1968.

25. Love, Eugene S.; Henderson, Arthur, Jr.; and Bertram, Mitchel H.: Some Aspects of Air-Helium Simulation and Hypersonic Approximations. NASA TN D-49, 1959.

26. Eckert, E. R. G.: Engineering Relations for Friction and Heat Transfer to Surfaces in High Velocity Flow. J. Aeronaut. Sci. (Readers' Forum), vol. 22, no. 8, Aug. 1955, pp. 585-587.

27. Wilson, M. P., Jr.: Thermodynamic and Transport Properties of Helium. MGCR-PR-60-1550, Gen. Dyn./Elec. Boat, Jan. 1960.

28. Lomax, Harvard; and Inouye, Mamoru: Numerical Analysis of Flow Properties About Blunt Bodies Moving at Supersonic Speeds in an Equilibrium Gas. NASA TR R-204, 1964.

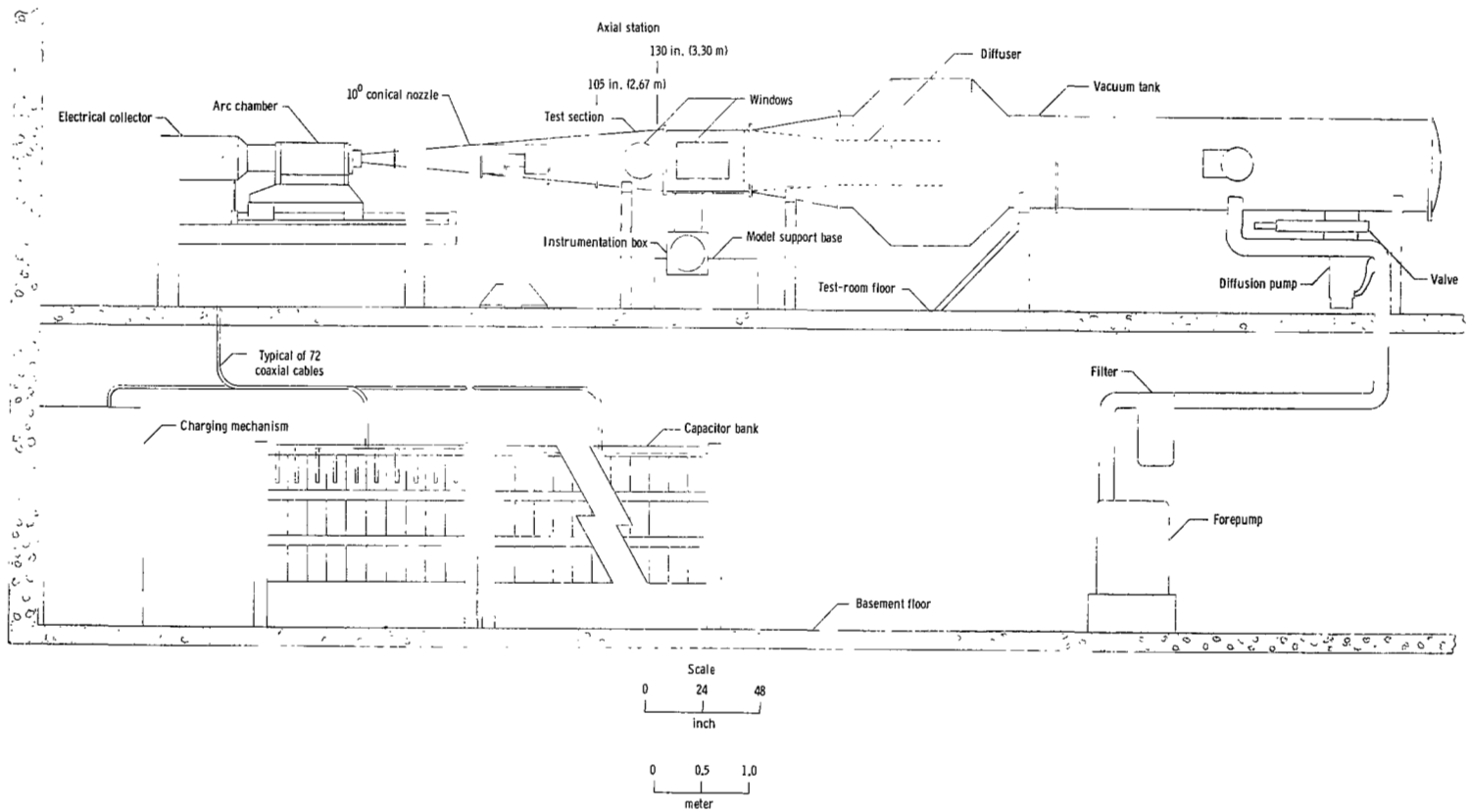

Figure 1.- Sketch of Langley hotshot tunnel.

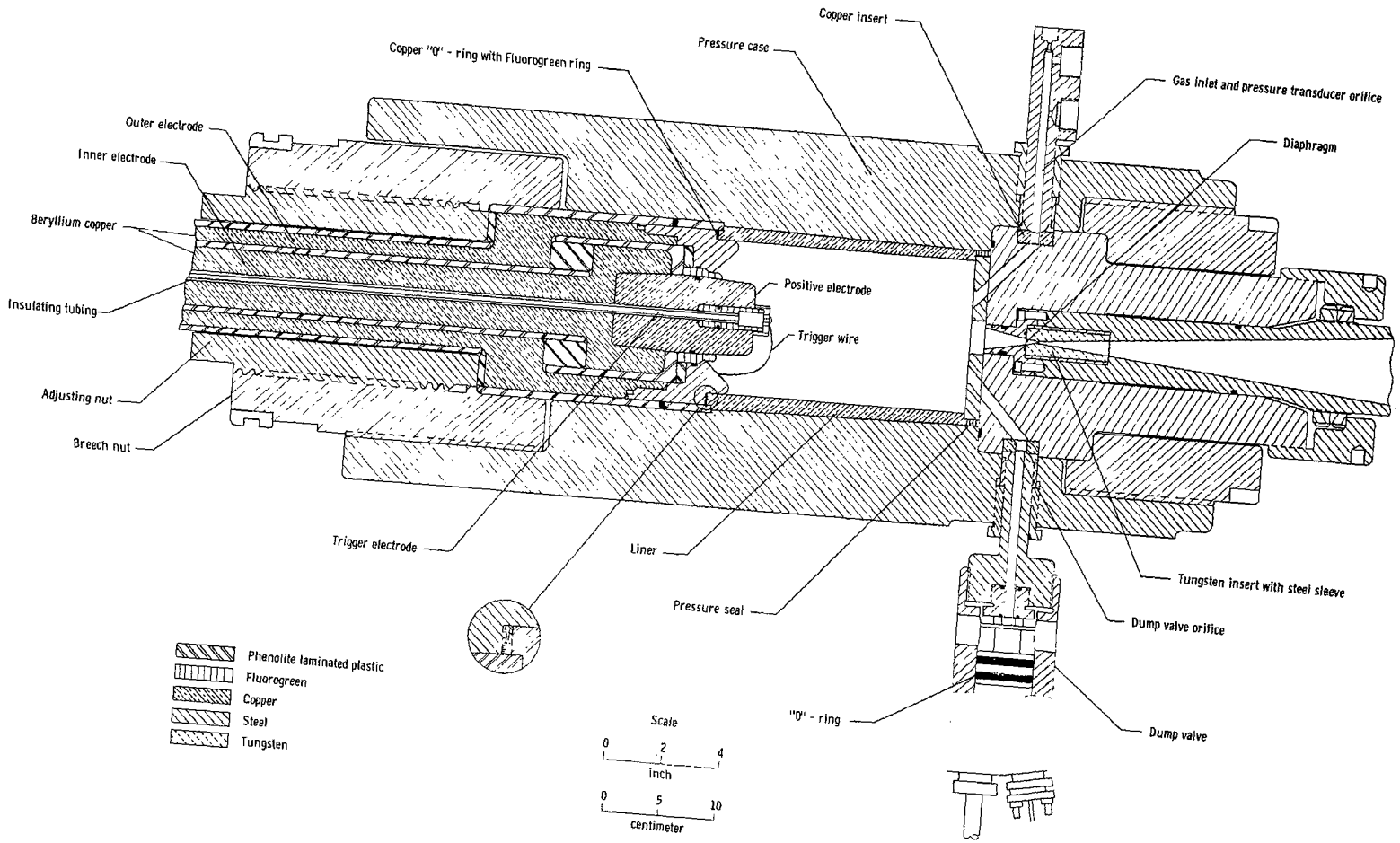

Figure 2.- Arc chamber for Langley hotshot tunnel.

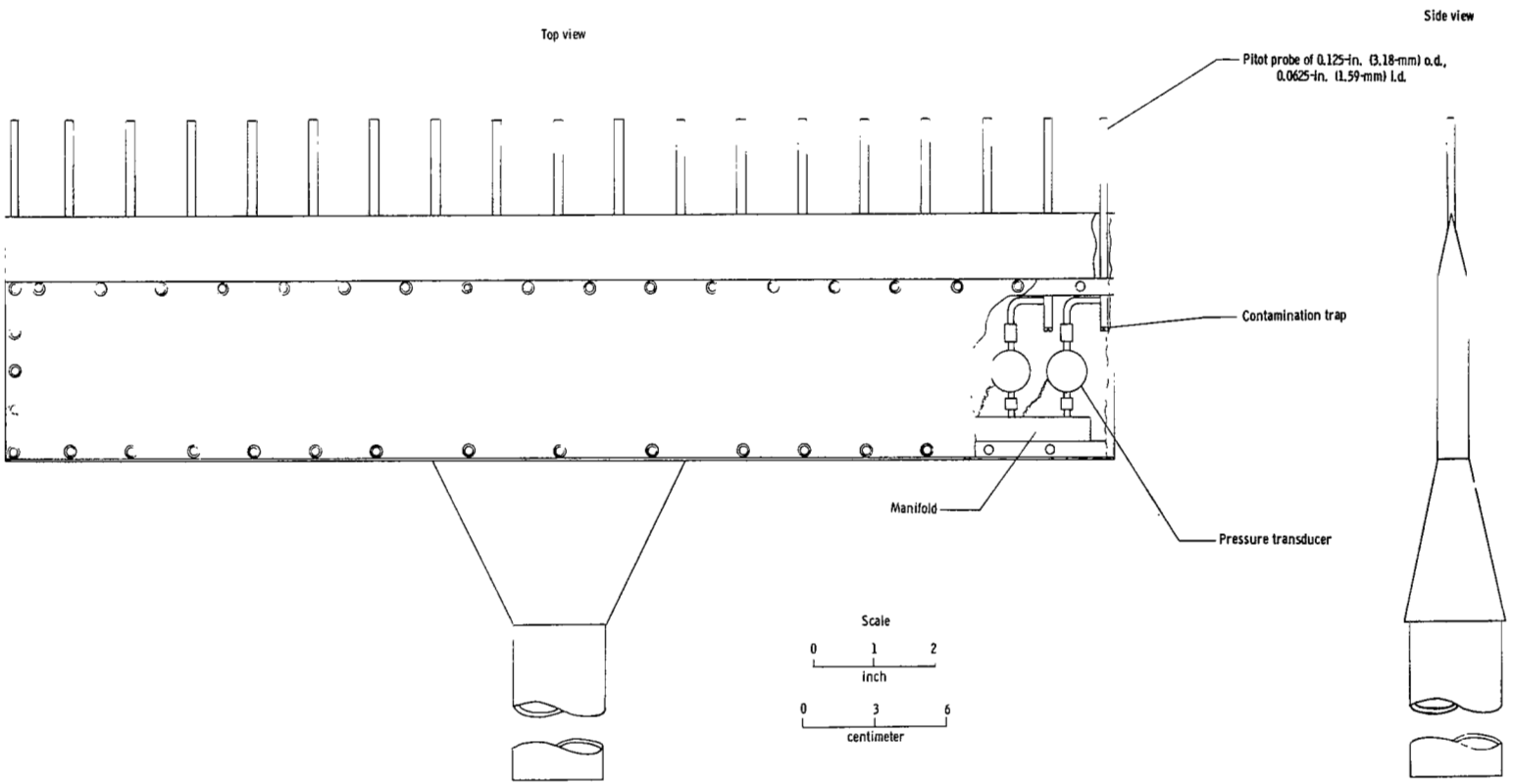

Figure 3.- Pitot-pressure survey rake. (The abbreviations o.d. and i.d. denote outside diameter and inside diameter, respectively.)

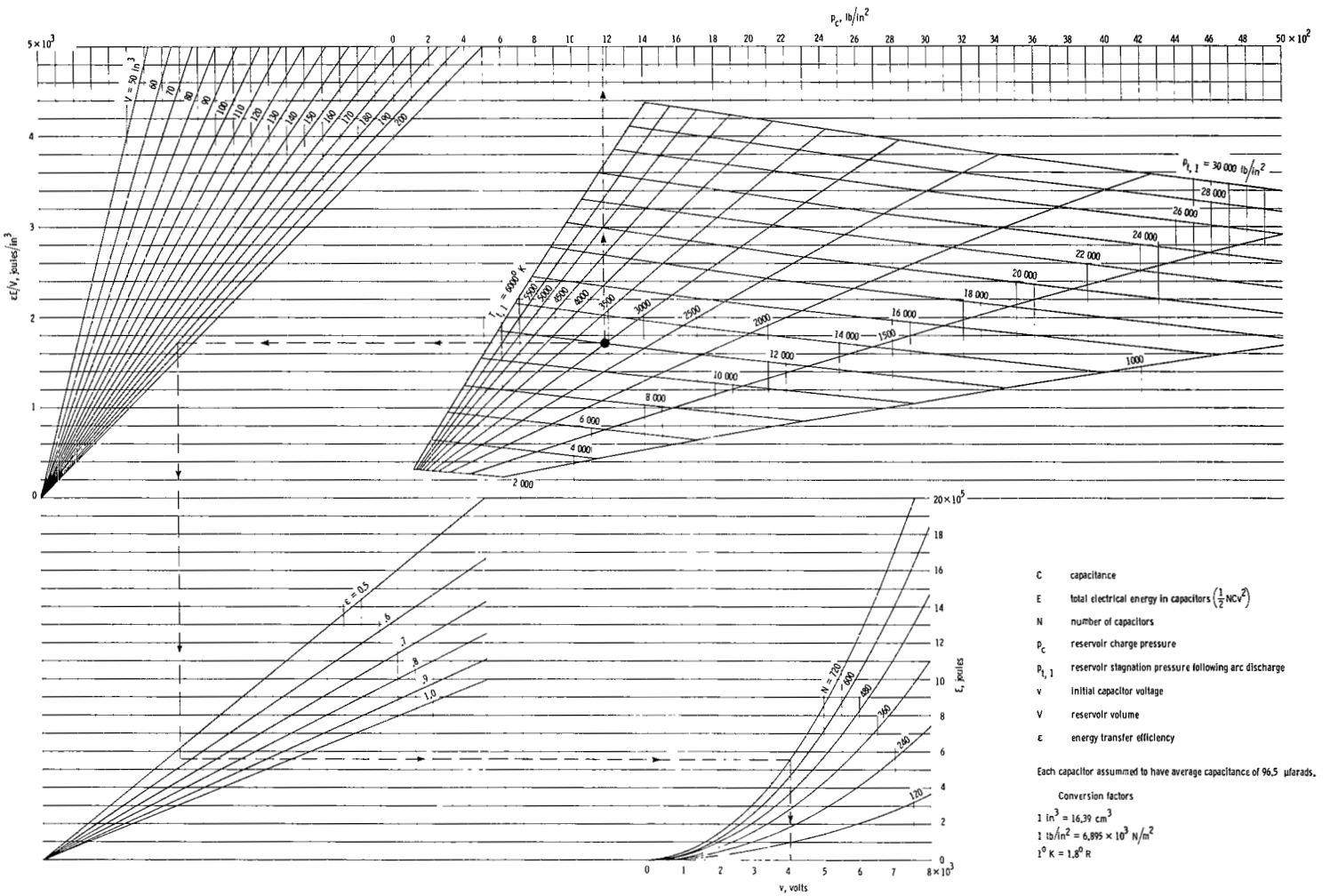

Figure 4.- Working chart for estimating reservoir conditions as functions of charge density and voltage for real helium in Langley hotshot tunnel.

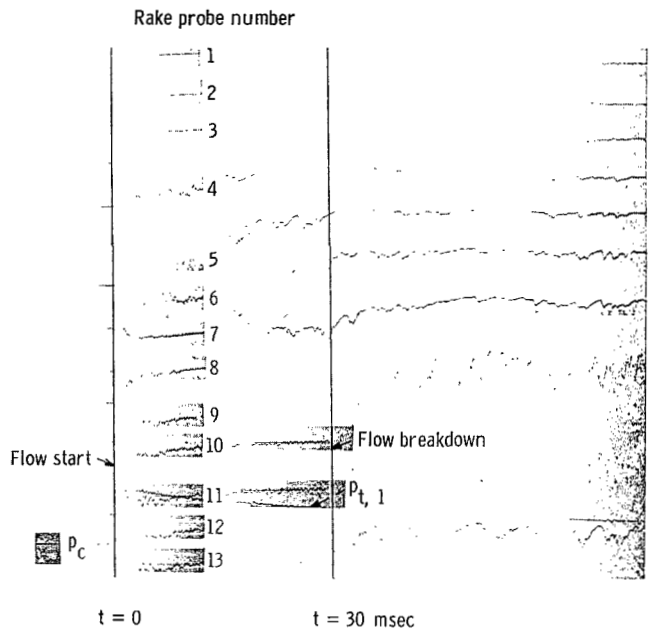

(a) Helium.

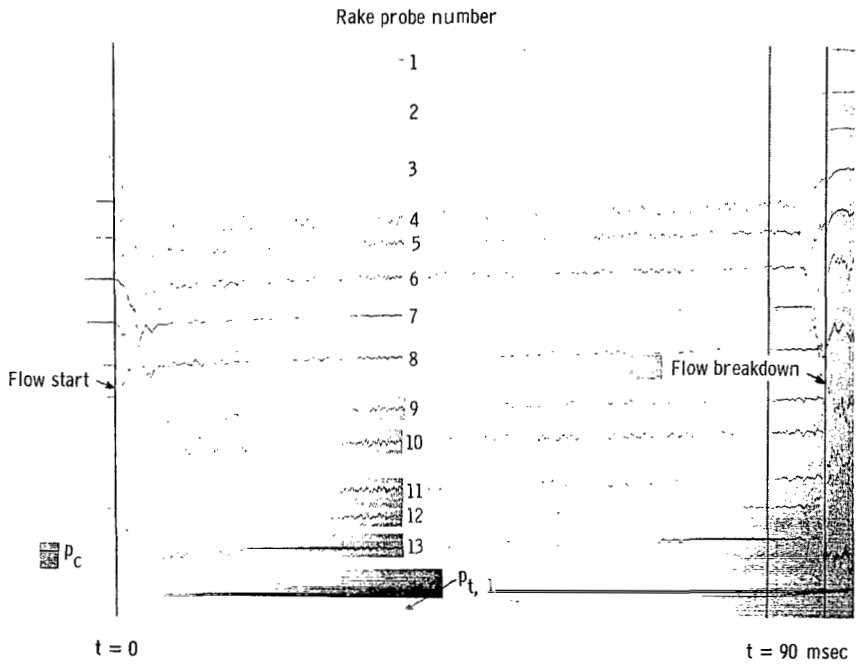

(b) Nitrogen.

Figure 5.- Representative oscillograph pressure traces obtained with survey rake in helium and nitrogen; d* = 0.15 in. (3.81 mm).

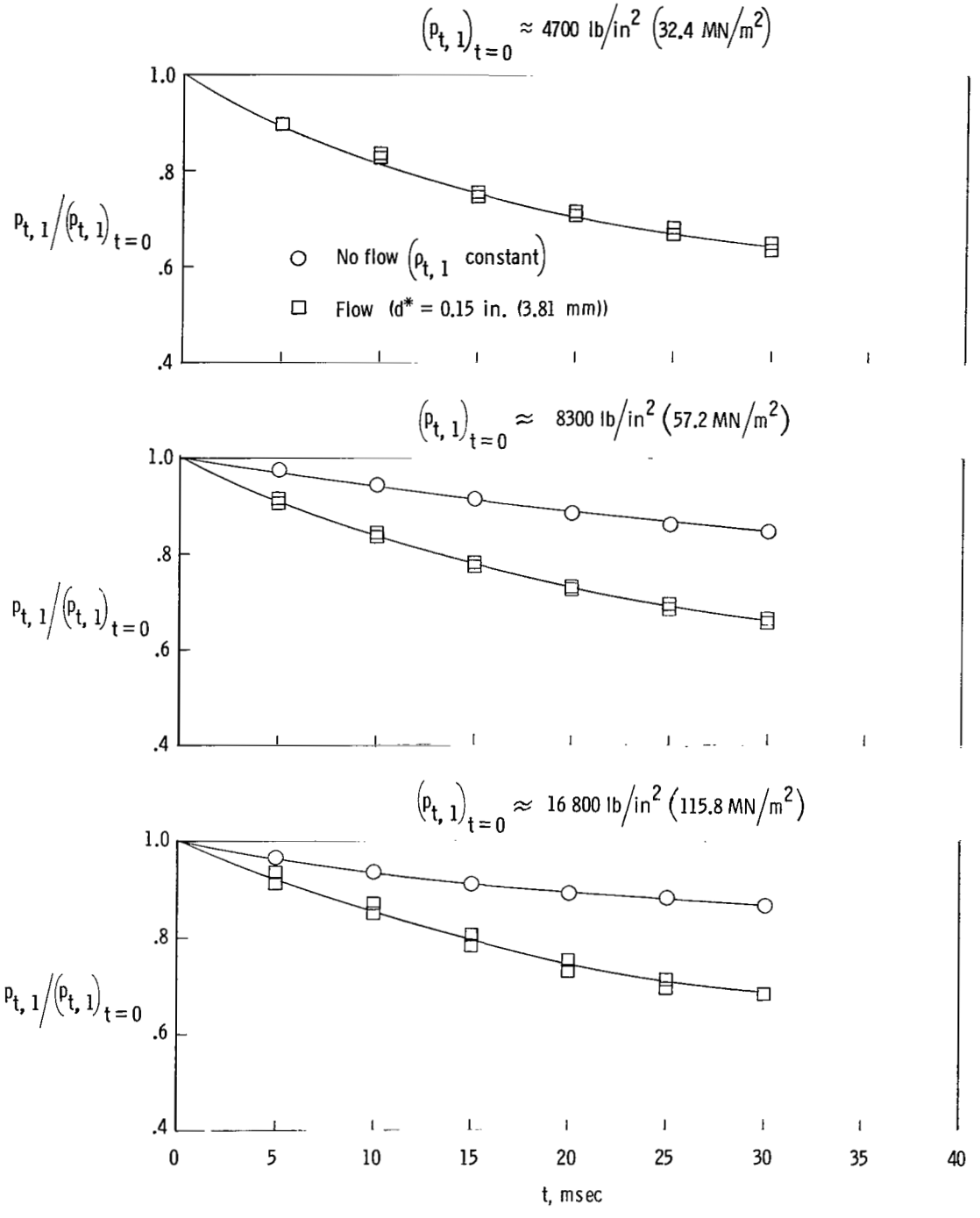

(a) Reservoir pressure.

Figure 6.- Decay of reservoir pressure and temperature for several levels of reservoir pressure and $(T_{t,1})_{t=0} \approx 5000^0$ R (2778^0 K).

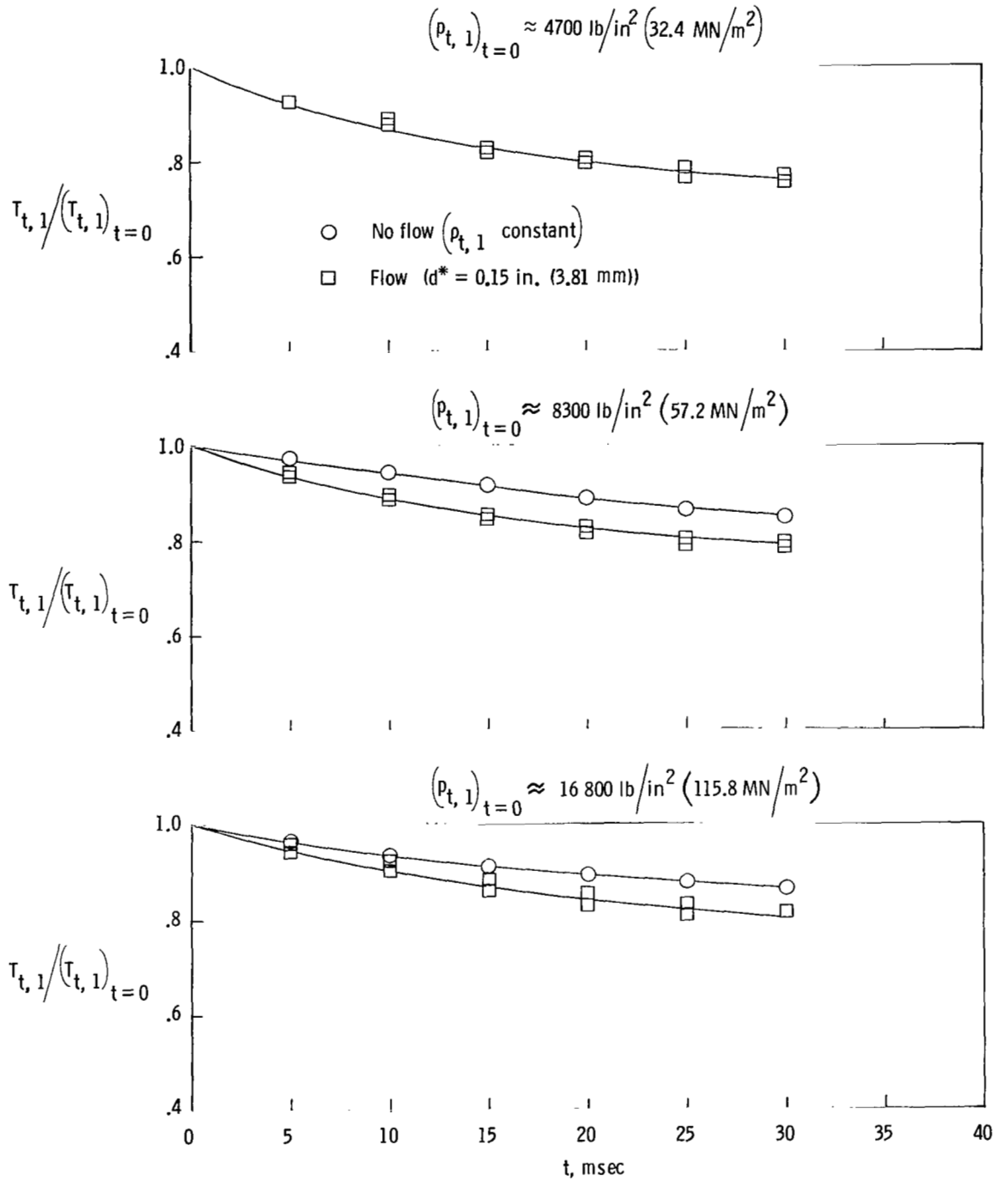

(b) Reservoir temperature.

Figure 6.- Concluded.

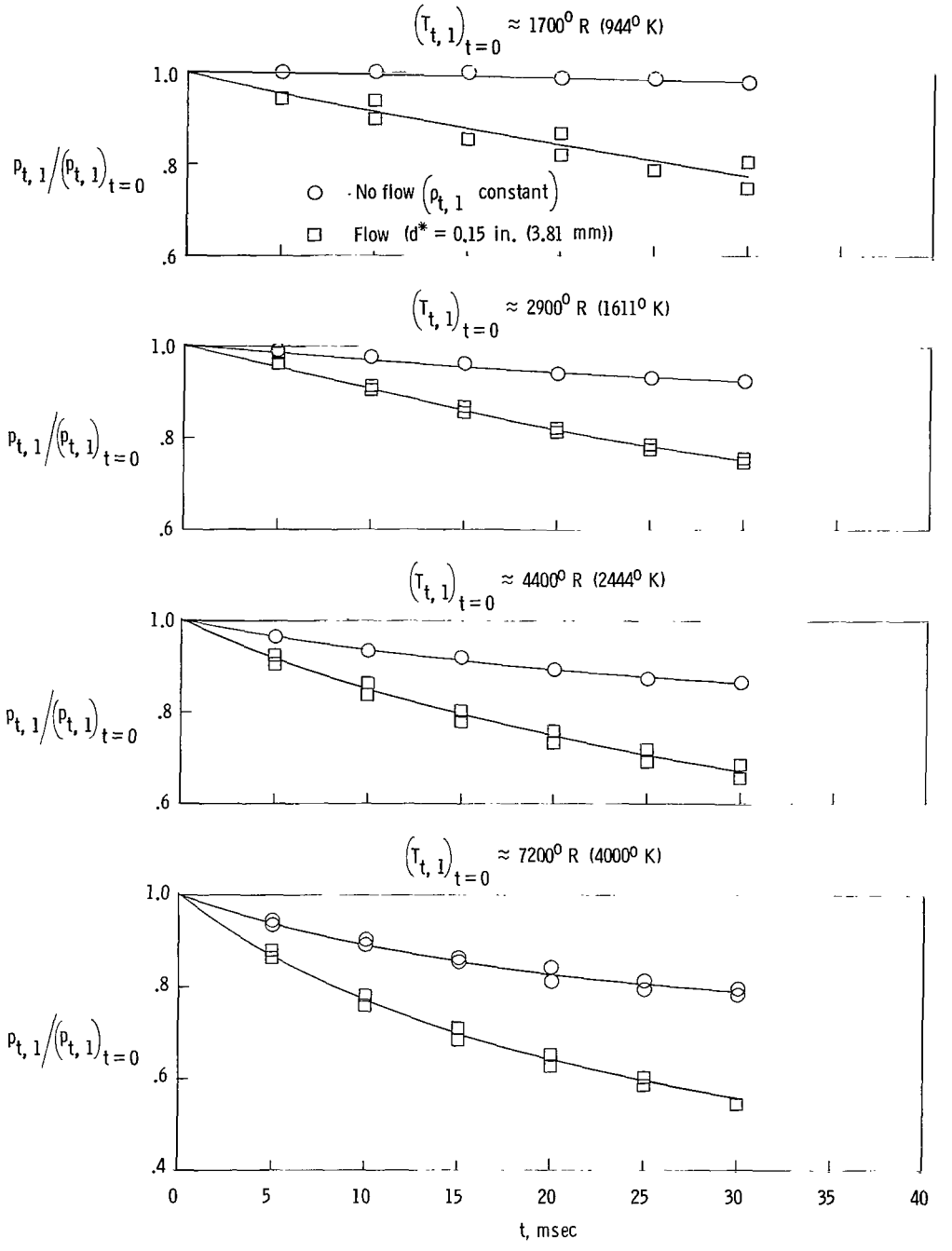

(a) Reservoir pressure.

Figure 7.- Decay of reservoir pressure and temperature for several levels of reservoir temperature and $(p_{t,1})_{t=0} \approx 11\,500$ lb/in^2 (79.3 MN/m^2).

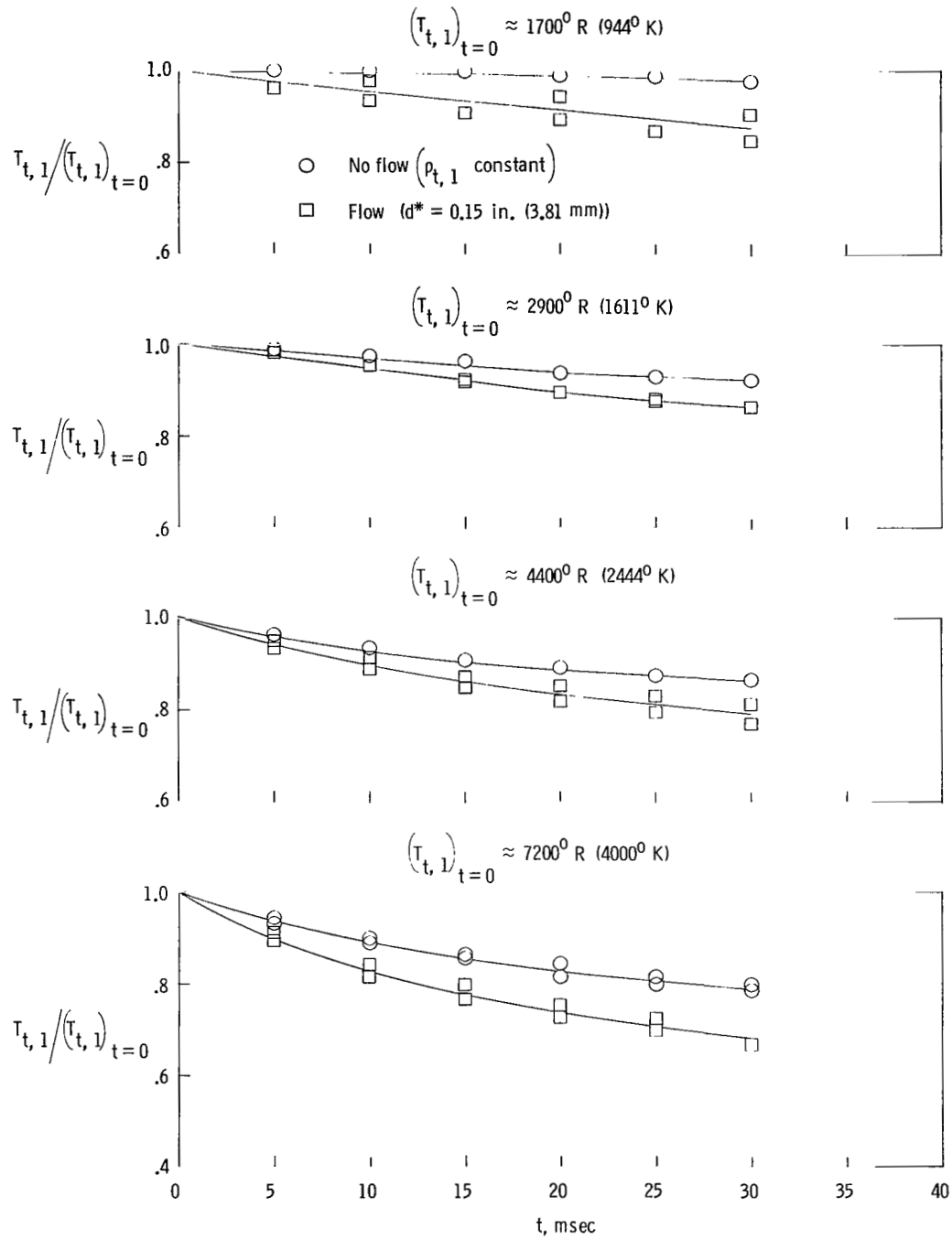

(b) Reservoir temperature.

Figure 7.- Concluded.

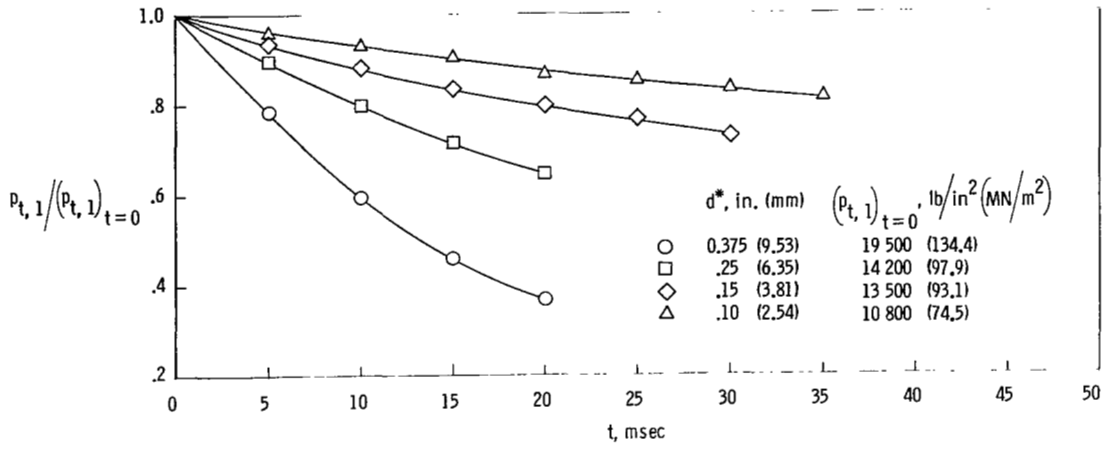

(a) Reservoir pressure.

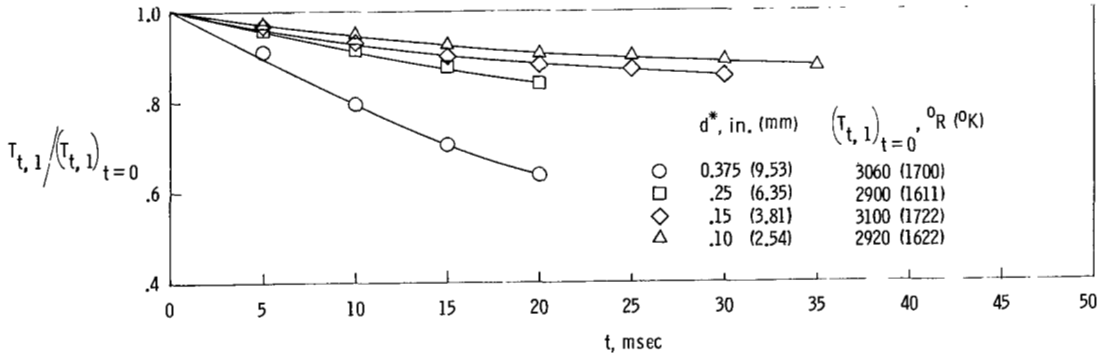

(b) Reservoir temperature.

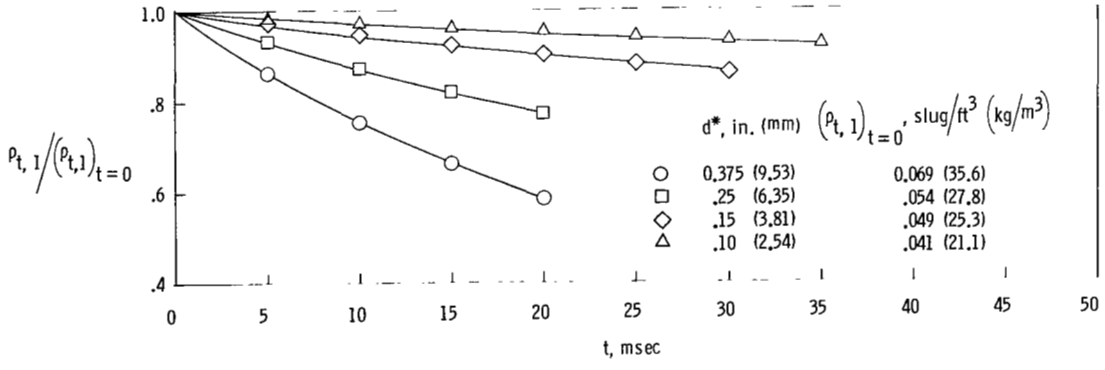

(c) Reservoir density.

Figure 8.- Decay of reservoir conditions for several nozzle-throat diameters.

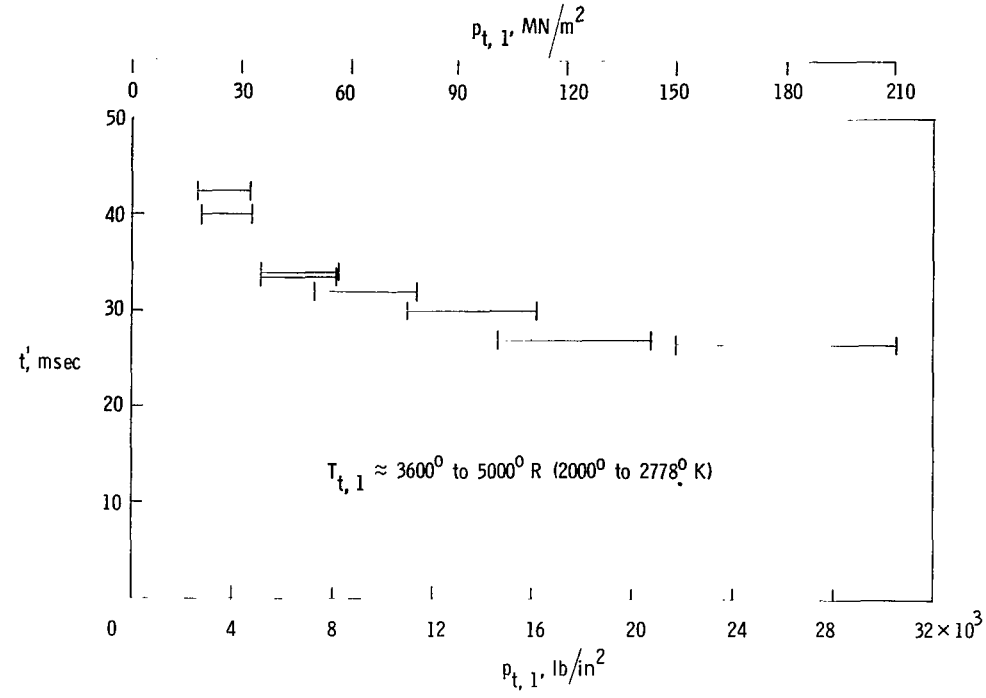

(a) $d^* = 0.15$ in. (3.81 mm).

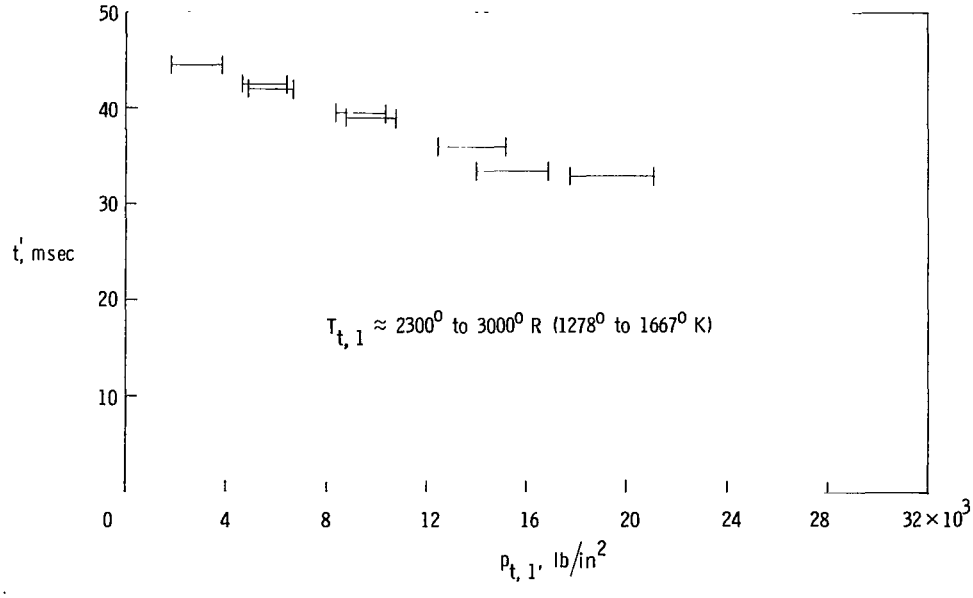

(b) $d^* = 0.10$ in. (2.54 mm).

Figure 9.- Variation in total tunnel run time with reservoir pressure for two nozzle-throat diameters.

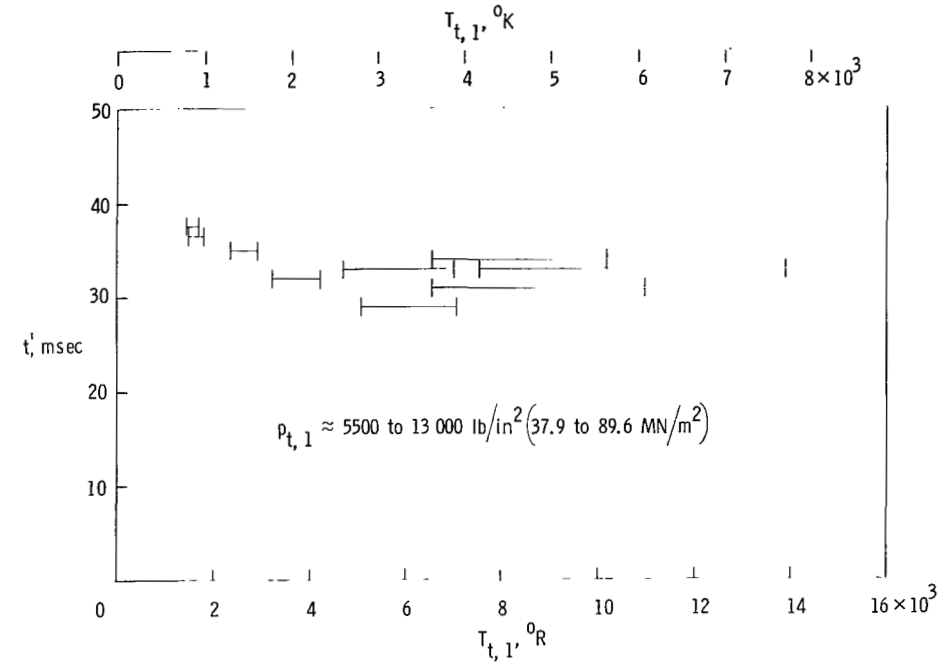

(a) d* = 0.15 in. (3.81 mm).

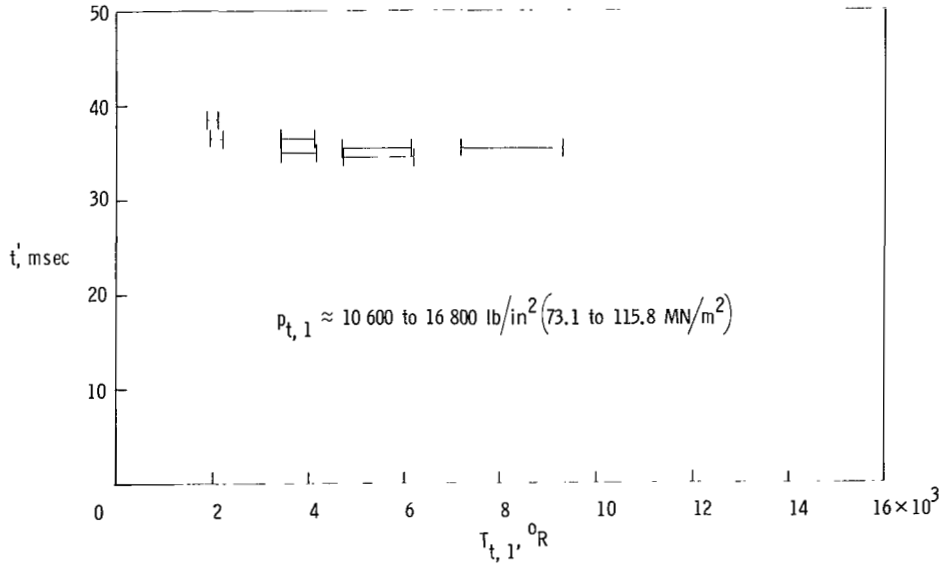

(b) d* = 0.10 in. (2.54 mm).

Figure 10.- Variation in total tunnel run time with reservoir temperature for two nozzle-throat diameters.

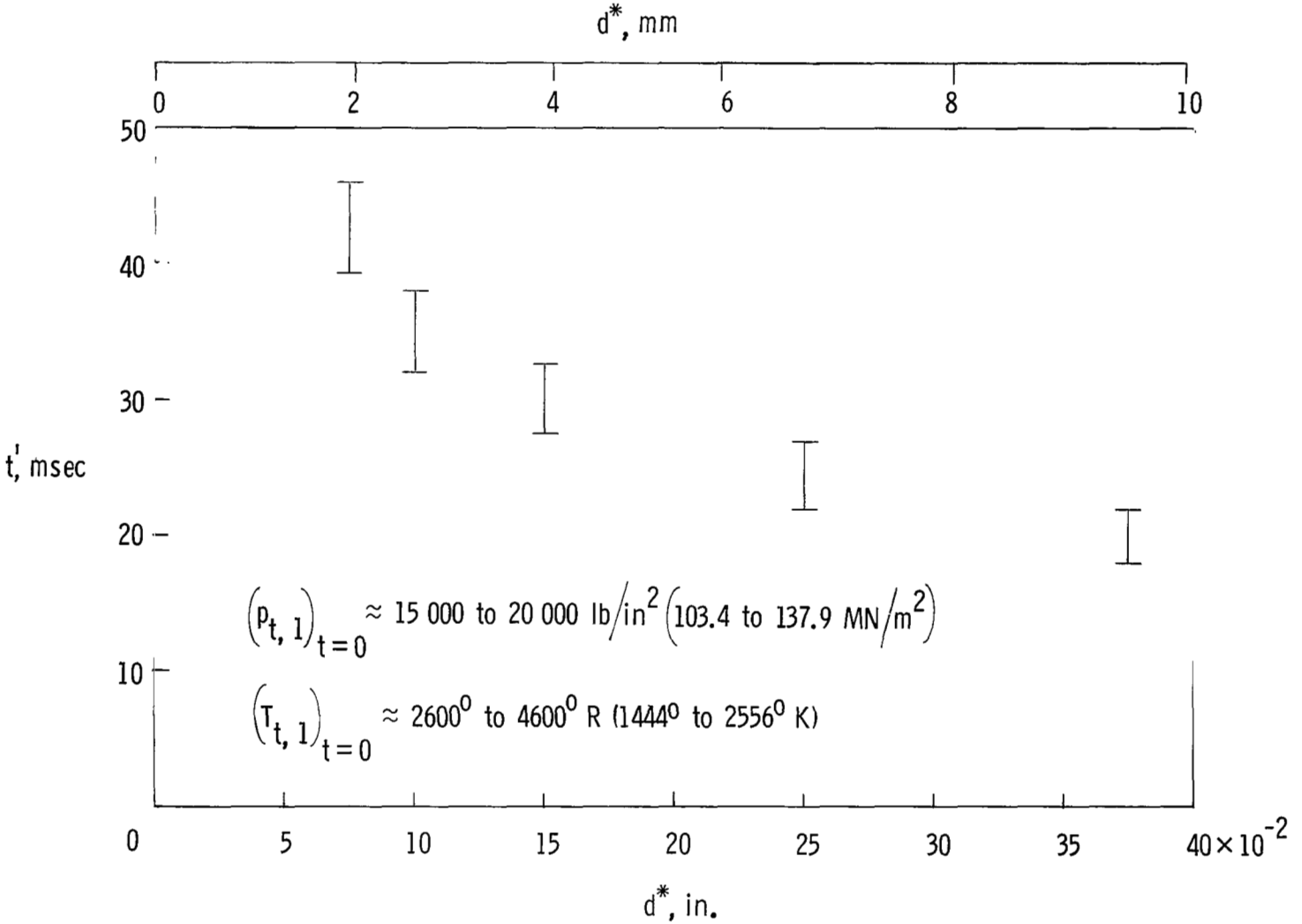

Figure 11.- Variation in total tunnel run time with nozzle-throat diameter.

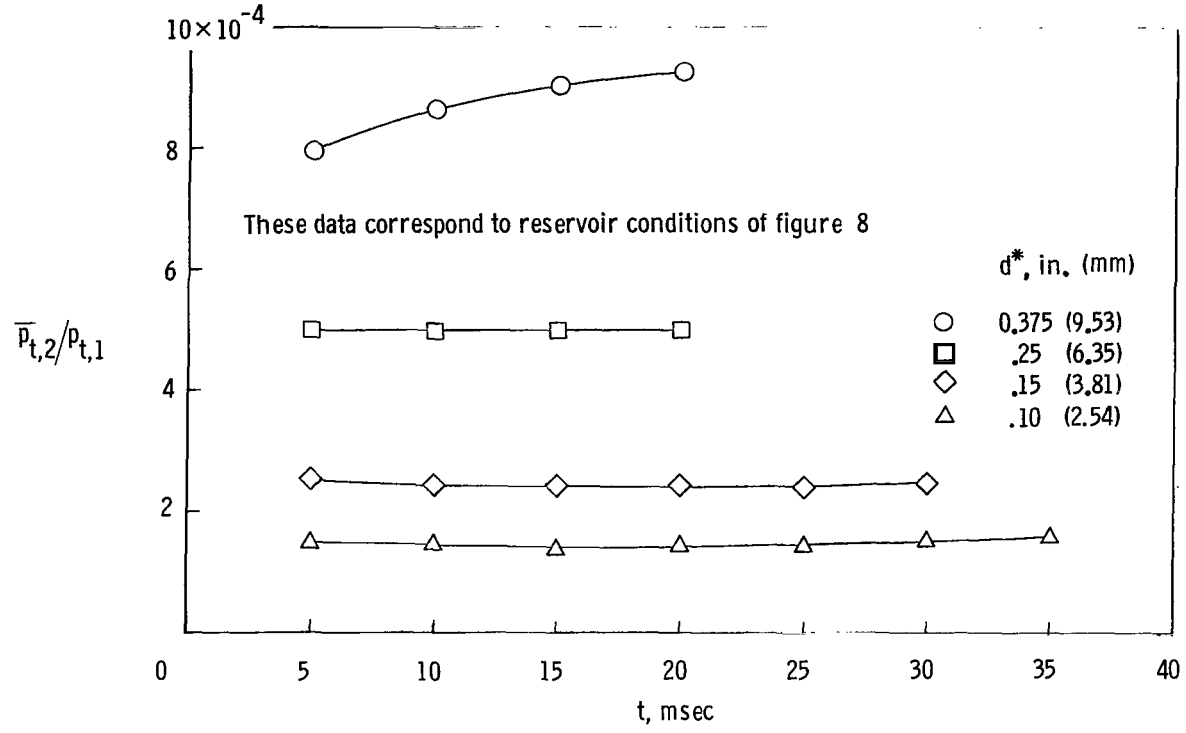

(a) Stagnation-pressure ratio.

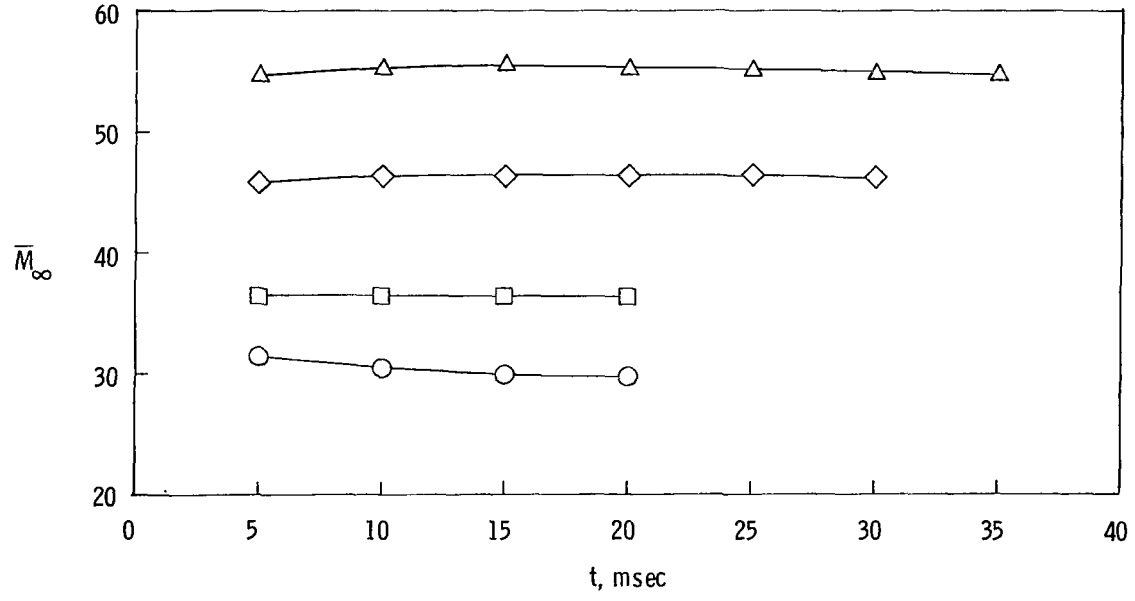

(b) Free-stream Mach number.

Figure 12.- Time variation of stagnation-pressure ratio and Mach number averaged across the inviscid core for several nozzle-throat diameters.

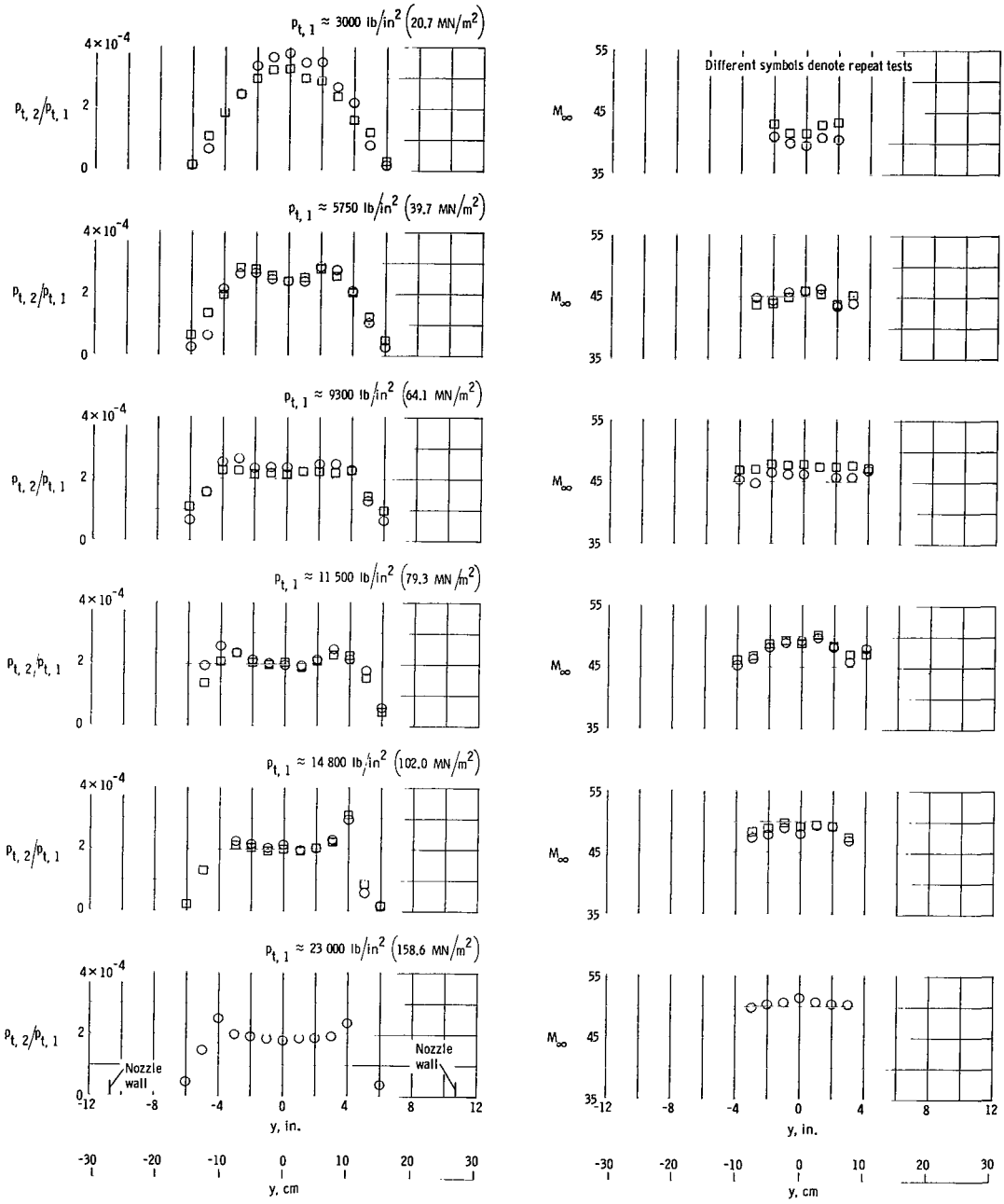

(a) $d^* = 0.15$ in. (3.81 mm); $T_{t,1} \approx 3800^0$ R (2111^0 K).

Figure 13.- Stagnation-pressure-ratio and Mach number profiles for various reservoir pressures and two nozzle-throat diameters at station x = 122 in. (3.10 m).

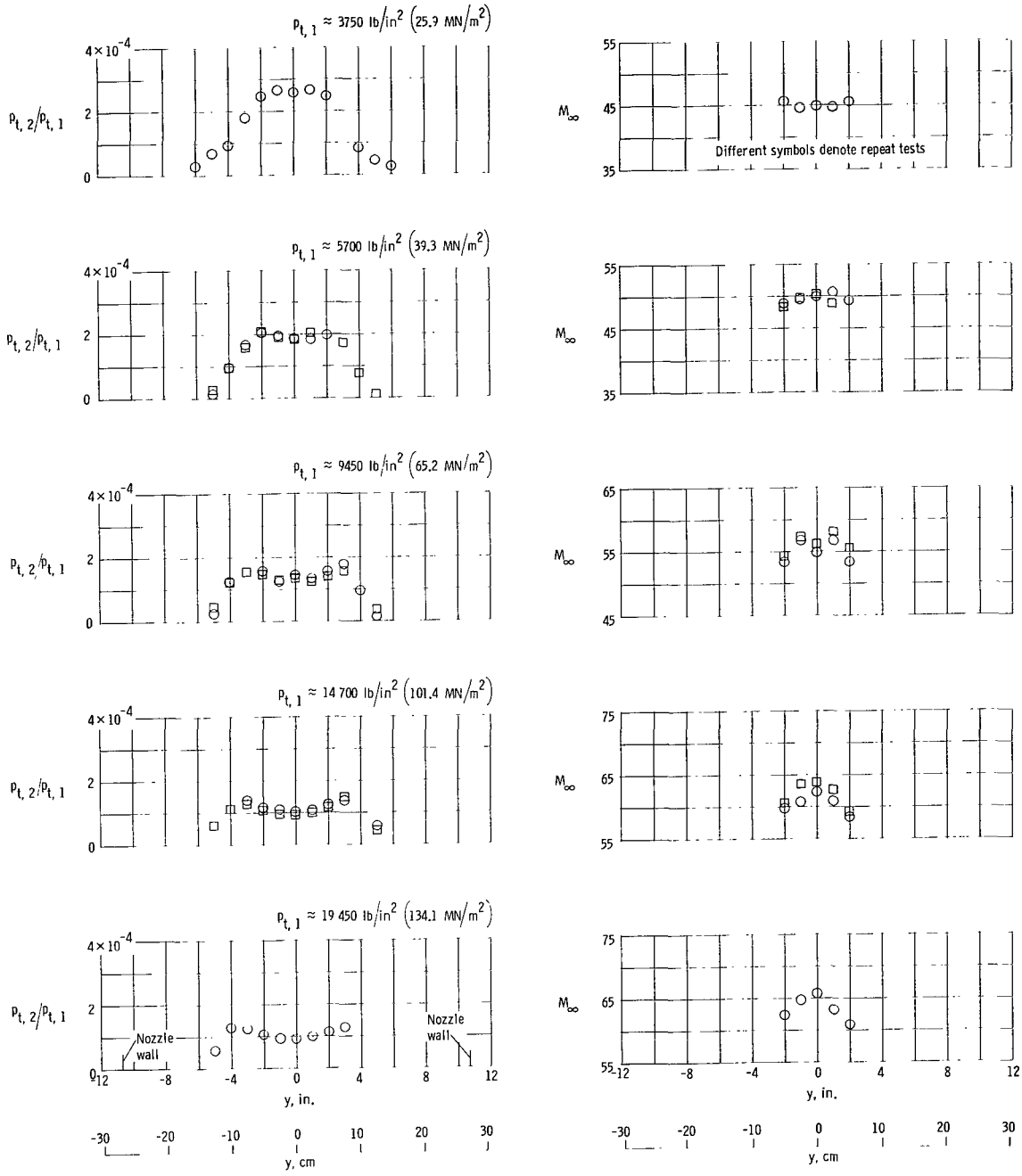

(b) d* = 0.10 in. (2.54 mm); $T_{t,1} \approx 2600^{\circ}$ R (1444° K).

Figure 13.- Concluded.

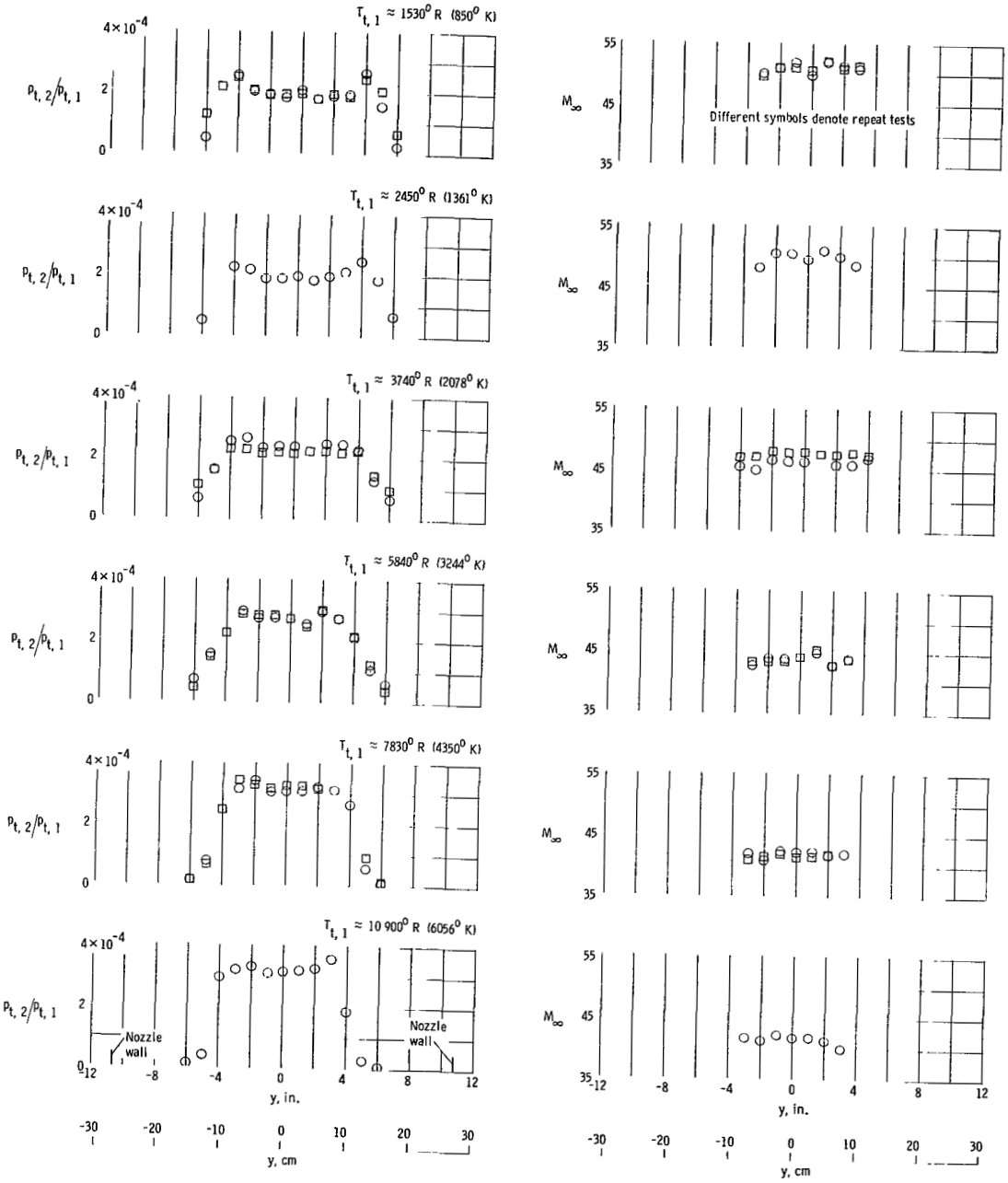

(a) $d^* = 0.15$ in. (3.81 mm); $p_{t,1} \approx 9200$ lb/in^2 (63.4 MN/m^2).

Figure 14.- Stagnation-pressure-ratio and Mach number profiles for various reservoir temperatures and two nozzle-throat diameters at station x = 122 in. (3.10 m).

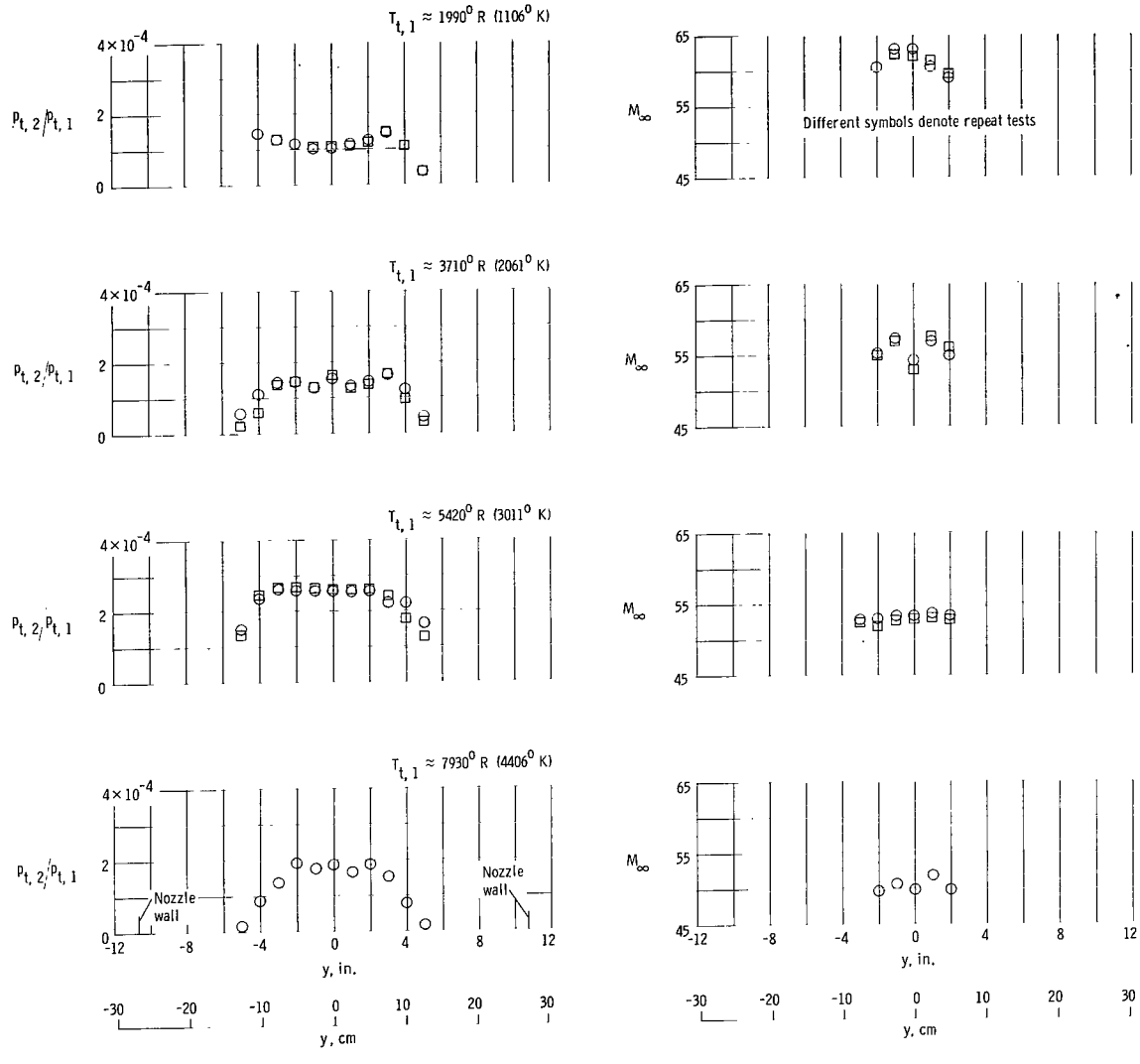

(b) $d^* = 0.10$ in. (2.54 mm); $p_{t,1} \approx 14\,500$ lb/in^2 (100.0 MN/m^2).

Figure 14.- Concluded.

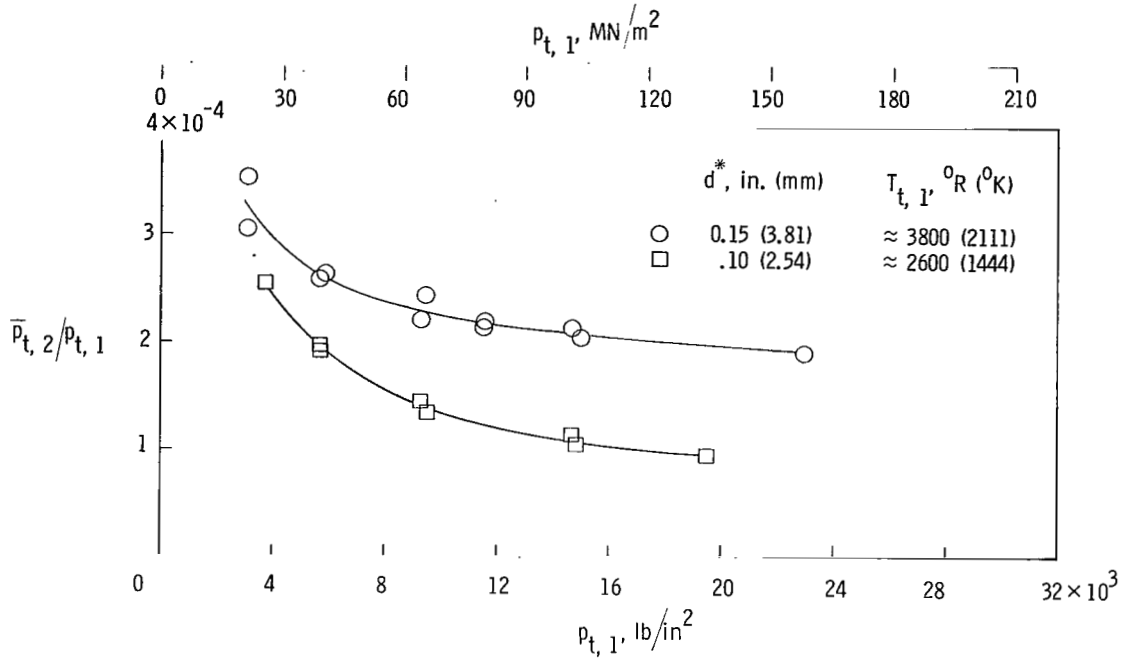

(a) Stagnation-pressure ratio.

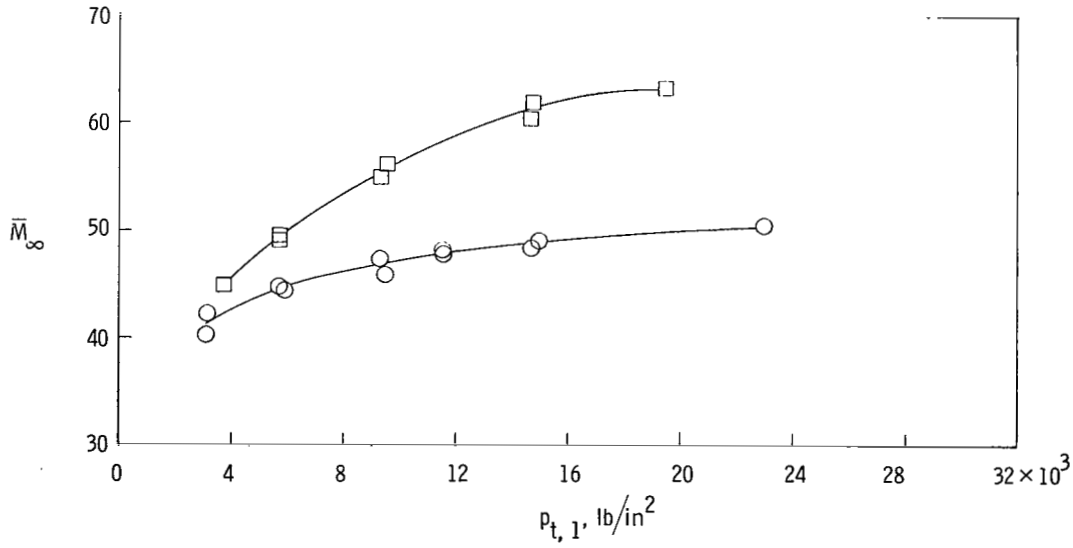

(b) Free-stream Mach number.

Figure 15.- Variation of several flow parameters averaged across the inviscid core with reservoir pressure at station x = 122 in. (3.10 m).

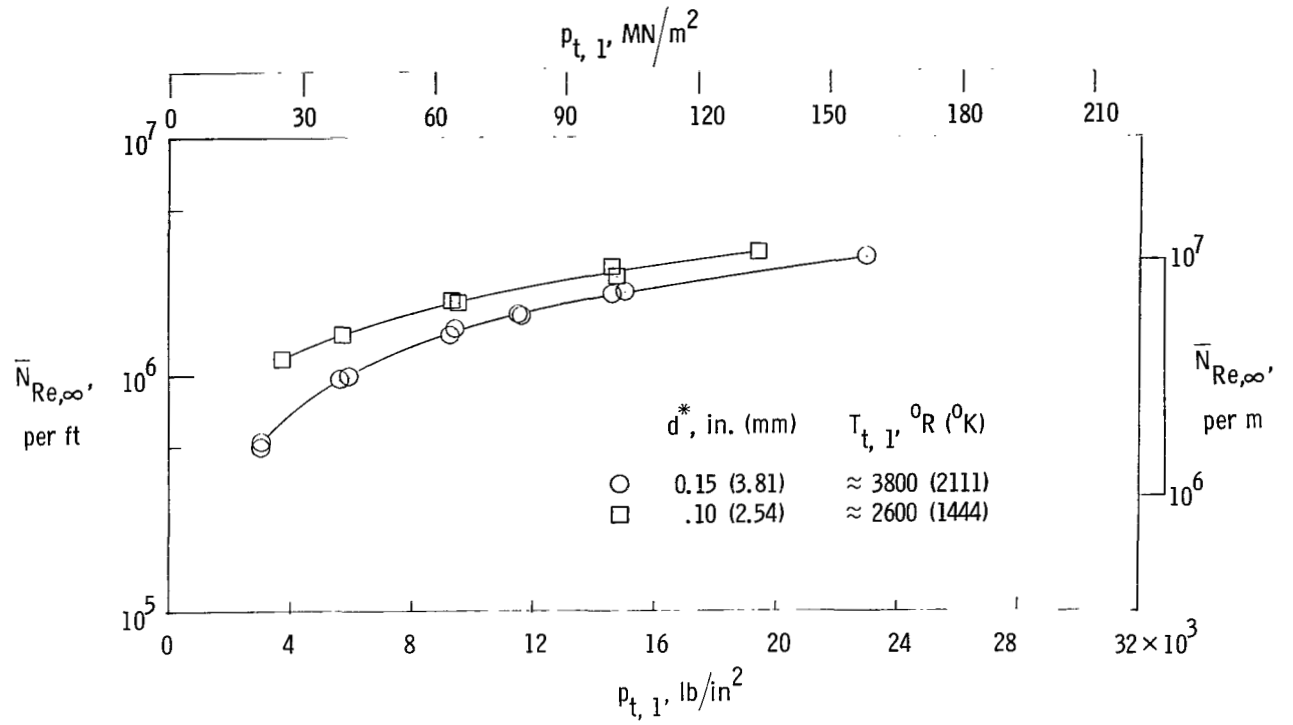

(c) Free-stream Reynolds number.

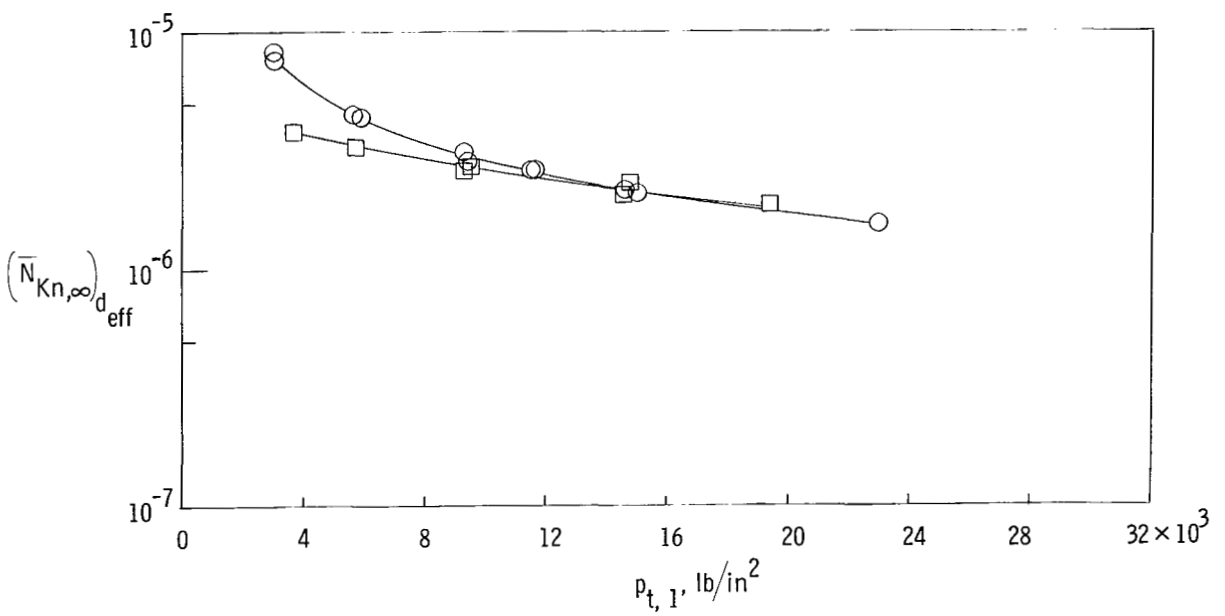

(d) Free-stream Knudsen number.

Figure 15.- Concluded.

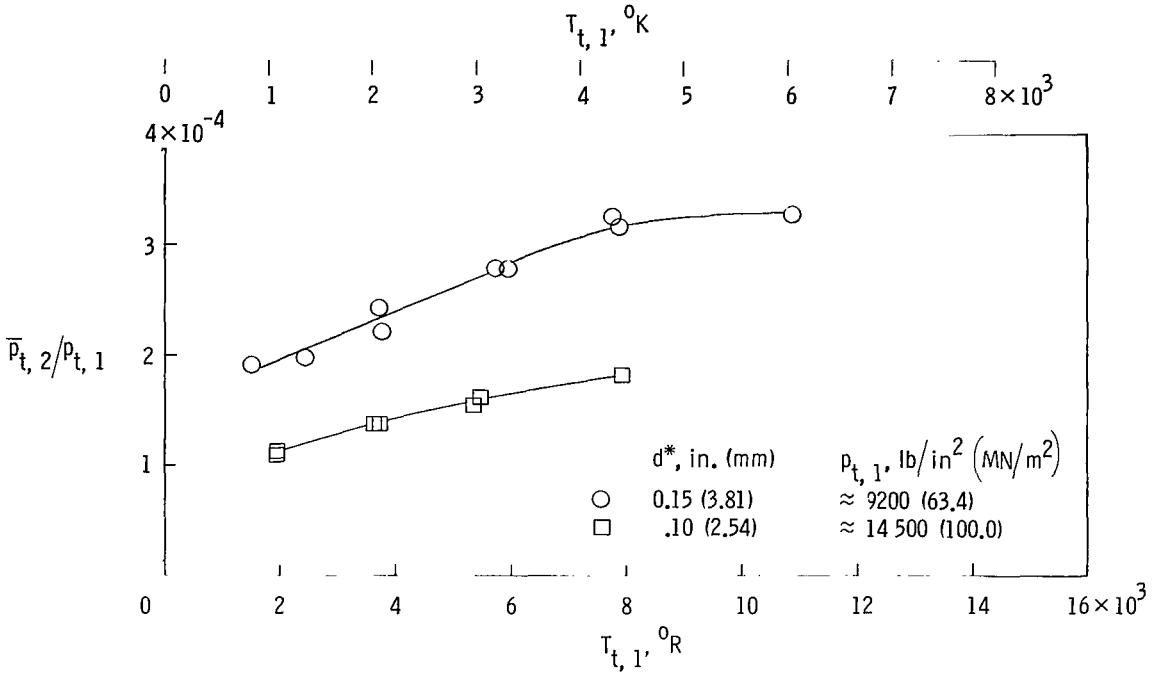

(a) Stagnation-pressure ratio.

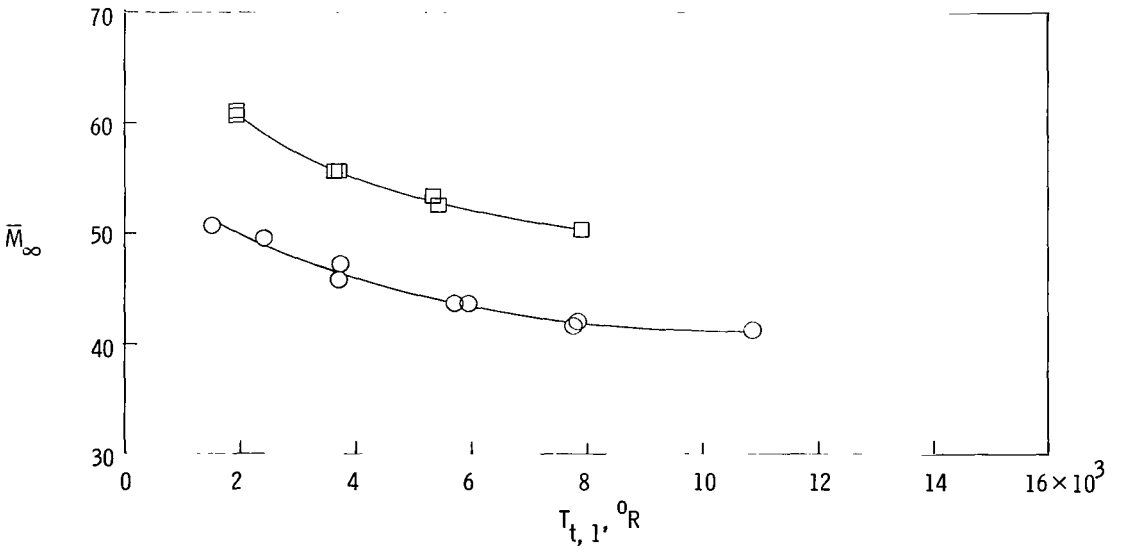

(b) Free-stream Mach number.

Figure 16.- Variation of several flow parameters averaged across the inviscid core with reservoir temperature at station x = 122 in. (3.10 m).

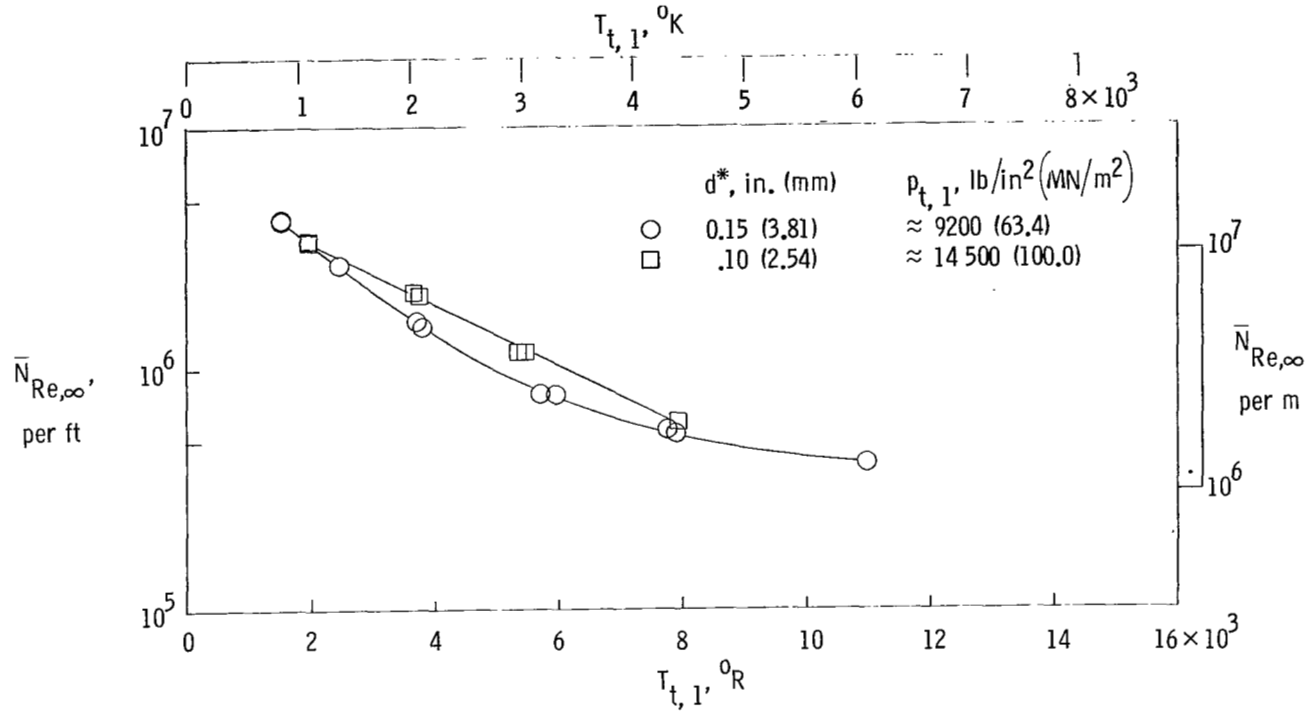

(c) Free-stream Reynolds number.

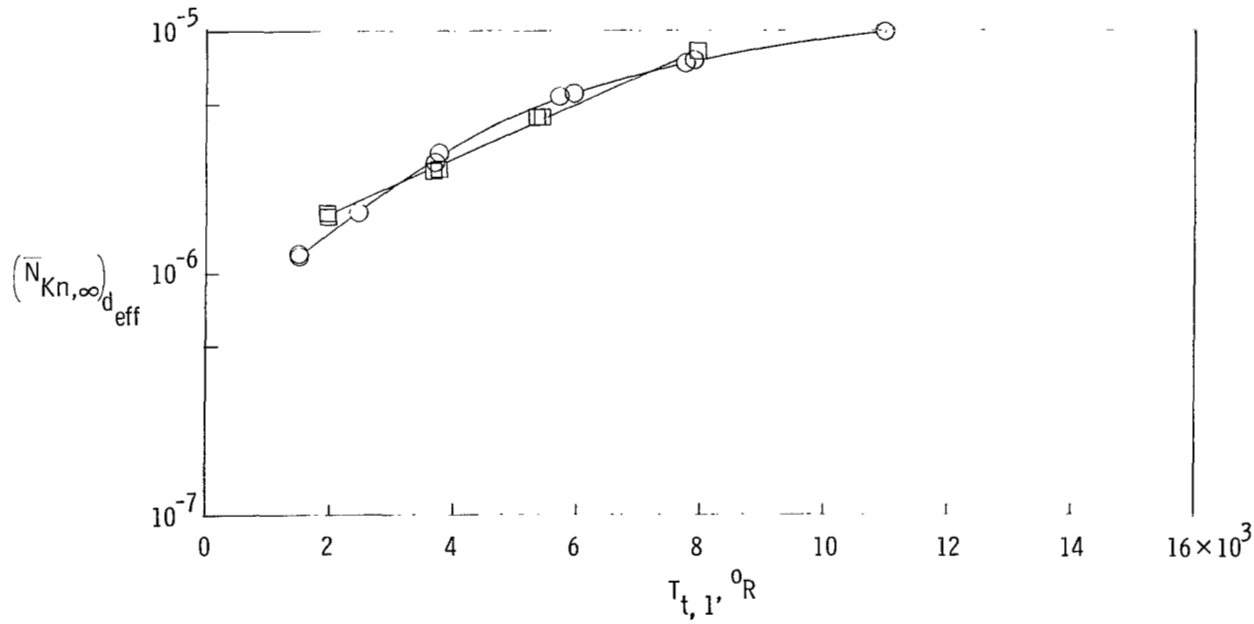

(d) Free-stream Knudsen number.

Figure 16.- Concluded.

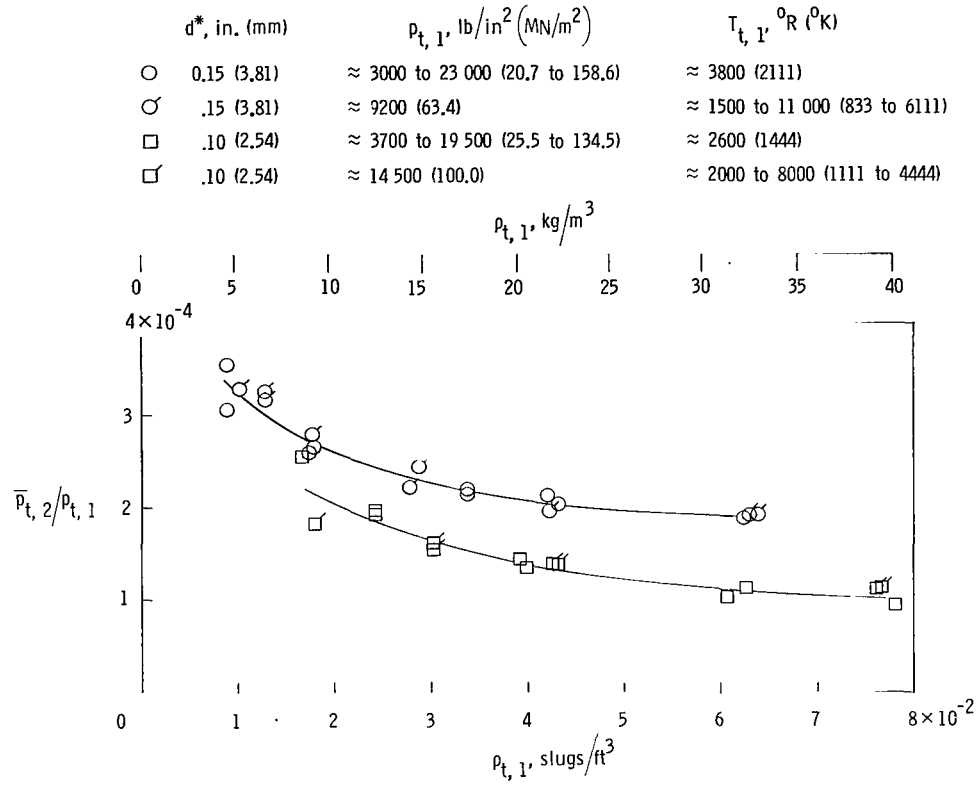

(a) Stagnation-pressure ratio.

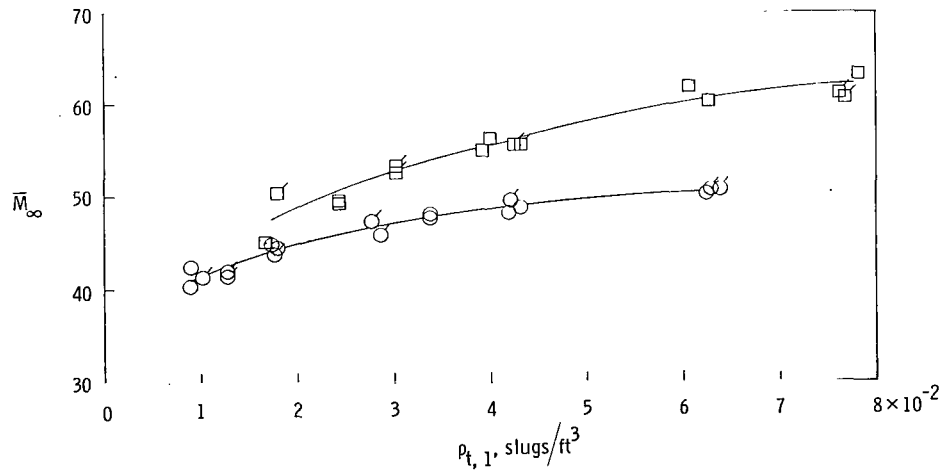

(b) Free-stream Mach number.

Figure 17.- Variation of stagnation-pressure ratio and Mach number averaged across the inviscid core with reservoir density at station x = 122 in. (3.10 m).

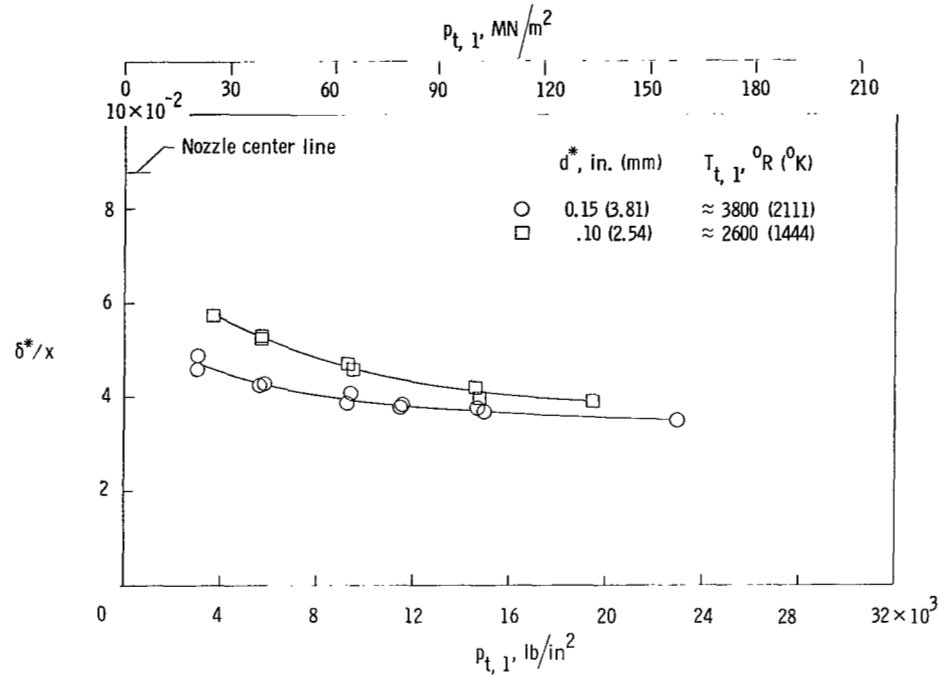

(a) Nozzle boundary-layer displacement thickness.

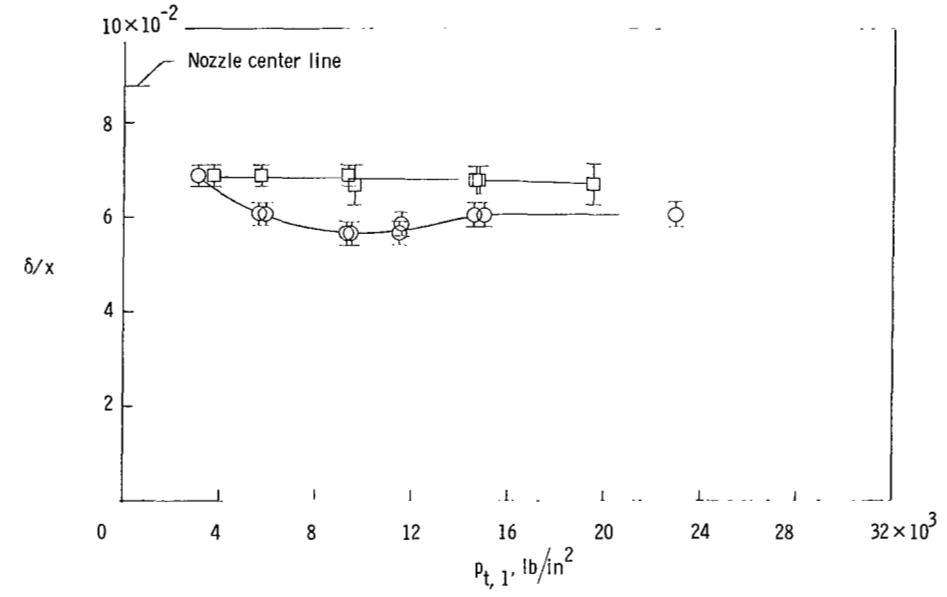

(b) Nozzle boundary-layer thickness.

Figure 18.- Variation of nozzle boundary-layer displacement thickness and nozzle boundary-layer thickness with reservoir pressure at station x = 122 in. (3.10 m).

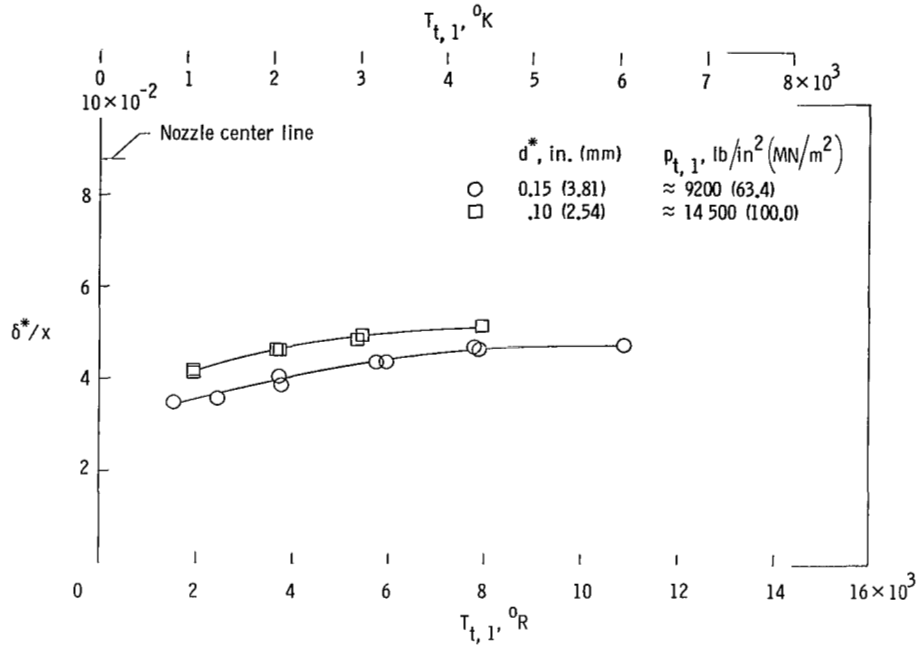

(a) Nozzle boundary-layer displacement thickness.

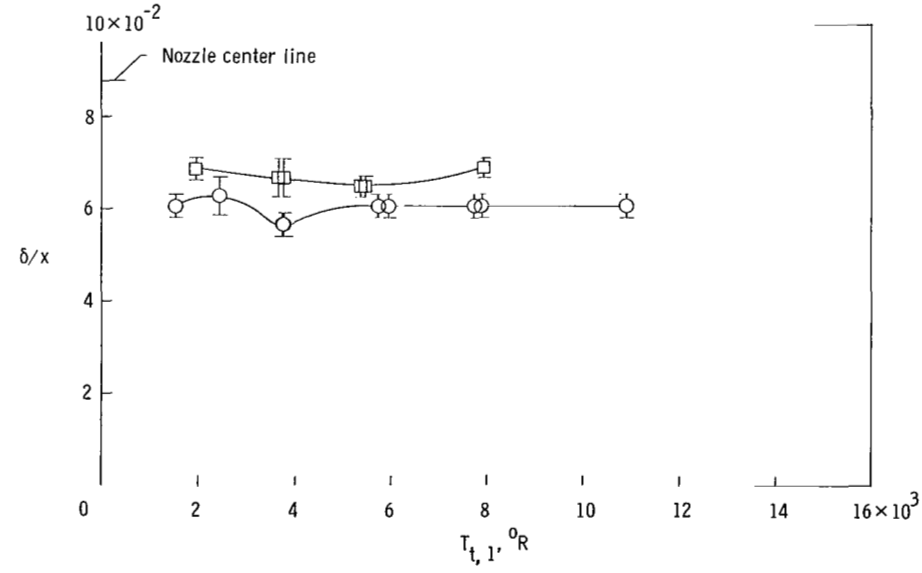

(b) Nozzle boundary-layer thickness.

Figure 19.- Variation of nozzle boundary-layer displacement thickness and nozzle boundary-layer thickness with reservoir temperature at station x = 122 in. (3.10 m).

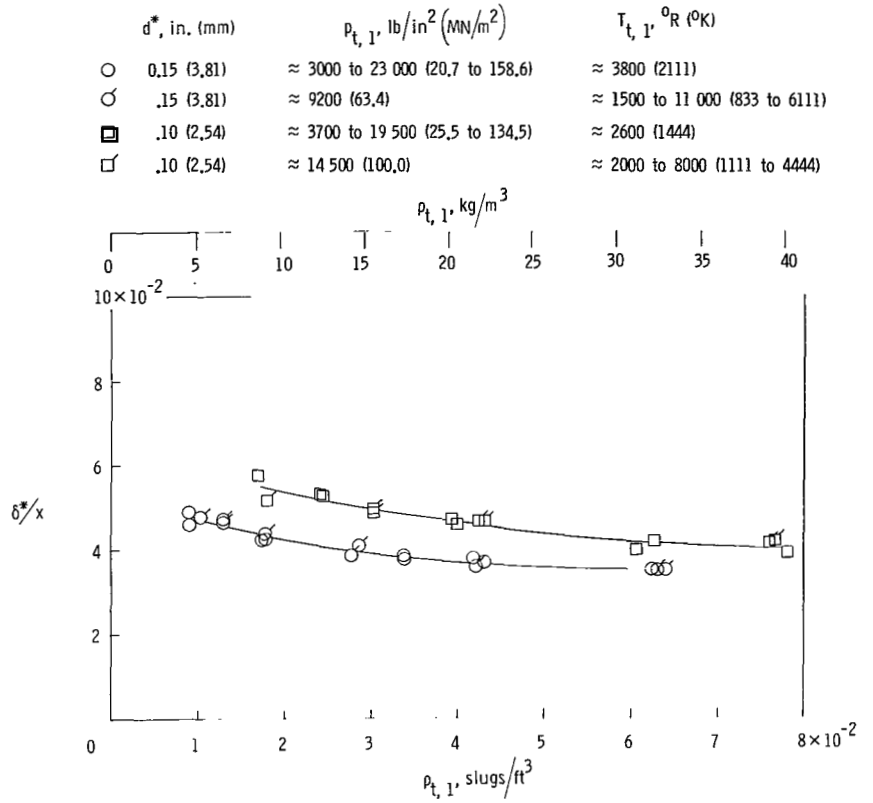

(a) Nozzle boundary-layer displacement thickness.

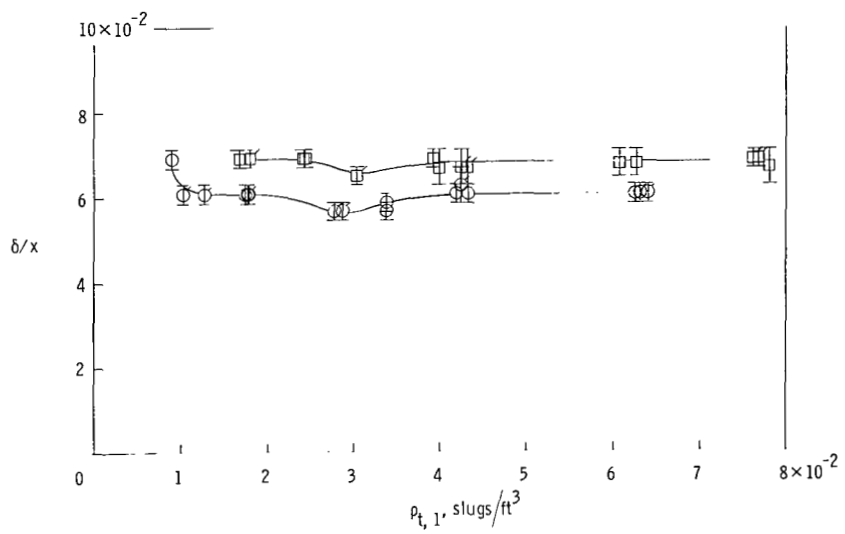

(b) Nozzle boundary-layer thickness.

Figure 20.- Variation of nozzle boundary-layer displacement thickness and nozzle boundary-layer thickness with reservoir density at station x = 122 in. (3.10 m).

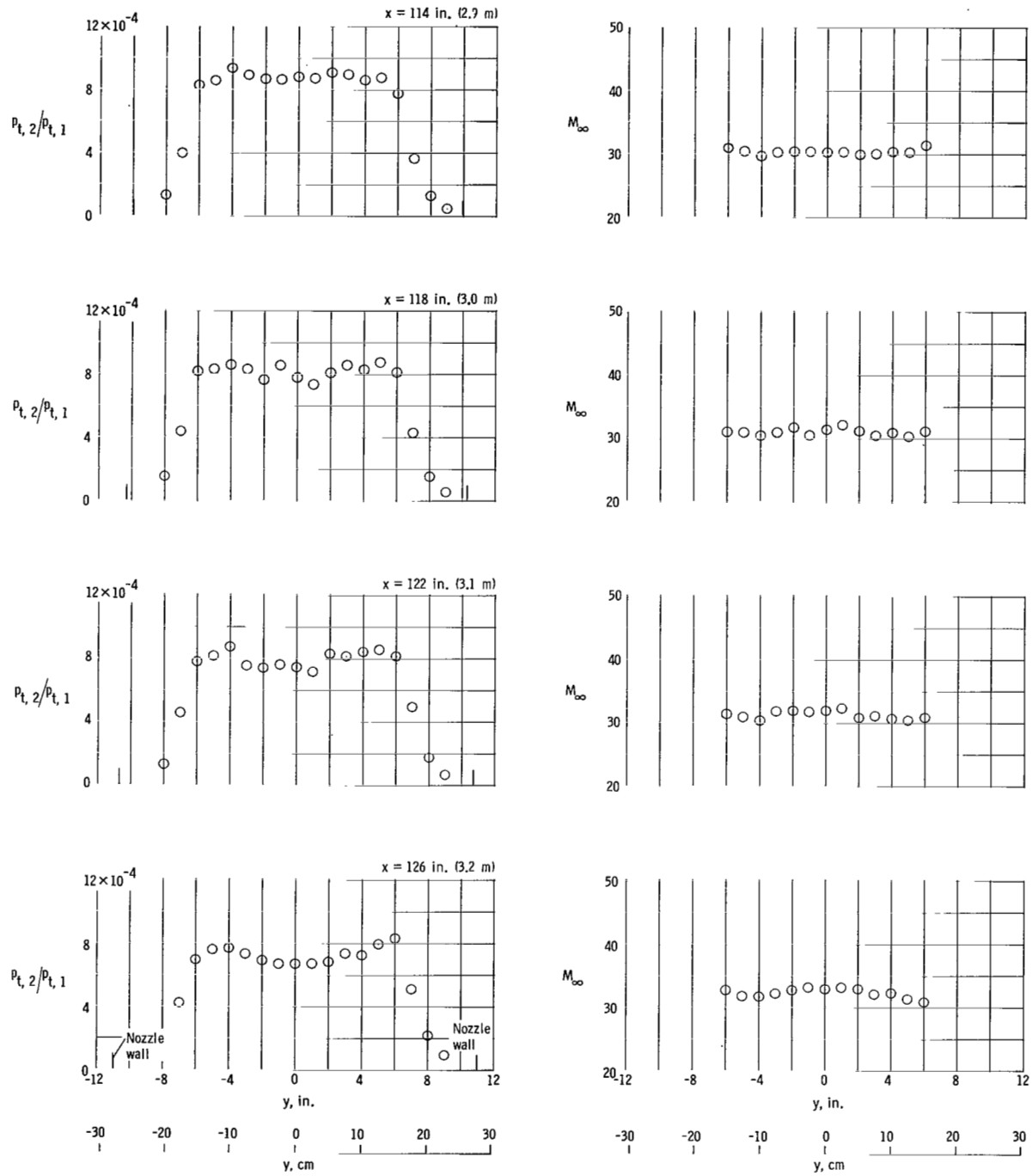

(a) $d^* = 0.375$ in. (9.53 mm); $T_{t,1} \approx 2400^0$ R (1333^0 K).

Figure 21.- Stagnation-pressure-ratio and Mach number profiles for various nozzle axial stations and nozzle-throat diameters; $p_{t,1} \approx 11\,500$ lb/in^2 (79.3 MN/m^2).

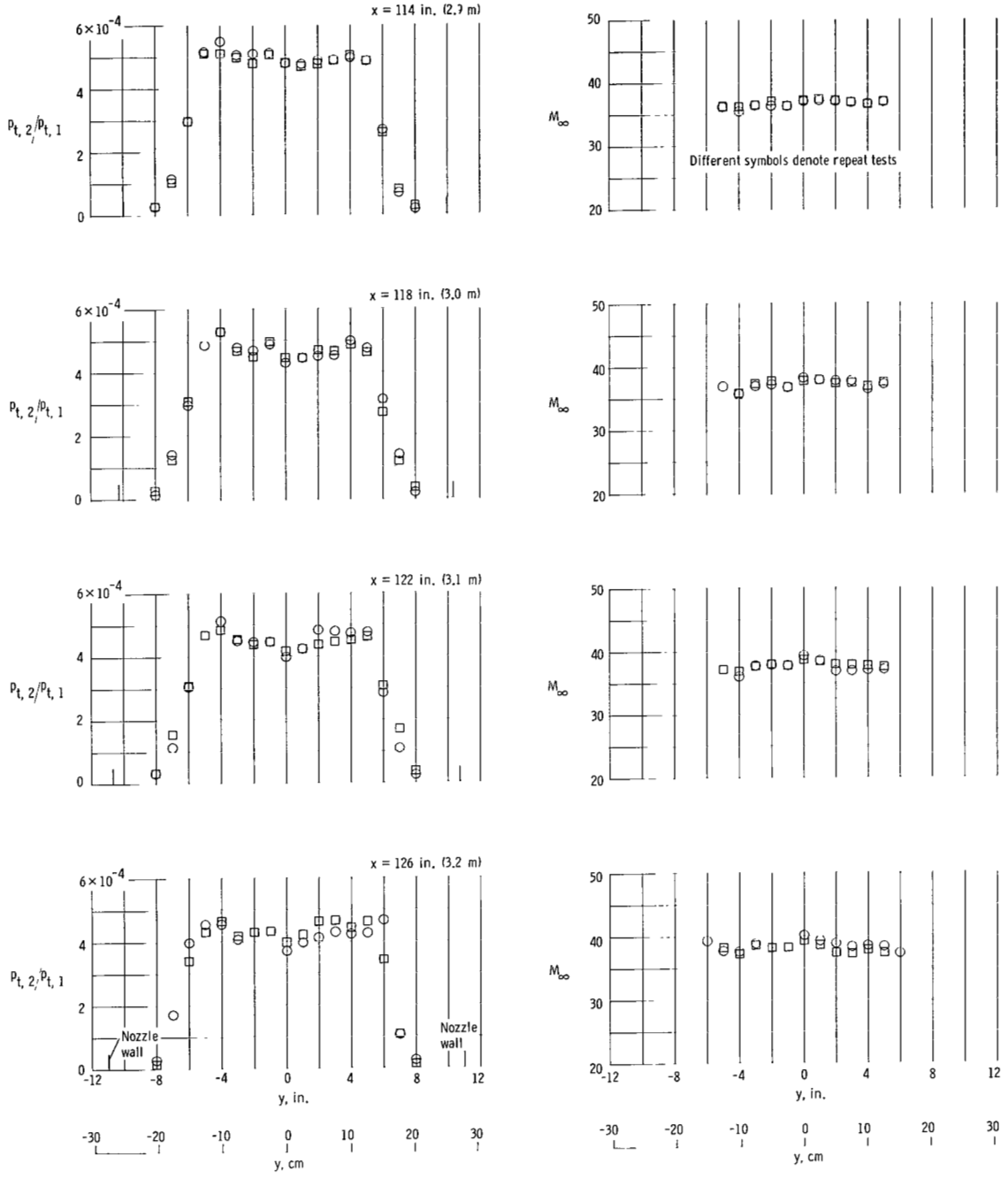

(b) $d^* = 0.25$ in. (6.35 mm); $T_{t,1} \approx 2600^0$ R (1444^0 K).

Figure 21.- Continued.

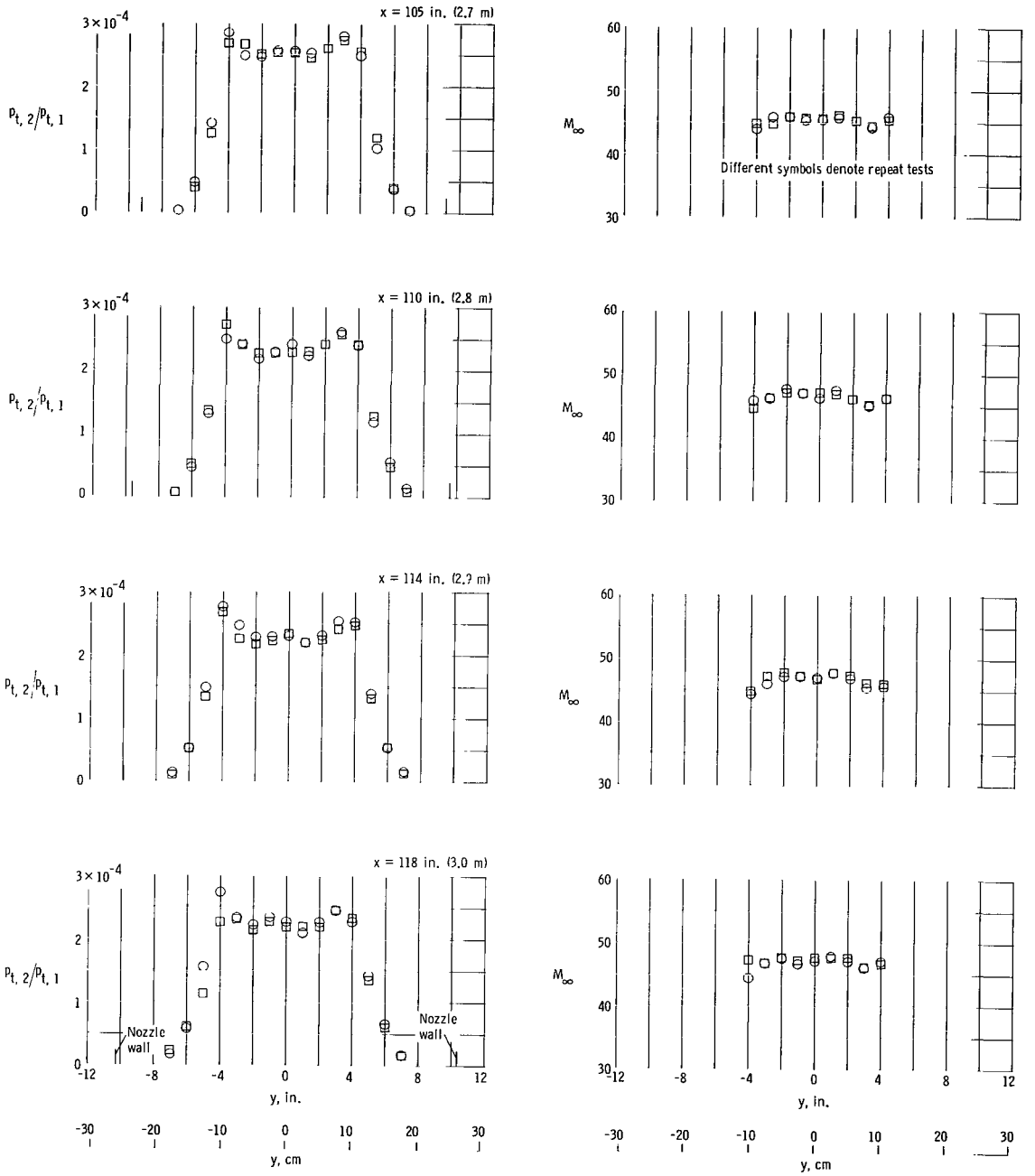

(c) $d^* = 0.15$ in. (3.81 mm); $T_{t,1} \approx 2800^0$ R (1556^0 K).

Figure 21.- Continued.

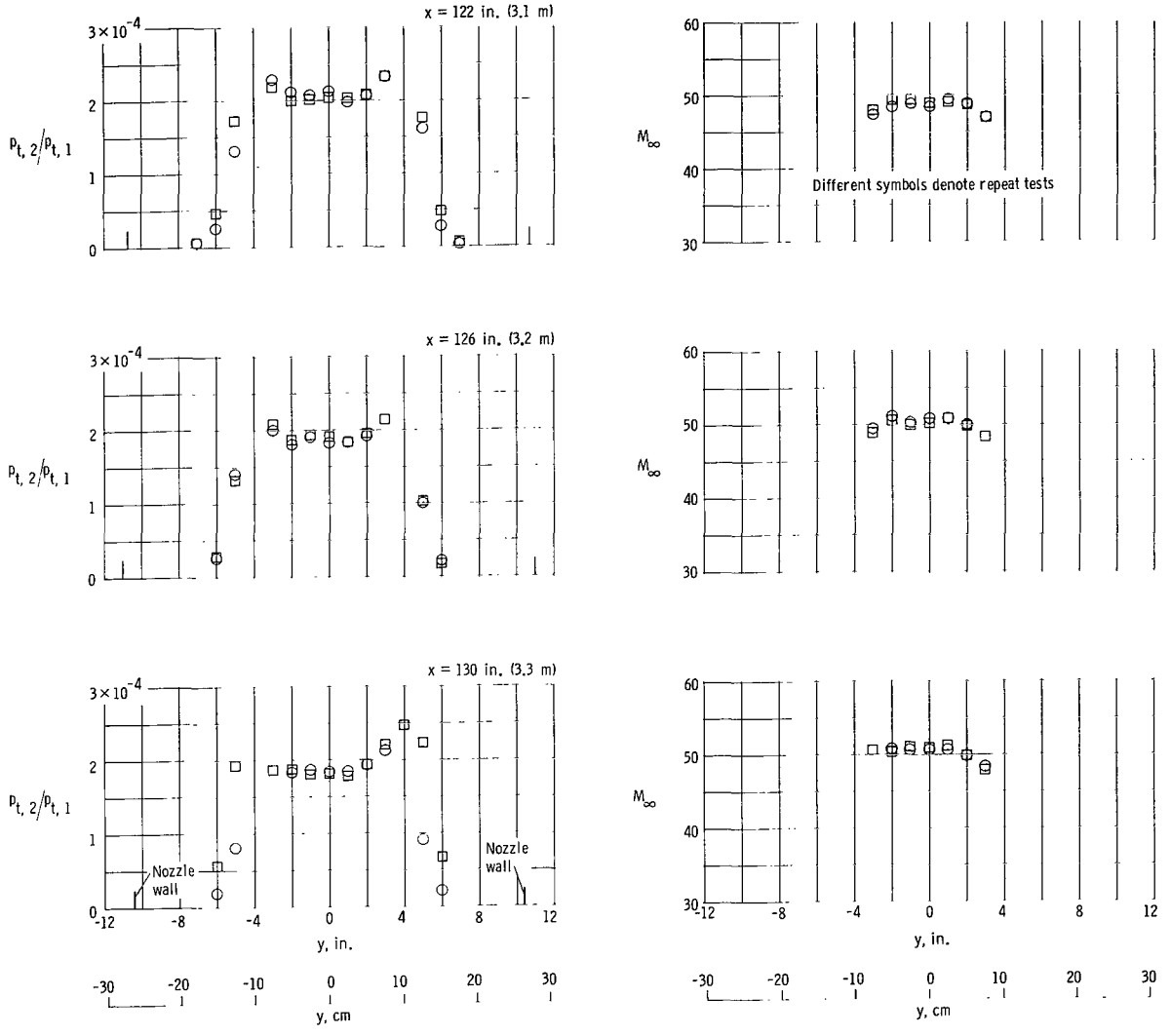

(c) Concluded.

Figure 21.- Concluded.

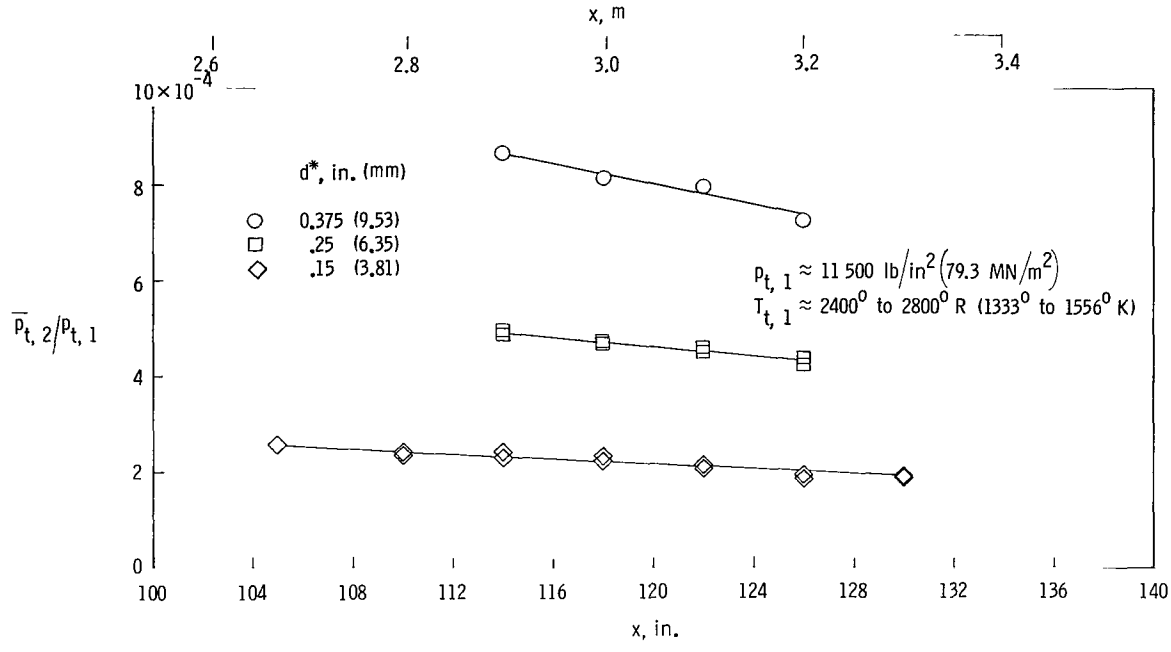

(a) Stagnation-pressure ratio.

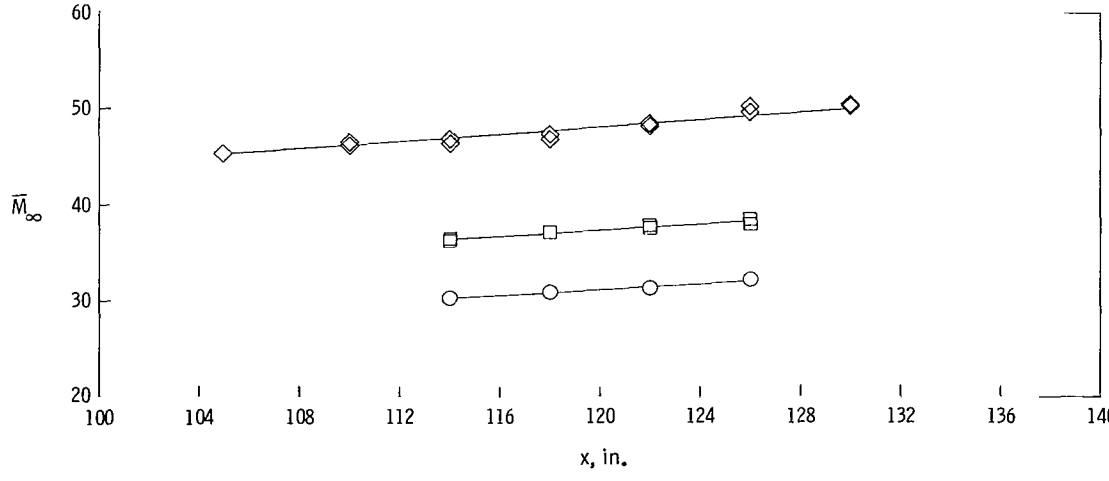

(b) Free-stream Mach number.

Figure 22.- Axial variation of various flow parameters averaged across the inviscid core for several nozzle-throat diameters.

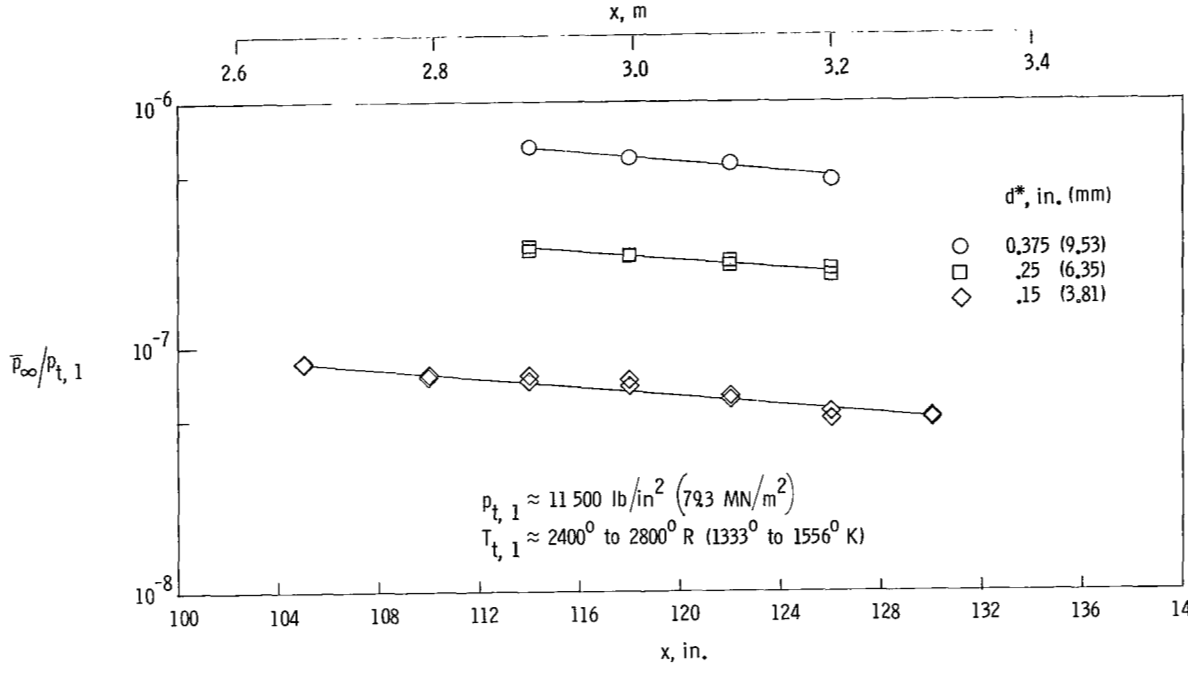

(c) Free-stream static-pressure ratio.

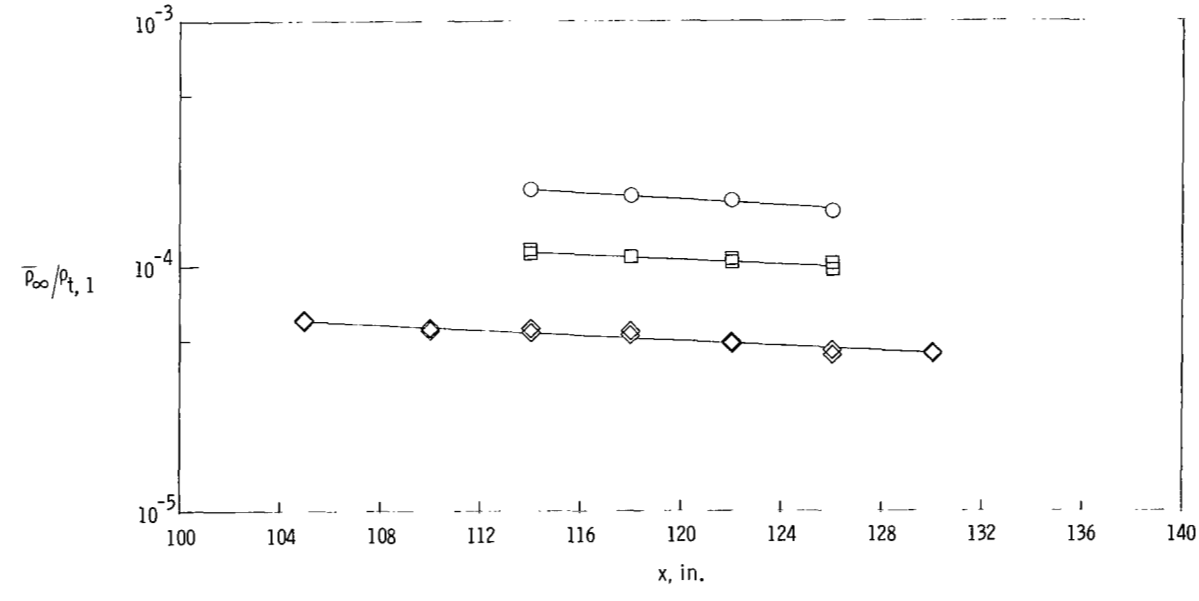

(d) Free-stream density ratio.

Figure 22.- Concluded.

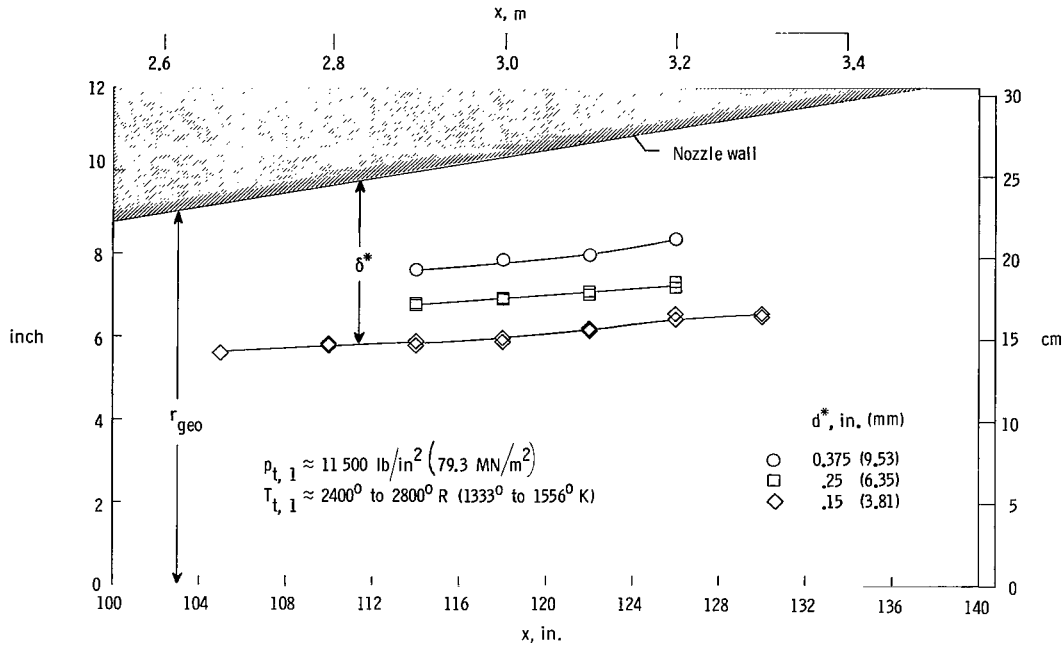

(a) Nozzle boundary-layer displacement thickness.

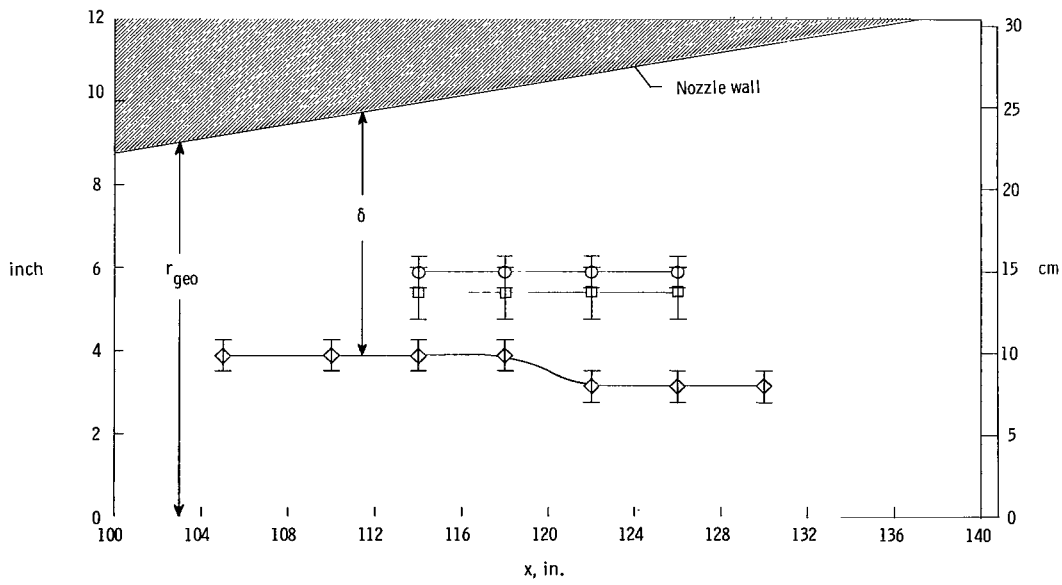

(b) Nozzle boundary-layer thickness.

Figure 23.- Axial variation of nozzle boundary-layer displacement thickness and nozzle boundary-layer thickness for several nozzle-throat diameters.

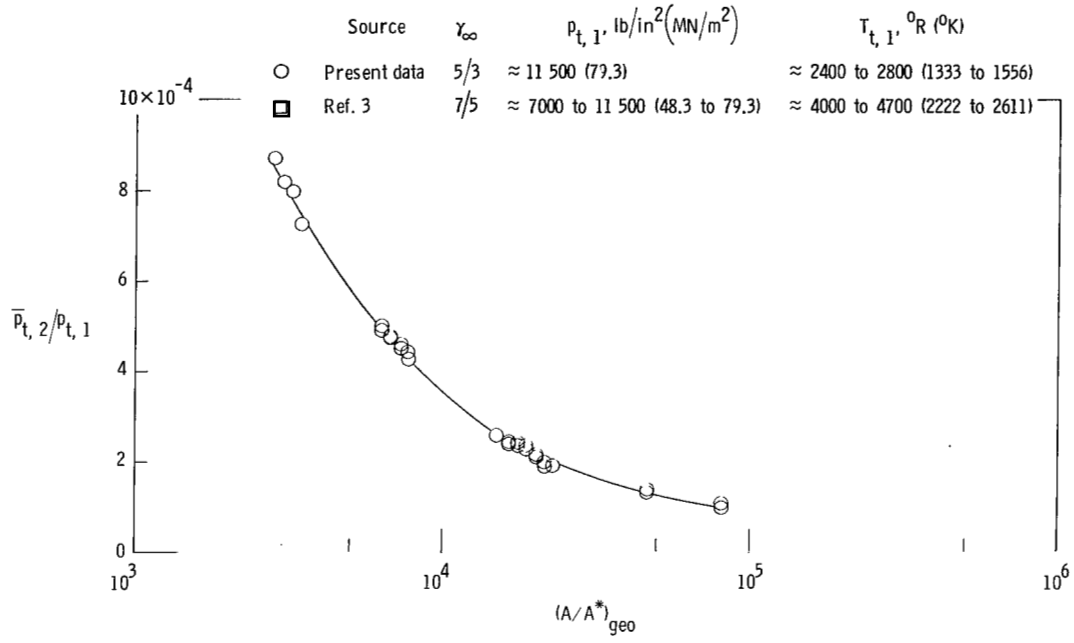

(a) Stagnation-pressure ratio.

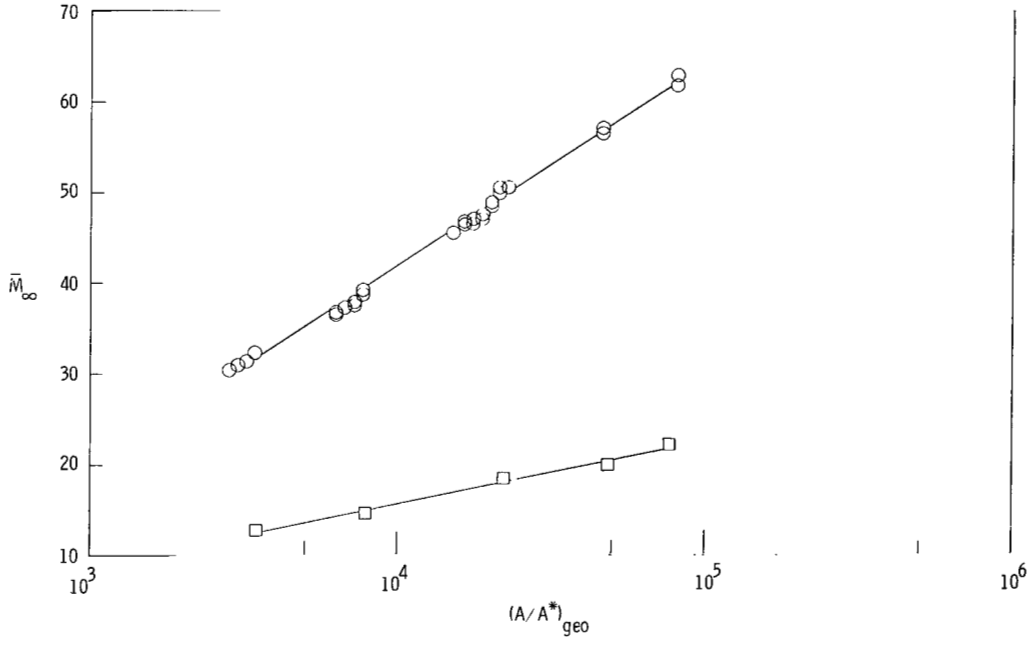

(b) Free-stream Mach number.

Figure 24.- Stagnation-pressure ratio and Mach number averaged across the inviscid core as functions of geometric-area ratio.

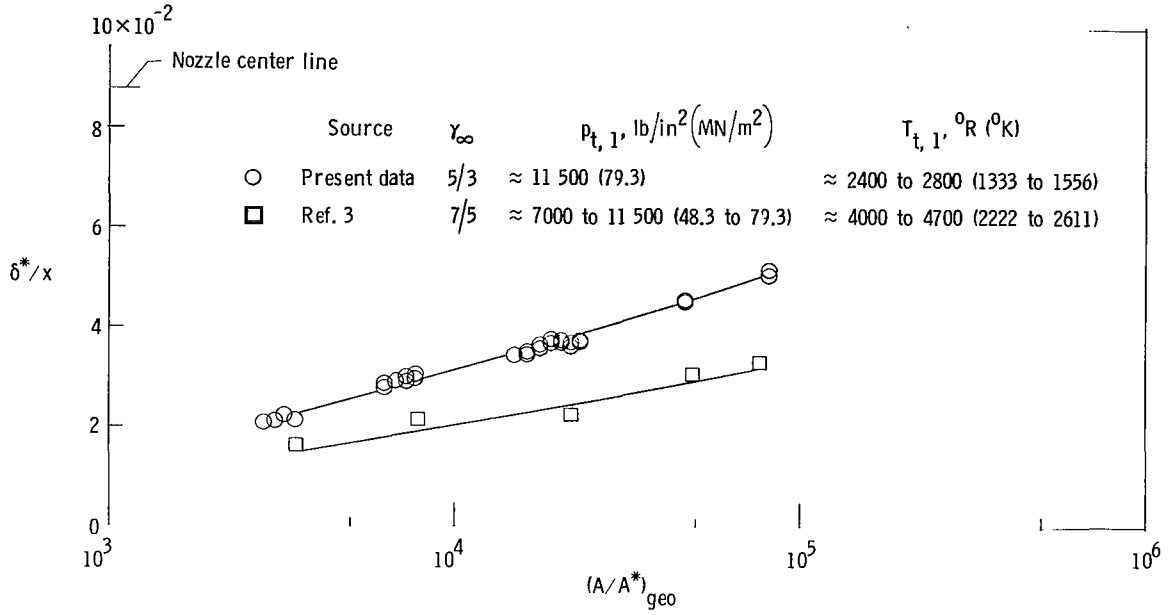

(a) Nozzle boundary-layer displacement thickness.

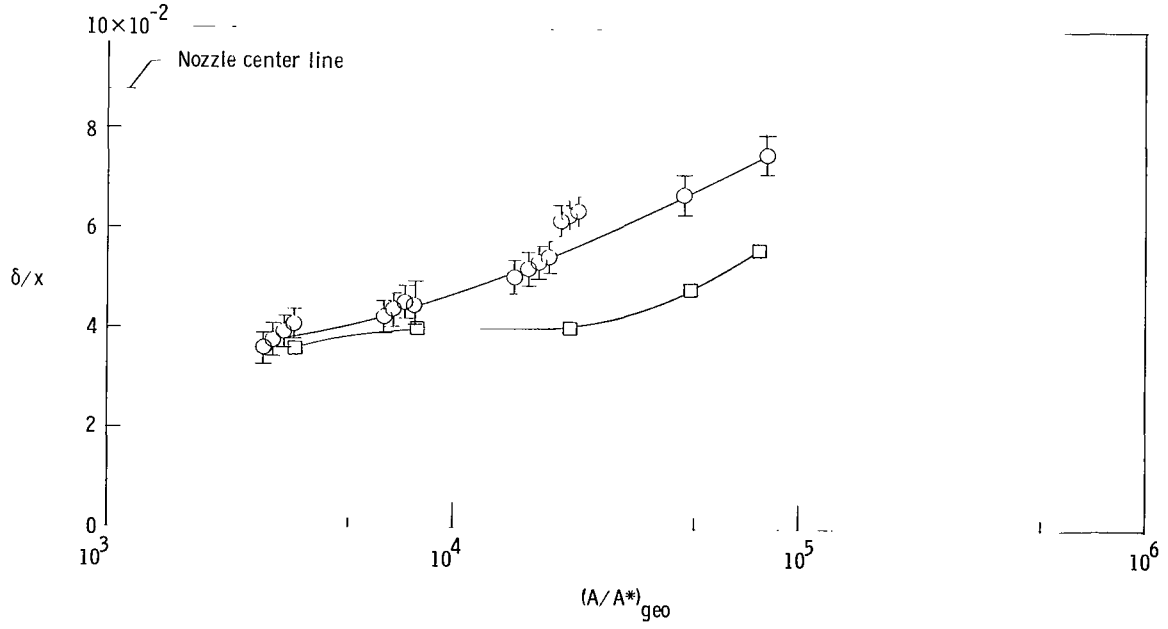

(b) Nozzle boundary-layer thickness.

Figure 25.- Variation of nozzle boundary-layer displacement thickness and nozzle boundary-layer thickness with geometric-area ratio.

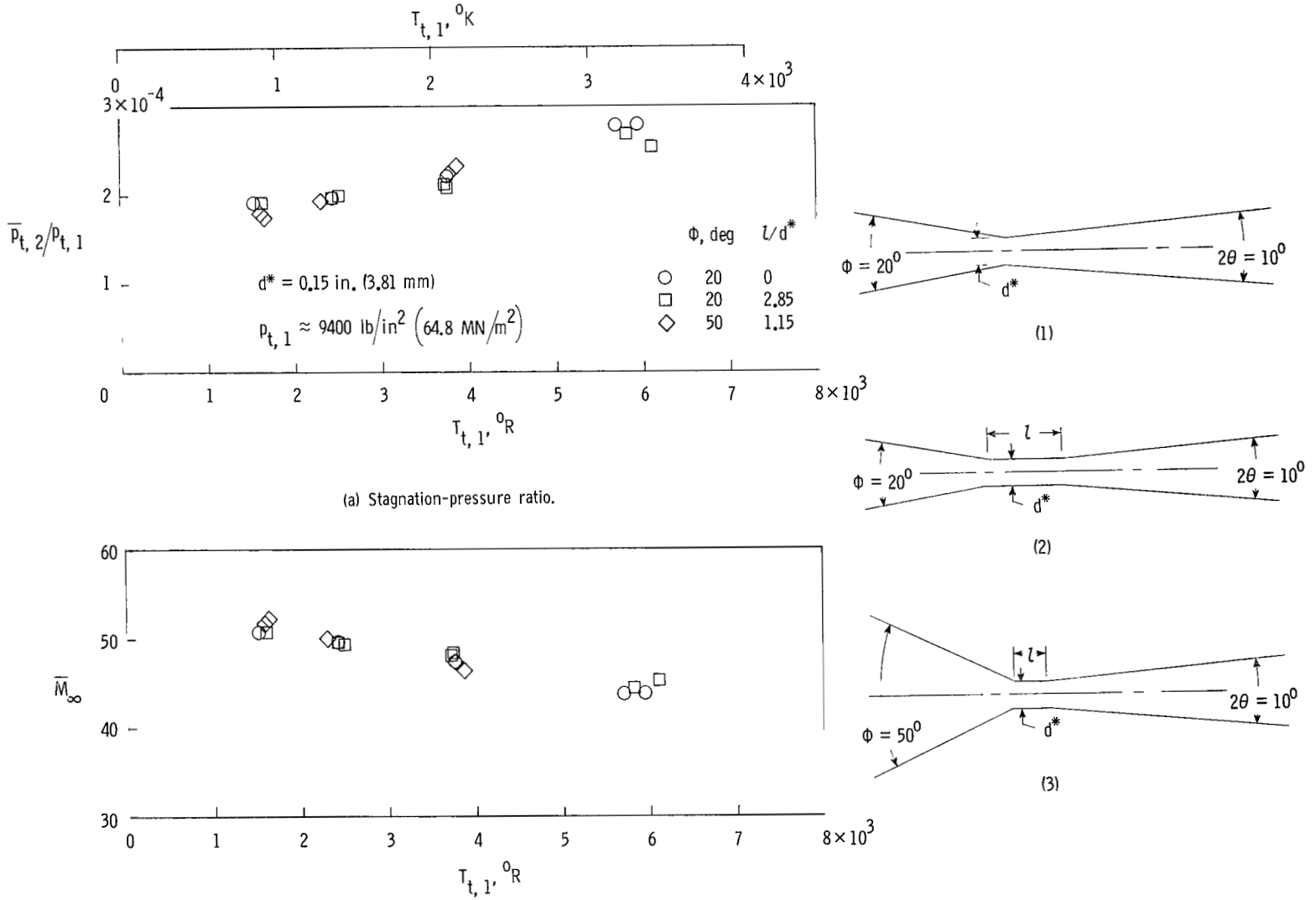

Figure 26.- Stagnation-pressure ratio and Mach number averaged across inviscid core as functions of reservoir temperature for several nozzle-throat geometries.

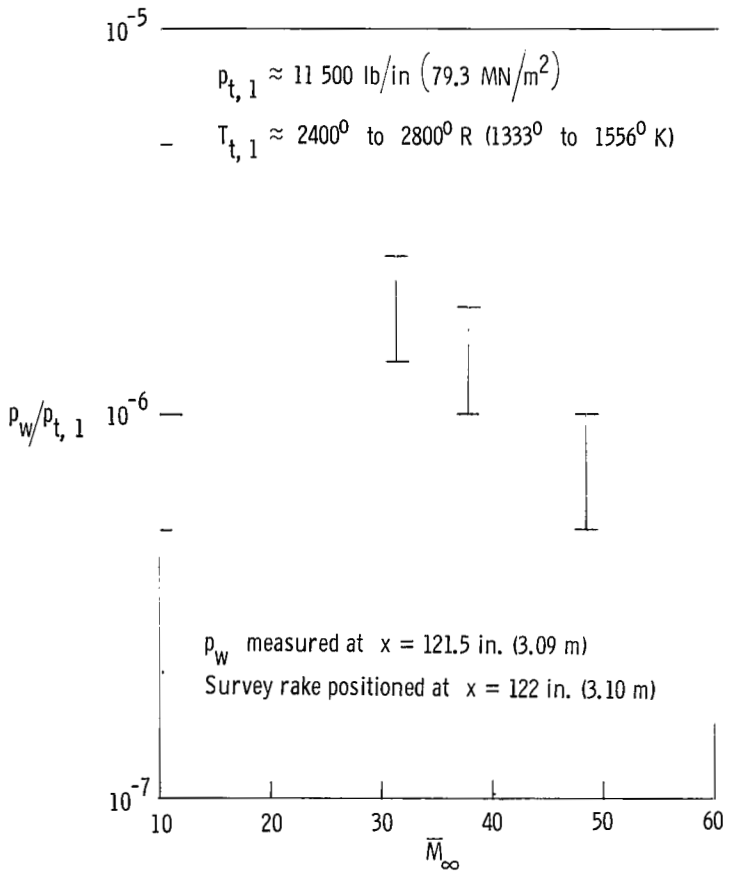

(a) Wall pressure nondimensionalized by reservoir pressure.

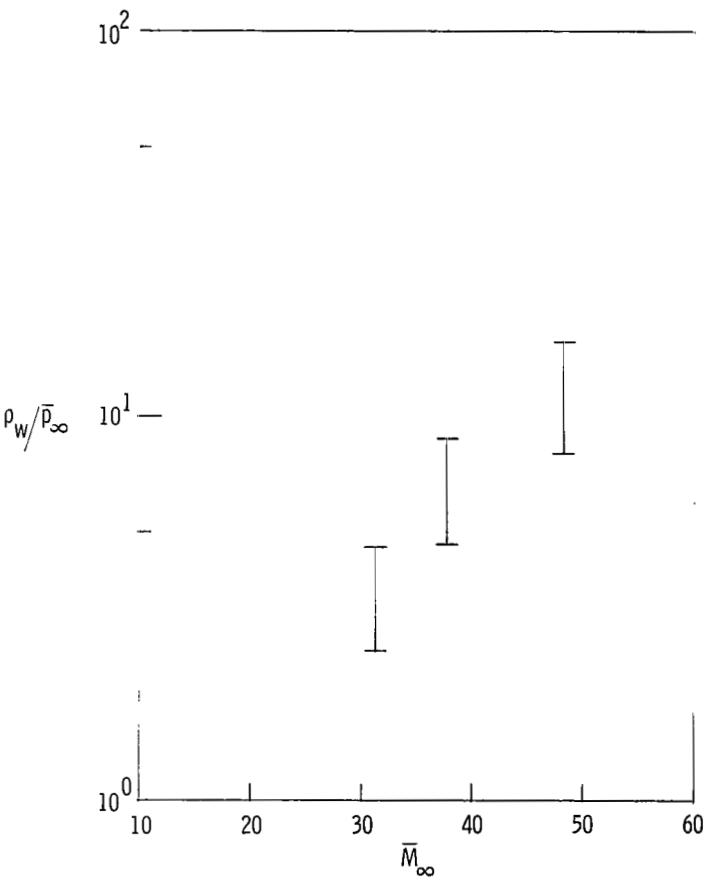

(b) Wall pressure nondimensionalized by average free-stream static pressure.

Figure 27.- Variation of nozzle-wall-pressure ratio with Mach number.

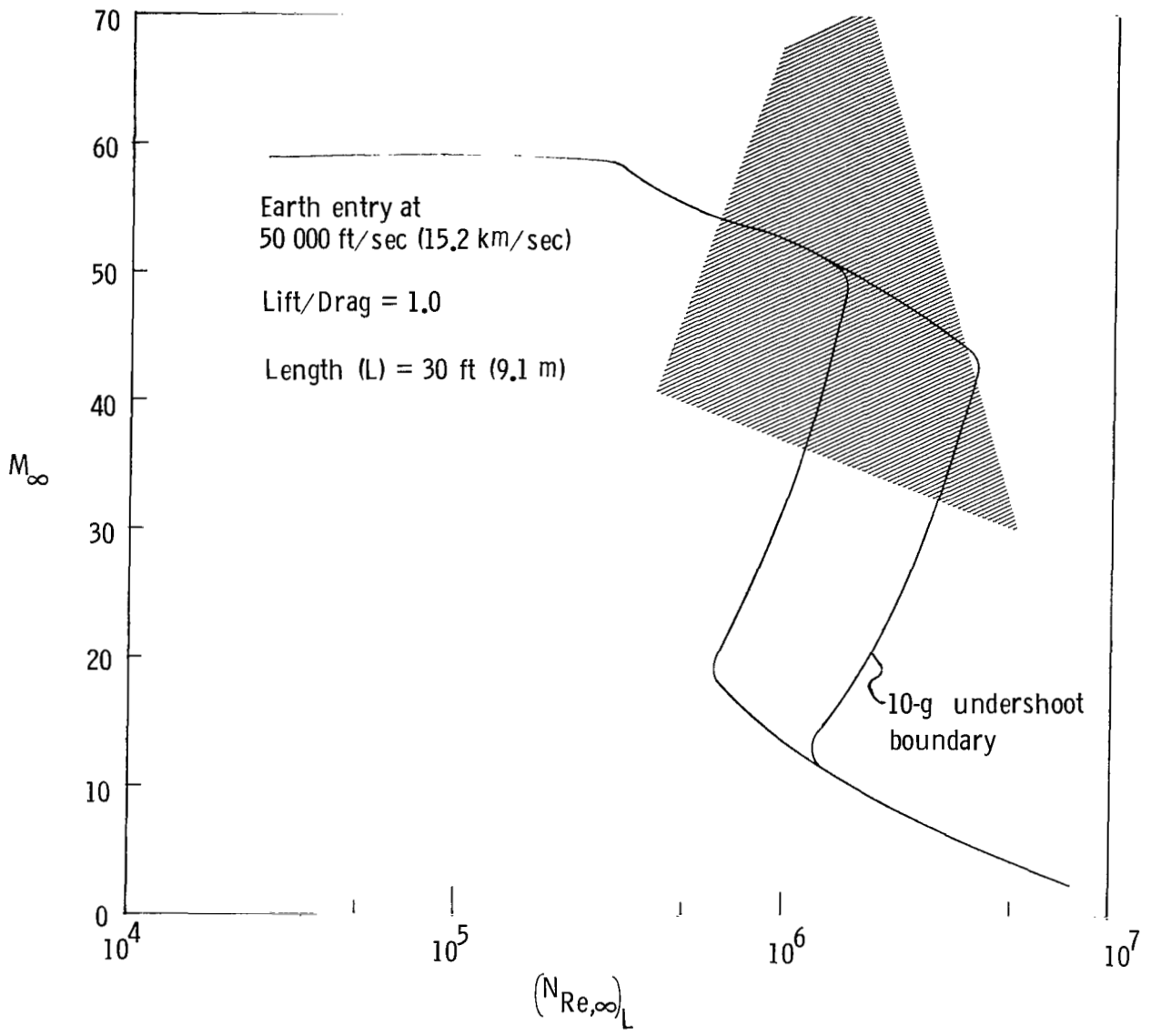

Figure 28.- Test experience in terms of free-stream Mach number and free-stream Reynolds number in the Langley hotshot tunnel with helium.

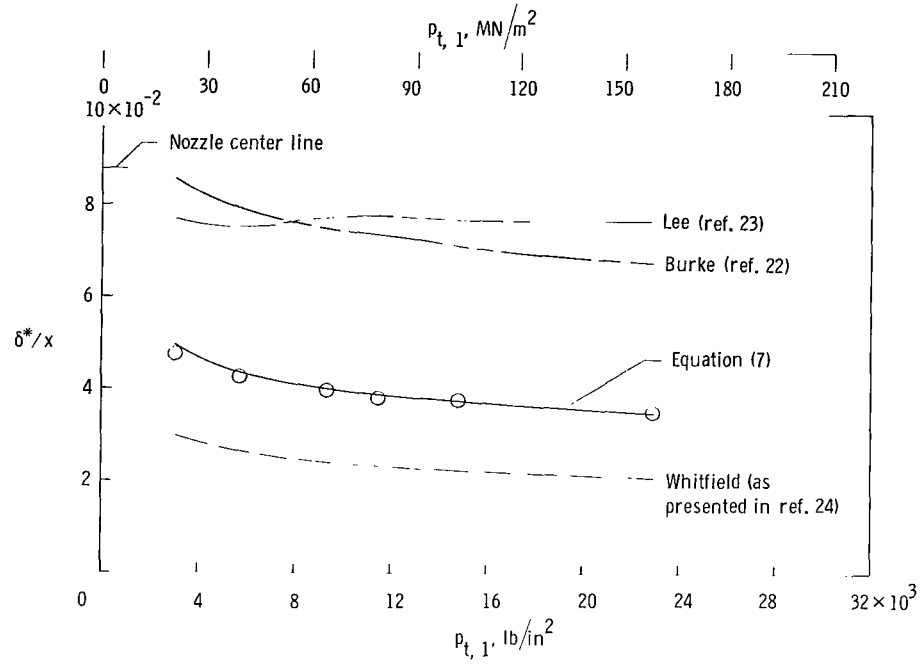

(a) $d^* = 0.15$ in. (3.81 mm); $T_{t,1} \approx 3800^0$ R (2111^0 K).

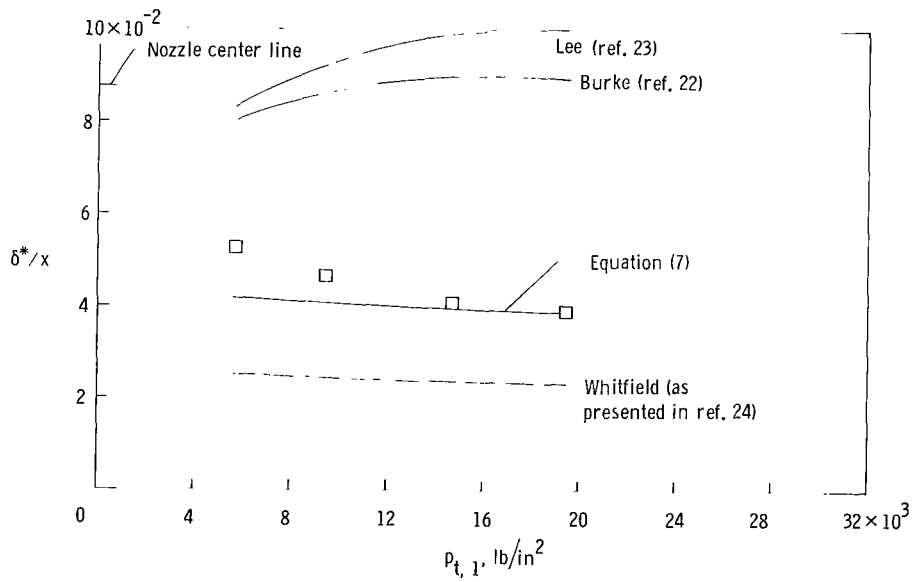

(b) $d^* = 0.10$ in. (2.54 mm); $T_{t,1} \approx 2600^0$ R (1444^0 K).

Figure 29.- Empirical methods for predicting nozzle boundary-layer displacement thickness for a range of reservoir pressure and two nozzle-throat diameters. (Symbols represent average values of data presented in fig. 18(a).)

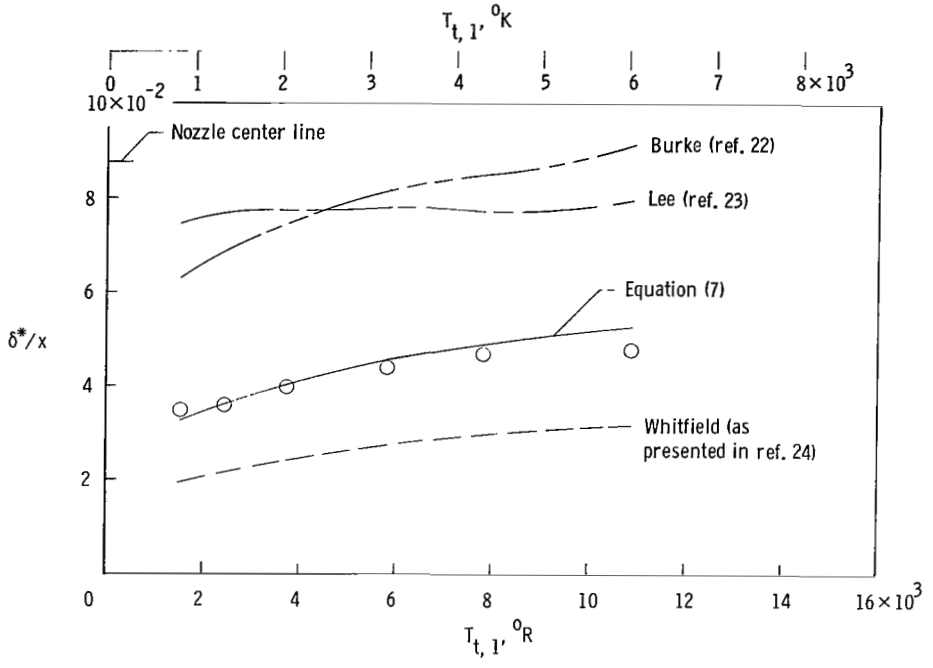

(a) $d^* = 0.15$ in. (3.81 mm); $p_{t,1} \approx 9200$ lb/in^2 (63.4 MN/m^2).

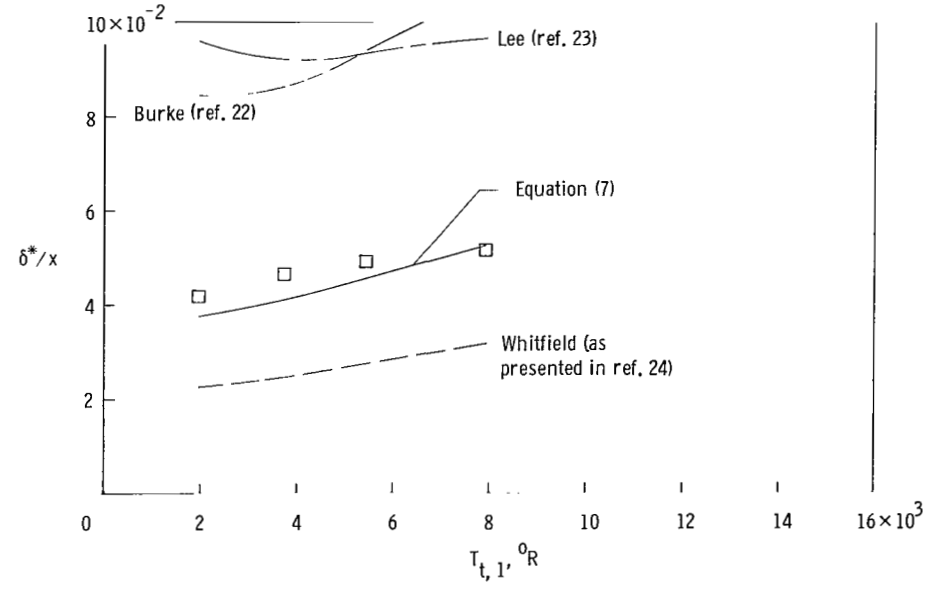

(b) $d^* = 0.10$ in. (2.54 mm); $p_{t,1} \approx 14\,500$ lb/in^2 (100.0 MN/m^2).

Figure 30.- Empirical methods for predicting nozzle boundary-layer displacement thickness for a range of reservoir temperature and two nozzle-throat diameters. (Symbols represent average values of data presented in fig. 19(a).)

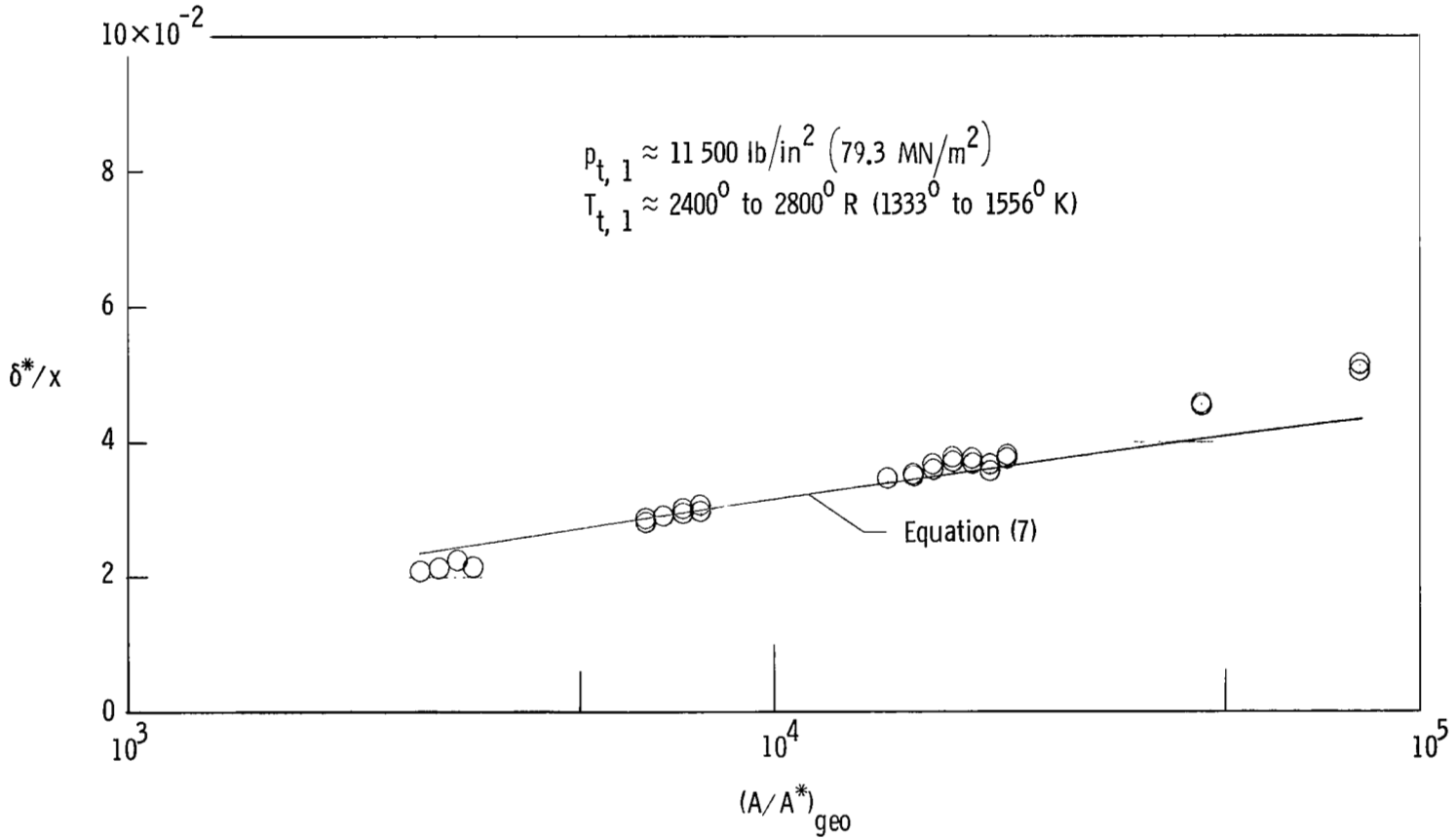

Figure 31.- Empirical prediction of nozzle boundary-layer displacement thickness as a function of geometric-area ratio.

	Source	γ_∞	M_∞	$p_{t,1}$, lb/in^2 (MN/m^2)	$T_{t,1}$, $^\circ$R ($^\circ$K)
○	Present data	5/3	≈ 30 to 60	≈ 3000 to 23 000 (20.7 to 158.6)	≈ 1500 to 11 000 (833 to 6111)
□	Ref. 14	5/3	≈ 27 to 47	950 to 4000 (6.6 to 27.6)	800 to 1650 (444 to 917)

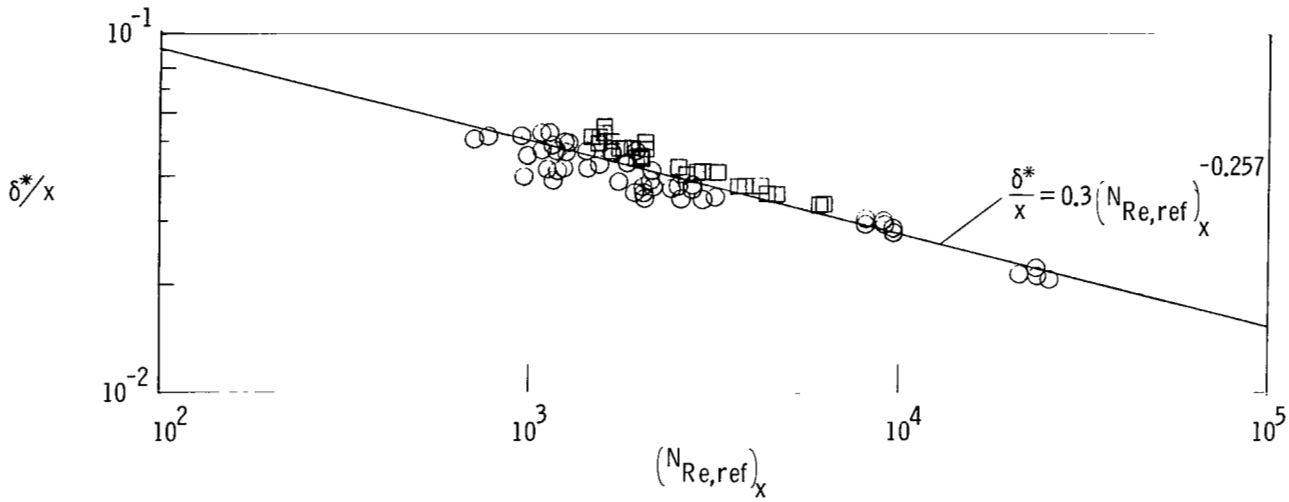

(a) Nozzle boundary-layer displacement thickness.

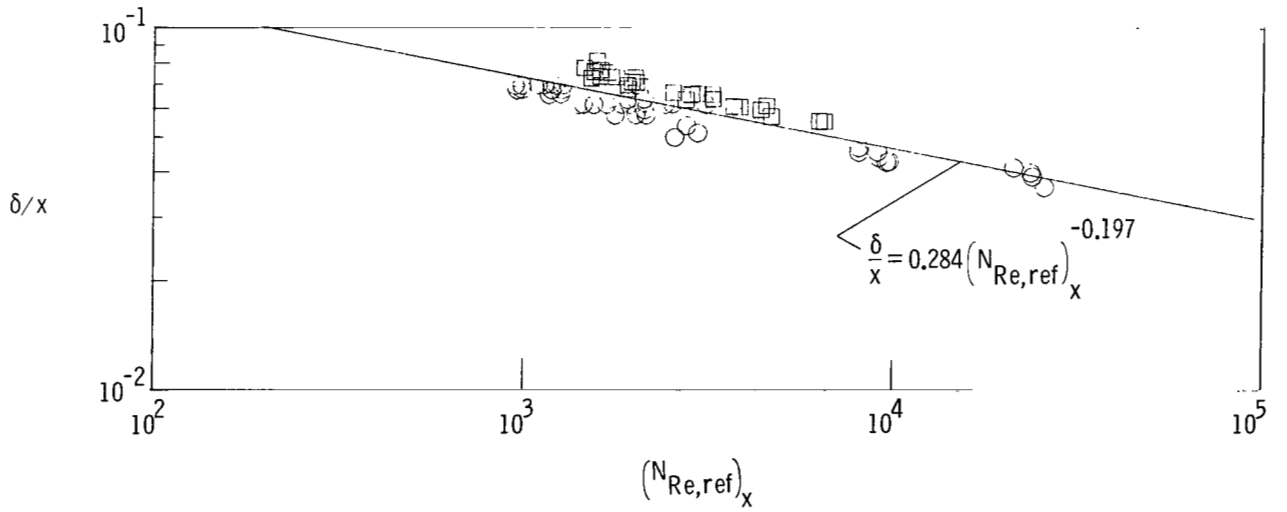

(b) Nozzle boundary-layer thickness.

Figure 32.- Nozzle boundary-layer displacement thickness and nozzle boundary-layer thickness in terms of Reynolds number based on a reference temperature.

	Source	γ_∞	M_∞	$p_{t,1}$, lb/in^2 (MN/m^2)	$T_{t,1}$, $^\circ$R ($^\circ$K)
○	Present data	5/3	≈ 30 to 60	≈ 3000 to 23 000 (20.7 to 158.6)	≈ 1500 to 11 000 (833 to 6111)
□	Ref. 14	5/3	≈ 27 to 47	950 to 4000 (6.6 to 27.6)	800 to 1650 (444 to 917)

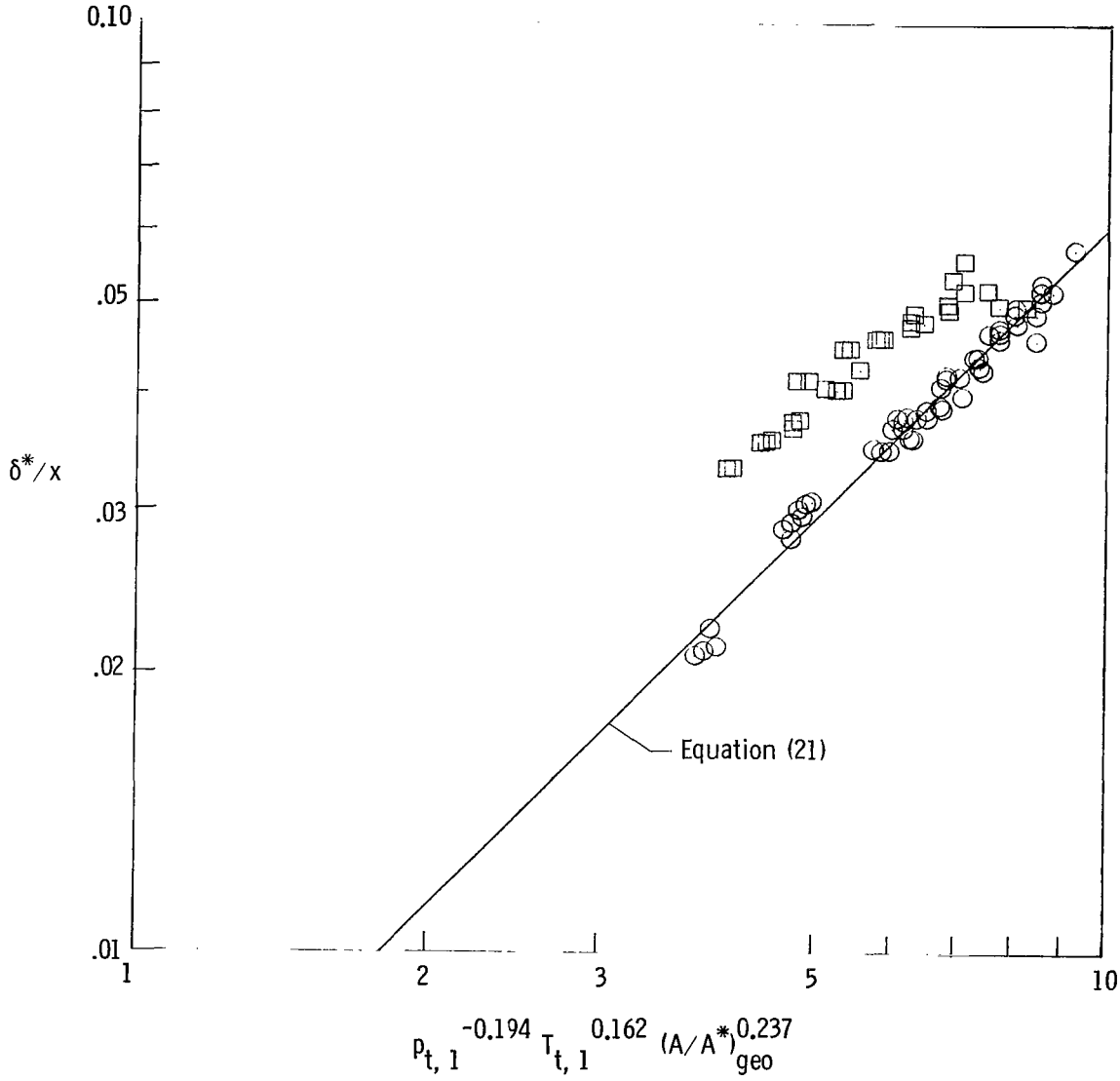

Figure 33.- Correlation of nozzle boundary-layer displacement thickness in terms of reservoir pressure, reservoir temperature, and geometric-area ratio.

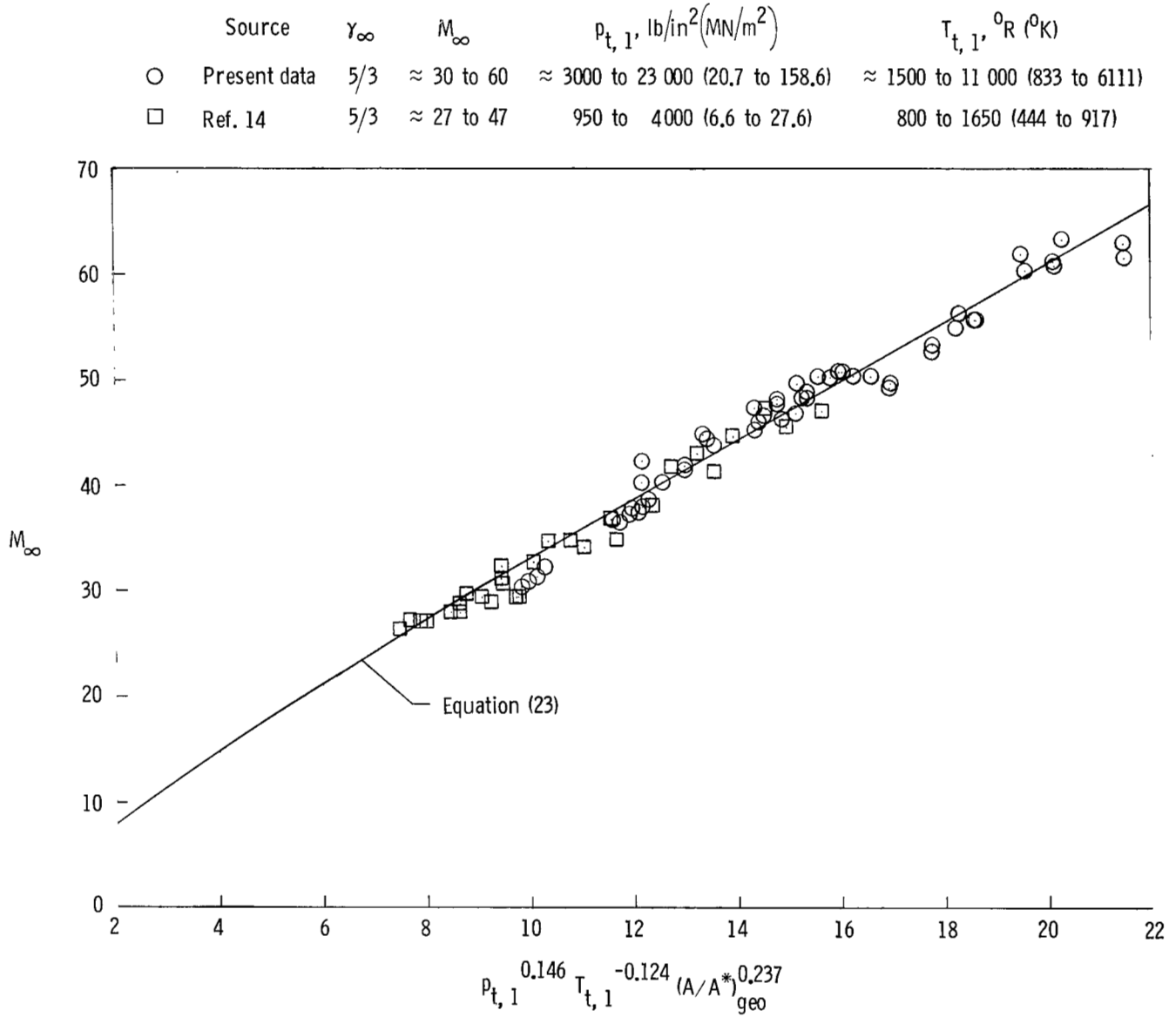

Figure 34.- Correlation of Mach number in terms of reservoir pressure, reservoir temperature, and geometric-area ratio.

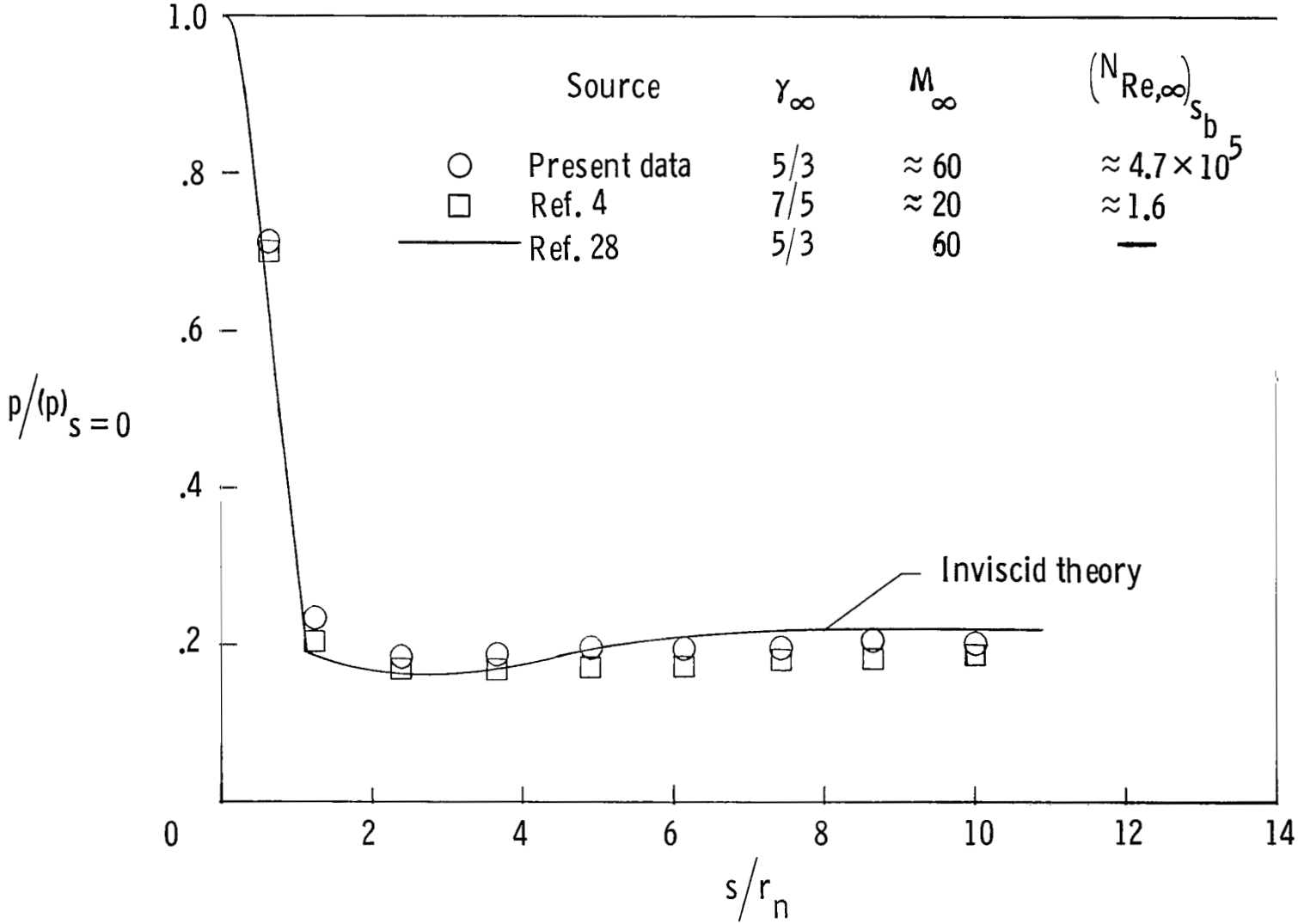

Figure 35.- Surface pressure distribution on a 25^0 half-angle spherically blunted cone.

"The aeronautical and space activities of the United States shall be conducted so as to contribute . . . to the expansion of human knowledge of phenomena in the atmosphere and space. The Administration shall provide for the widest practicable and appropriate dissemination of information concerning its activities and the results thereof."

—NATIONAL AERONAUTICS AND SPACE ACT OF 1958

NASA SCIENTIFIC AND TECHNICAL PUBLICATIONS

TECHNICAL REPORTS: Scientific and technical information considered important, complete, and a lasting contribution to existing knowledge.

TECHNICAL NOTES: Information less broad in scope but nevertheless of importance as a contribution to existing knowledge.

TECHNICAL MEMORANDUMS: Information receiving limited distribution because of preliminary data, security classification, or other reasons.

CONTRACTOR REPORTS: Scientific and technical information generated under a NASA contract or grant and considered an important contribution to existing knowledge.

TECHNICAL TRANSLATIONS: Information published in a foreign language considered to merit NASA distribution in English.

SPECIAL PUBLICATIONS: Information derived from or of value to NASA activities. Publications include conference proceedings, monographs, data compilations, handbooks, sourcebooks, and special bibliographies.

TECHNOLOGY UTILIZATION PUBLICATIONS: Information on technology used by NASA that may be of particular interest in commercial and other non-aerospace applications. Publications include Tech Briefs, Technology Utilization Reports and Notes, and Technology Surveys.

Details on the availability of these publications may be obtained from:

SCIENTIFIC AND TECHNICAL INFORMATION DIVISION

NATIONAL AERONAUTICS AND SPACE ADMINISTRATION

Washington, D.C. 20546